

March 2022

Fiber-based Electrical Energy Storage and Harvesting Devices for Wearable Electronics

Tareq Kareri
University of South Florida

Follow this and additional works at: <https://digitalcommons.usf.edu/etd>



Part of the [Electrical and Computer Engineering Commons](#), and the [Oil, Gas, and Energy Commons](#)

Scholar Commons Citation

Kareri, Tareq, "Fiber-based Electrical Energy Storage and Harvesting Devices for Wearable Electronics" (2022). *USF Tampa Graduate Theses and Dissertations*.
<https://digitalcommons.usf.edu/etd/10304>

This Dissertation is brought to you for free and open access by the USF Graduate Theses and Dissertations at Digital Commons @ University of South Florida. It has been accepted for inclusion in USF Tampa Graduate Theses and Dissertations by an authorized administrator of Digital Commons @ University of South Florida. For more information, please contact digitalcommons@usf.edu.

Fiber-based Electrical Energy Storage and Harvesting Devices for Wearable Electronics

by

Tareq Kareri

A dissertation submitted in partial fulfillment
of the requirements for the degree of
Doctor of Philosophy
Department of Electrical Engineering
College of Engineering
University of South Florida

Major Professor: Arash Takshi, Ph.D.
Elias Stefanakos, Ph.D.
Sylvia Thomas, Ph.D.
Manoj Ram, Ph.D.
Ryan Toomey, Ph.D.

Date of Approval:
March 17, 2022

Keywords: Hybrid Device, Flexible Device, Supercapacitor, Solar Cell,
Photoactive Electrolyte, Thread

Copyright © 2022, Tareq Kareri

Dedication

This dissertation is dedicated to my great parents, Mohammed Kareri and Aisha Maswadi, for their endless love and support in every step of my life. I also dedicate this dissertation to my beloved wife, Nada Rajhi, and my lovely daughter, Dalia, who have been a constant source of inspiration and motivation during my graduate studies.

Acknowledgments

I would like first to thank my advisor Dr. Arash Takshi who made this dissertation possible, for his help, invaluable advice, and constant motivation throughout my Ph.D. studies, and for providing a perfect and well-organized working environment in his lab.

Also, I would like to express my thanks to the Ph.D. committee members Dr. Lee Stefanakos, Dr. Sylvia Thomas, Dr. Manoj Ram, and Dr. Ryan Toomey for being on my committee and their valuable comments and recommendations.

I would like to extend my thanks to my friends and colleagues in the Bio-Organic Electronics lab for their help and support over these years. I am also thankful to the Ministry of Education and Najran University in Saudi Arabia for their financial and moral support throughout my graduate studies.

Table of Contents

List of Tables	iv
List of Figures	v
Abstract	ix
Chapter 1: Introduction	1
1.1 Background	1
1.2 Motivation of the Work	2
1.3 Research Objectives	3
1.4 Scope of the Dissertation	4
Chapter 2: A Critical Review on the Voltage Requirement in Hybrid Cells with Solar Energy Harvesting and Energy Storage Capability	5
2.1 Abstract	5
2.2 Introduction	5
2.3 Two Basic Types of Hybrid Devices	7
2.4 Conventional Approach of Solar Panels with External Batteries	8
2.5 Circuit Topologies Using a Hybrid Cell for Powering Low-Voltage Electronics	12
2.6 Review of Hybrid Cells	17
2.6.1 Three-Terminal Hybrid Cells	18
2.6.1.1 Si PV-SC Hybrid Cells	18
2.6.1.2 PSC-SC Hybrid Cells	20
2.6.1.3 OPV-SC Hybrid Cells	22
2.6.1.4 DSSC-SC Hybrid Cells	24
2.6.1.5 Fabric-Base DSSC-SC Hybrid Cells	26
2.6.2 Two-Terminal Hybrid Cells	27
2.6.2.1 Photogalvanic Cells	28
2.6.2.2 DSSC-Redox Flow Battery Hybrid Cells	31
2.6.2.3 Photoactive SCs	32
2.7 Suggestions and Outlook	37
2.8 Conclusions	38
Chapter 3: Impedance Spectroscopy Study of Hybrid Photovoltaic Supercapacitors	39
3.1 Abstract	39
3.2 Introduction	40
3.3 Experimental	42
3.3.1 Materials and Equipment	42
3.3.2 Electrode Fabrication	42

3.3.3 Electrolytes Preparation	43
3.4 Results and Discussion	43
3.5 Conclusion	49
Chapter 4: Hybrid Photovoltaic-Supercapacitors: Effect of the Counter Electrode on the Device Performance	50
4.1 Abstract	50
4.2 Introduction	51
4.3 Experimental	53
4.3.1 Materials and Instrumentation	53
4.3.2 Electrodes Fabrication	53
4.3.3 Electrolyte Preparation	54
4.4 Results and Discussion	54
4.5 Conclusion	59
Chapter 5: Image Processing Analysis of Supercapacitors with Twisted-Fiber Structures and a Gel Electrolyte	60
5.1 Abstract	60
5.2 Introduction	61
5.3 Experimental Section	63
5.3.1 Materials	63
5.3.2 Preparation of Gel Electrolytes	63
5.3.3 Device Fabrication and Characterization	63
5.4 Results and Discussion	64
5.4.1 Device Characterization	64
5.4.2 Image Processing	70
5.5 Conclusion	76
Chapter 6: A Flexible Fiber-Shaped Hybrid Cell with a Photoactive Gel Electrolyte for Concurrent Solar Energy Harvesting and Charge Storage	77
6.1 Abstract	77
6.2 Introduction	78
6.3 Experimental Section	80
6.3.1 Materials	80
6.3.2 Preparation of the Gel Electrolyte and the CNT Ink	81
6.3.3 Preparation of Electrodes	81
6.3.4 Device Fabrication and Characterization	83
6.4 Results and Discussion	83
6.4.1 Characterization	83
6.4.2 Electrochemical Properties of Fiber-Shaped Hybrid Devices	86
6.5 Conclusion	95
Chapter 7: Conclusion and Recommendations for Future Work	96
7.1 Conclusion	96
7.2 Recommendations for Future Work	97

References.....	98
Appendix A: Copyright Permissions	112
Appendix B: Supporting Information for Chapter 5.....	117
Appendix C: Supporting Information for Chapter 6.....	120

List of Tables

Table 1: Summary of the reviewed works with their reported V_{oc}	34
Table 2: Impedance parameters of different concentrations of Aniline in the dark and light.....	48
Table 3: Summary of the hybrid device characteristics with different counter electrodes	58
Table 4: Impedance parameters of different fiber supercapacitors based on the number of twists per length	69
Table 5: Measured dimensions of the samples using the image processing tool in MATLAB and calculated the uniformity factor in the twisted structures	73
Table S1: Impedance parameters of the fiber-shaped hybrid devices in dark and under illumination.....	122

List of Figures

Figure 1: Schematic of (a) a three-terminal and (b) a two-terminal hybrid cell.....	7
Figure 2: Typical I-V characteristics of a solar cell.....	9
Figure 3: (a) Conventional solar energy system with a smart charge controller; (b) series connection of two-terminal hybrid cells; and (c) three-terminal cells each equipped with a charge control unit.....	10
Figure 4: Block-diagram of Si1000 from Silicon Labs	13
Figure 5: Various topologies where a hybrid single cell can be used for powering a circuit: (a) direct connection of a two-terminal cell, (b) impractical usage of a three-terminal as a two-terminal device, (c) impractical combination of a battery and a single PV, (d) using a DC-DC converter to charge a battery via a PV cell, and (e) a simple solution of using a diode in a three-terminal device with a SC storage	15
Figure 6: Three different Si PV-SC hybrid cells designed and reported by: (a) Westover et al., [64] (b) Thekkekara et al., [65] and (c) Liu et al. [66].....	19
Figure 7: Three different PSC-SC hybrid cells designed and reported by: (a) Liang et al., [35] (b) Zhou et al., [71] and (c) Liu et al. [56]	20
Figure 8: Examples of combination of a PV and a SC in series not acting as a hybrid cell reported by (a) Liu et al. [75] and (b) Xu et al. [76]	21
Figure 9: Three different OPV-SC hybrid cells reported by: (a) Kim et al., [80] (b) Lechêne et al., [81] and (c) Zhang et al. [82].....	23
Figure 10: Four different examples of power packs with OPV or PSC cells in series and a supercapacitor reported by: (a) Chien et al., [83] (b) Wee et al., [84] (c) Li et al., [53] and (d) Xu et al. [54].....	23
Figure 11: Examples of DSSC-SC hybrid device reported by: (a) Nagai et al., [90] (b) Bagheri et al., [96] (c) Cohn et al., [97] (d) Yang et al., [98] (e) Skunik-Nuckowska et al., [99] and (f) Xu et al. [100].....	25

Figure 12: Example of fabric based hybrid cells reported by: (a) Fu et al., [110] (b) Chen et al., [112] (c) Zhang et al., [115] (d) Fu et al., [110] (e) Chai et al., [114] and (f) Liang et al. [113].....	27
Figure 13: Examples of PG cells reported by: (a) Lal et al., [117] (b) Xiao et al., [129] and (c) Halls et al.[130].....	29
Figure 14: Examples of hybrid cells made from biomaterials reported by: (a) De La Garza et al. [136] and (b) Usui et al. [137]	30
Figure 15: Examples of hybrid cells with flow batteries reported by: (a) Liu et al. [139] and (b) Cao et al. [140].....	31
Figure 16: Examples of two-terminal photoactive supercapacitors reported by: (a) Takshi et al., [145] (b) Aljafari et al., [133] (c) Huang et al., [147] (d) Cai et al., [148] and (e) Roy et al. [150].....	33
Figure 17: Schematic diagram of hybrid device based on composite gel electrolyte.....	41
Figure 18: Cyclic voltammetry (CV) results of the hybrid device with PVA-PANI composite gel electrolyte, 0.3 mM of Aniline, under the dark and light conditions	44
Figure 19: (a) UV-visible absorption spectrum, (b) open circuit voltage result of a hybrid photovoltaic supercapacitor with PVA-(0.3 mM)PANI composite gel electrolyte	45
Figure 20: Short circuit current result of a hybrid photovoltaic supercapacitor with PVA-(0.3 mM)PANI composite gel electrolyte under dark and light pulses.....	45
Figure 21: Nyquist impedance results of the hybrid devices with (a) different concentrations of Aniline, and (b) 0.3 mM of Aniline in dark and light	46
Figure 22: Experimental and simulation results for (a) Magnitude and (b) phase of impedance for the device with PVAPANi composite gel electrolyte containing of 0.3 mM of Aniline.....	47
Figure 23: Schematic diagram of the hybrid device with different counter electrodes	52
Figure 24: Cyclic voltammetry results of the hybrid device with (a) MWCNT, (b) PEDOT:PSS, (c) carbon monolithic, and (d) carbon fiber fabric electrode.....	55
Figure 25: (a) UV-visible absorption spectrum of PVA/PANI gel, (b) open circuit voltage results of the hybrid device with different counter electrodes	56

Figure 26: Short circuit current results of the hybrid device with different counter electrodes.....	57
Figure 27: Nyquist plot of the hybrid device with MWCNT, PEDOT:PSS, carbon monolithic, and carbon fiber counter electrodes	58
Figure 28: (a) Schematic and (b) the image of a twisted fiber supercapacitor, made by first coating a thin layer of the gel on two pieces of fibers	62
Figure 29: CV curves of the supercapacitors with (a) Jameco, (b) JL, and (c) BCP fibers at different twisting turns	66
Figure 30: Experimental and fitted results of the impedance magnitude and phase for the supercapacitors with (a,b) Jameco, (c,d) JL, and (e,f) BCP fibers at T_1 and T_6	68
Figure 31: SEM images of (a,b) Jameco, (c,d) JL, and (e,f) BCP threads.....	70
Figure 32: Image processing steps: (a) reading the image files, (b) converting to the black and white, (c) opening the adjust contrast tool, (d) adjusting the minimum and maximum of the contrast range to get (e) the images with high contrasts.....	71
Figure 33: The magnitude of the capacitances and the effective length of the twisted structures vs. number of the twisting turns in the (a) Jameco, (b) JL, and (c) BCP devices	74
Figure 34: (a) Schematic illustration of the fabrication steps of the Ny66-Ag/CNT/ZnO-NWs anode electrode and the final device structure, (b,c) photographs of the fiber-shaped hybrid devices	80
Figure 35: SEM images of (a,b) Ny66-Ag conductive thread at different magnifications, (c,d) Ny66-Ag/CNT electrode surface, (e,f) ZnO nanowires growth on Ny66-Ag/CNT/ZnO-NWs electrode, and (g,h) SS conductive thread at different magnifications.....	84
Figure 36: EDS analysis of (a) Ny66-Ag conductive thread, (b) Ny66-Ag/CNT, and (c) Ny66-Ag/CNT/ZnO-NWs electrodes.....	85
Figure 37: Comparative (a) CV and (b) galvanostatic charge-discharge curves of the fiber-shaped hybrid device with Ny66-Ag, Ny66-Ag/CNT, and Ny66-Ag/CNT/ZnO-NWs anode electrodes tested in dark	87

Figure 38: Comparative measurements of (a) open circuit potential of the fiber-shaped hybrid devices with Ny66-Ag, Ny66-Ag/CNT, and Ny66-Ag/CNT/ZnO-NWs anode electrodes and (b) short circuit current under light pulses	89
Figure 39: Nyquist plots of the fiber-shaped hybrid device with (a) Ny66-Ag, (b) Ny66-Ag/CNT, and (c) Ny66-Ag/CNT/ZnO-NWs anode electrodes in the dark and under illumination; (d) comparative Nyquist plots of the devices in the dark condition.....	90
Figure 40: Stability measurements of the device with the Ny66-Ag/CNT/ZnO-NWs electrode	91
Figure 41: Energy diagram of the fiber-shaped hybrid device with (a) the Ny66-Ag, (b) Ny66-Ag/CNT, and (c) the Ny66-Ag/CNT/ZnO-NWs electrode.....	93
Figure S1: Galvanostatic charge-discharge results of the supercapacitor with (a) Jameco, (b) JL, and (c) BCP fibers and different twisting turns.....	117
Figure S2: Nyquist plots of the device with (a) Jameco, (b) JL, and (c) BCP fibers.....	118
Figure S3: Jameco thread coated with a layer of gel electrolyte before making the twisted-fiber capacitor	118
Figure S4: Cropped images of the Jameco, JL, and BCP devices at different number of turns	119
Figure S5: Zoomed in picture of T2 in the JL sample, showing the double layer structure of each JL thread and its effect on the structure of twisted two threads	119
Figure S6: A picture of the 3D printed threads holder for the hydrothermal process	120
Figure S7: Cyclic voltammetry results of the fiber-shaped hybrid devices with (a) Ny66-Ag, (b) Ny66-Ag/CNT, and (c) Ny66-Ag/CNT/ZnO-NWs electrode in dark and under illumination	120
Figure S8: I-V response of the fiber-shaped hybrid devices with (a) Ny66-Ag, (b) Ny66-Ag/CNT, and (c) Ny66-Ag/CNT/ZnO-NWs electrode in dark and under illumination.....	121
Figure S9: UV-visible absorption spectrum of the photoactive PANI gel in emeraldine salt form	121

Abstract

Over the past few years, smart textiles and wearable technologies have received tremendous attention due to their functionalities and characteristics, which could be used in a variety of ways in healthcare, sports/leisure, fashion, military, personal protective, and energy applications. These technologies depend on self-power systems, which require energy sources (e.g., batteries, supercapacitors, and solar cells) to power their projected functionalities in the future. Therefore, fabricating energy harvesting cells (i.e., solar cells) and energy storage cells (i.e., batteries and supercapacitors) in the form of fibers are promising solutions for powering wearable electronics due to their unique features such as flexibility and stretchability.

In this dissertation work, several projects and research works were carried out to fabricate and characterize two-terminal energy harvesting and storage devices based on a photoactive gel electrolyte. First, the photoactive composite gel containing polyaniline (PANI) was investigated by studying the effect of aniline (ANI) concentration in the bulk of the gel electrolyte on the impedance, capacitance, and photovoltaic performance of the devices. It was found that 0.3 M of ANI improves the energy storage and reduces the device's impedance, while the photovoltaic (PV) performance can be improved with 0.2 M of ANI.

The performance of the two-terminal hybrid cell can also be enhanced by optimizing the counter electrode materials. As a part of this research work, the impact of the counter electrode on the electrochemical and photovoltaic properties of the hybrid cell was considered by studying various counter electrodes made from carbon nanotubes (CNTs), a conducting polymer, carbon

monolithic, and carbon fibers. The results showed improvement in the hybrid cell's impedance, self-discharge, and energy storage performance with PEDOT:PSS as a conducting polymer. However, improving the capacitance of the hybrid cell with carbon fiber fabric and carbon monolithic electrodes negatively affects the PV performance and vice versa.

Moreover, three different symmetric thread-based supercapacitors with twisted structures were fabricated in order to study the electrochemical properties of the conductive threads (i.e., Jameco, JL, and BCP) and the impact of the structure on the device performance. The results revealed that the Jameco-based device provides a higher capacitance, and the capacitance is directly related to the number of twists due to the uniformity of the Jameco thread surface.

Finally, a flexible fiber-shaped hybrid device was successfully fabricated using the photoactive gel electrolyte and two conductive threads. The device was also examined with three different anode electrodes (i.e., Ny66-Ag, Ny66-Ag/CNT, and Ny66-Ag/CNT/ZnO-NWs) to improve the energy storage and PV response of the device. The results showed that the energy storage improved with the Ny66-Ag/CNT electrode, while the PV response increased with the Ny66-Ag/CNT/ZnO-NWs electrode.

Chapter 1: Introduction

1.1 Background

Over the past half-century, fossil fuel consumption has increased significantly due to the industrial revolution and global population growth, leading to climate change [1]. Recently, the interest in renewable energy has grown significantly to address the climate change [2, 3]. Therefore, governments, organizations, and researchers have made a great effort to develop and improve the efficiency of systems using renewable energies, especially solar and wind. However, there are still major obstacles that limit the applications of renewable sources including their high cost, stability, availability, and challenges in energy harvesting and energy storage devices. Improving the performance of energy storage devices, such as batteries and supercapacitors, and the efficiency of solar energy harvesting devices (i.e., solar cells) is a crucial factor in the development of renewable energy technologies.

Supercapacitors are electrochemical energy storage devices with a higher power density and the ability of being charged and discharged faster than batteries [4, 5]. With the rising development of the electric vehicles market, as well as the renewable energy industry, supercapacitors can play an important role in some applications where high-power density is needed. Supercapacitors can be classified into three types based on their energy storage mechanism: electric double-layer capacitors, pseudocapacitors, and hybrid capacitors. Supercapacitors, including electric double-layer capacitors (EDLCs) and pseudocapacitors, have a low energy density, at least 10 times lower than batteries, and a relatively high self-discharge

rate that restrict their use as an alternative to batteries [6, 7]. To improve the low energy density in supercapacitors, developing new electrode materials that have high porosity is needed [8]. Several approaches and electrode materials have been studied to enhance capacitance and energy density in supercapacitors [8, 9]. Generally, the electrode materials of supercapacitor can be classified into three main types: carbon-based materials, conducting polymers, and metal oxides [10].

In recent years, the need to develop flexible supercapacitors has increased due to the increasing demand for portable and wearable electronics equipment and applications. Among different flexible supercapacitors, fiber-based supercapacitors are promising devices, which could be used in several industrial fields such as electronics manufacturing, sports apparel, military garments, and medical applications [11-13].

1.2 Motivation of the Work

Science is making rapid steps towards the era of artificial intelligence and the internet of things to provide an intelligent future that can enhance the speed, accuracy, and effectiveness of research, human, and industrial efforts. Therefore, the new generation of electronics must keep pace with this development and if it is necessary those can be completely unlike traditional electronics in terms of shape, flexibility, functionality, and performance. According to Grand View Research, the global market size for the wearable electronics market was USD 32.63 billion in 2019, and it is expected to reach USD 104.39 billion in 2027 [14].

Currently, majority of the wearable electronics are made of circuits being fabricated on a flexible substrate and glued/sewn to fabrics [15]. Such structures lack the required flexibility for convenient wearable electronics. Hence, the focus is drifting toward fiber-based devices and systems that can be integrated into a fabric. Considering the required powers for such electronics,

fiber-shaped supercapacitors and fiber-shaped solar cells have attracted some scientific attentions. However, the low efficiency in the fiber-shape solar cells, the low energy density, and high self-discharge in supercapacitors are among challenges that require scientific studies [16].

Integration of electrochemical energy storage and harvesting in a single fiber-based hybrid device is a promising feature for wearable applications. However, some issues and challenges need to be overcome, such as low efficiency, low mechanical and electrochemical stability and performance, complexity and high cost of fabrication, and safety issues [17]. Therefore, there are great research opportunities to contribute to improving the performance and solving problems related to such devices.

1.3 Research Objectives

This dissertation aims to design and fabricate fiber-shaped hybrid energy storage and harvesting device with a photoactive gel electrolyte, low cost, simple structure, high mechanical, photoelectric, and energy storage performance for wearable applications. Three main objectives were determined to achieve the aim of this dissertation. The first objective was to study the effect of aniline ($C_6H_5NH_2$) concentration in polyaniline (PANI)-based gel electrolyte on the impedance and energy harvesting and storage performance of a two-terminal hybrid device. The device was made using a titanium dioxide (TiO_2) coated fluorine-doped tin oxide (FTO) glass electrode, a carbon nanotube (CNT) electrode, and the photoactive gel electrolyte.

The second objective was to investigate the effect of device structure on the capacitance and impedance of fiber-shaped supercapacitors. More focus was placed on studying the effect of twist on the electrochemical properties of three thread-based symmetric supercapacitors. The devices were fabricated using three conductive threads (silver-coated nylon 66, stainless steel

blended with polyester, and stainless steel thread) as electrodes and polyvinyl alcohol (PVA)-based gel electrolyte.

After studying the photoactive gel electrolyte, (in the first objective), and fiber-shaped device structure (in the second objective), the third objective was to transfer the approach used to fabricate the two-terminal flat hybrid devices for making fiber-shaped flexible hybrid energy harvesting and storage devices. The devices were made using two conductive threads and the photoactive composite gel electrolyte with a twisted configuration and simple fabrication method.

1.4 Scope of the Dissertation

This dissertation work focuses on the fabrication and characterization of fiber-shaped hybrid energy harvesting and storage devices based on a photoredox active gel electrolyte for wearable electronics applications. A number of studies have been conducted regarding the electrochemical properties and structure of the devices. Chapter 2 provides a review and discussion on different types of hybrid cells and their applications in electronics and wearable electronics. Chapter 3 presents the experimental results of different concentrations of aniline in the composite gel electrolyte and their effects on the performance of the hybrid cells. In order to optimize the energy storage of the two-terminal hybrid device, different materials for the counter electrode are investigated in Chapter 4. The structures of fiber-shaped supercapacitors and their effect on the electrochemical properties are studied and discussed in Chapter 5. A flexible fiber-shaped hybrid device based on a photoactive gel electrolyte is reported in Chapter 6. Chapter 7 presents the conclusion of the dissertation and recommendations for future work.

Chapter 2: A Critical Review on the Voltage Requirement in Hybrid Cells with Solar Energy Harvesting and Energy Storage Capability¹

2.1 Abstract

Energy storage is essential in many electrical and electronic applications powered through solar cells. This has motivated many research groups around the world to design single hybrid cells with the capability of both energy harvesting and charge storage. Despite the general perception of being able to make more compact and lower-cost solar panels with hybrid cells, as compared to conventional energy systems with separated panels and batteries, there are drawbacks in the series connection of hybrid cells in a panel form. These drawbacks are discussed in this review. The focus of the current manuscript is on the application of single hybrid cells in low-voltage and low-power electronics and wearable electronics. The voltage requirements in those applications are discussed and two-terminal and three-terminal hybrid cells are reviewed. Promising technologies are highlighted in the conclusions.

2.2 Introduction

The constant growing concerns on global warming have been a great motivation for the development of green energy technologies in recent years. Particularly, methods and devices for solar energy harvesting have been improved significantly [18, 19]. However, due to the intermittent nature of solar power, a mechanism has to be employed to store energy and supply it

¹ This chapter was published in Batteries & Supercaps journal (Takshi, A., Aljafari, B., Kareri, T., & Stefanakos, E. (2021). A critical review on the voltage requirement in hybrid cells with solar energy harvesting and energy storage capability. Batteries & Supercaps, 4(2), 252-267). Permissions are included in Appendix A.

during times that the consumption is higher than electricity production. That includes not only night times, but also early morning and before sunset hours when the harvested solar power is significantly low. In most places, solar power is reliable on average for less than 8 hours a day [20]. Further, weather conditions can have a significant impact on the availability of solar energy during a day. In this regard, designing a system with adequate output power and storage capacity is critical to ensure electric power availability.

Along with the fast-growing technologies of photovoltaic (PV) cells and electrochemical storage devices (i.e. batteries and supercapacitors), many research groups have been working on hybrid devices and systems for solar energy harvesting and storage. A broad range of novel approaches, some as simple as integrating two devices in one package and some with devised structures using emerging materials, have been demonstrated to address the interest in developing hybrid cells. Also, in recent years, a few good review papers and book chapters have been published explaining the mechanisms used in various designs [21-32]. Almost all the review articles in this field include tables with reported energy conversion efficiency, capacitance density, cell voltage, and other parameters. While the information may help a reader learn about different approaches, the conditions under which each device has been tested are different. Hence, their performances cannot be easily compared, making the development of a standard testing procedure for hybrid devices very desirable. Taking into consideration the contributions of scientists and researchers to the field of hybrid devices, this paper is written as a critical review to address the need of using hybrid devices and discussing challenges in different approaches to meet the requirements for practical applications. The focus of this review is to emphasize that hybrid devices address a niche market that must be considered in designing and developing new devices, because the use of hybrid devices in every solar energy systems is not

commercially justified. In the next section we will review the following: (i) the conventional method of using solar panels with external batteries; (ii) the technical challenges in using hybrid devices for making a hybrid solar panel; (iii) the specific market for hybrid devices for powering low-power and low-voltage electronics; and (iv) The various topologies of using a solar cell and a storage unit. The rest of the paper is dedicated to reviewing the output voltage of various types of hybrid devices, emphasizing the promising technologies for powering low-voltage electronics.

2.3 Two Basic Types of Hybrid Devices

In this review, hybrid cells are classified into two categories: three-terminal and two-terminal devices. As shown in Figure 1 (a), many of the hybrid devices contain a single solar cell and an energy storage cell in a single package. The storage part is usually a battery or a supercapacitor (SC). In this configuration, the two devices are sharing an electrode and a switching mechanism (S1 in Figure 1 (a)) to control charging and discharging cycles. On the other hand, two-terminal devices (Figure 1 (b)) rely on photoelectrochemical reactions for concurrent energy conversion and storage. It should be noted that the designs with an integrated miniaturized solar panel (i.e., several PV cells connected in series) and an energy storage cell are called solar energy systems or power packs and not considered as hybrid cells.

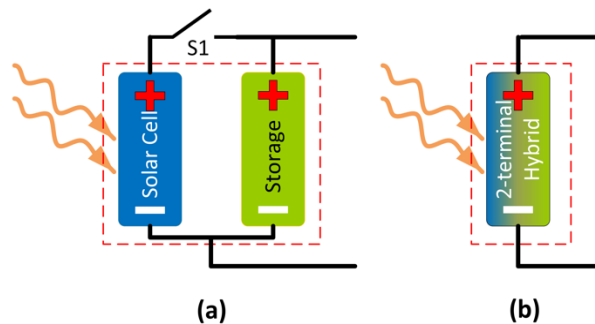


Figure 1: Schematic of (a) a three-terminal and (b) a two-terminal hybrid cell. (a) Switch S1 is needed for controlling the charging and discharging cycles in the storage.

2.4 Conventional Approach of Solar Panels with External Batteries

Semiconductor or semiconductor-like materials (e.g. dyes in dye-sensitized solar cells-DSSCs) are required for making PV cells. The energy gap in those materials allows photons to be absorbed and generates an electron-hole pair for each absorbed photon. Considering the solar radiation spectrum, theoretical calculations, known as “Shockley-Queisser Limit”, give the highest conversion efficiency in material with the energy gap of 1.1 eV [33]. Regardless of the type of PV cell, the material property (energy gap) defines the energy difference between the photogenerated electrons and holes and consequently the highest voltage that can be achieved from a single PV cell (i.e., equal to the open-circuit voltage (V_{oc})) will be less than the voltage associated to the material bandgap. In fact, due to the voltage drop inside a PV cell, V_{oc} in all devices is less than the energy gap of the photovoltaic material. For example, typical V_{oc} in a crystalline silicon-based solar cell is ~ 0.7 V while the silicon bandgap is 1.12 eV [34]. Although the highest reported V_{oc} of a perovskite solar cell (PSC) is 1.22 V [35], the majority of solar cells have $V_{oc} < 1.0$ V. As shown in the current-voltage (I-V) characteristics of a typical solar cell (Figure (2)), the value of V_{oc} depends on the light intensity.

On the other hand, almost in all applications, voltages much higher than 1.0 V are required. For instance, solar-powered traffic lights use voltages of 12-48 V DC. To generate the required voltage, in each application, solar panels are made with several cells connected in series. To store the energy produced by a panel with a voltage much higher than 1.0 V, the most energy efficient and economical option is to use a battery and a solar charge controller module (Figure 3 (a)). Most of the commercially available charge controller modules have an internal circuit for tracking the maximum power from the solar panel and monitoring the state of charge in rechargeable batteries [36, 37].

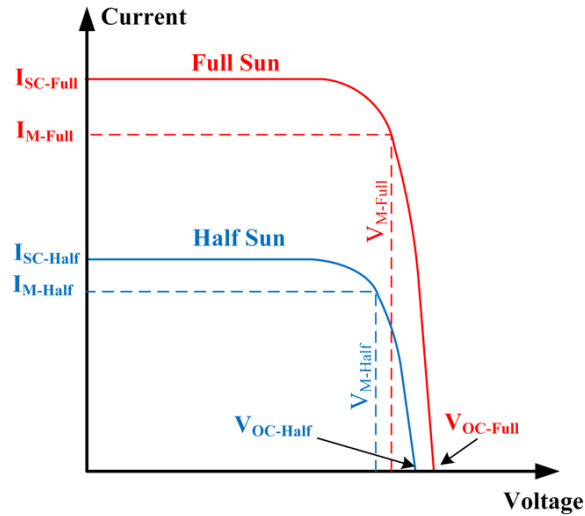


Figure 2: Typical I-V characteristics of a solar cell. The responses for operation under full and half sunlight intensities are shown.

As shown in Figure 2, the maximum output power of a solar cell is obtained when the solar cell operates at the point where VI is a maximum (V_M and I_M), for a specific solar intensity (I_M and V_M are not constant and change with sunlight intensity (Figure 2)). Therefore, a direct connection of a solar cell (or a panel) to a load or an energy storage device does not produce maximum power and can result in large power waste. For this reason, smart charge controller units are designed to constantly monitor the I-V response of the solar cell (or panel) and adjust their input impedance so that the cell operates at its maximum power output at any sunlight intensity. Additionally, the output of a smart charge control unit matches the output voltage and current for the efficient charging of an external battery. Even with all these excellent features, smart chargers are priced substantially lower than the cost of solar panels (in \$/watt).

While the conventional solar energy system (shown in Figure 3 (a)) is efficient, the question is if a panel made of hybrid cells can be superior to a conventional system. A general perception is that, potentially, using single hybrid cells, more compact and less-expensive panels

can be made than the conventional solar energy systems. Some publications have also justified the usage of hybrid cells instead of regular PVs in solar panels to achieve lower fluctuations in their output power when some solar panels are temporarily blocked by clouds [38, 39].

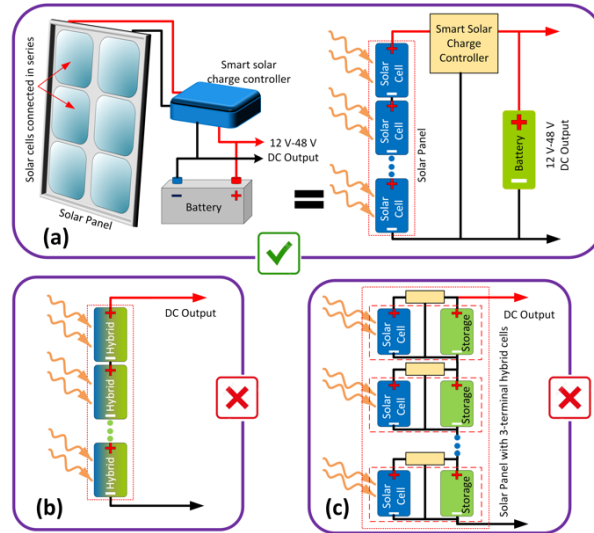


Figure 3: (a) Conventional solar energy system with a smart charge controller; (b) series connection of two-terminal hybrid cells; and (c) three-terminal cells each equipped with a charge control unit. (✓= Practical scheme, X= Not efficient).

Unfortunately, as explained here, the application of hybrid cells for making solar panels is not justified. It is important to consider that the overall energy conversion efficiency in any approach is critical for designing a compact and low-cost system. Optimizing efficiency in a solar cell requires choosing materials and design suitable for energy harvesting. Similarly, for optimum energy storage, the materials and the design of the energy storage unit are critical. In a hybrid cell, the choice of materials and design of the cell are often compromised (both in two-terminal and three-terminal devices). Hence, it is very likely that the energy conversion and charge storage efficiencies in a hybrid device would almost always be lower than the efficiencies obtained from separated solar and storage cells of similar technologies. Additionally,

complications in using smart charge controllers for hybrid cells becomes a drawback. As shown in Figure 3 (b), a solar panel can simply be made by the series connection of two-terminal hybrid cells. However, not being able to use a smart charge controller, the overall energy conversion efficiency under various sunlight intensities is expected to be lower than the conventional approach with an external smart unit. Even for three-terminal devices where it is feasible to equip each cell with a maximum power tracking module, the solution is not economical when each panel is made of several cells and requires a separate charger module for each cell (Figure 3 (c)). Further, in the conventional approach, a solar energy system can be easily customized for a required power by choosing large enough panels and battery packs with the capacity matching the generation power and the application need. Customizing the storage capacitance in a hybrid device for a specific power generation by the PV part requires manufacturing devices with different geometries or designs, increasing the cost of customized hybrid devices. Hence, despite the common perception that hybrid PV cells can be used to make PV panels with the integrated storage feature for at least having low-voltage fluctuation when clouds temporarily block the sunlight, the system shown in Figure 3.a is more efficient and cost-effective than the alternatives shown in Figures 3 (b) and 3 (c).

Another motivation for developing hybrid cells is to take advantage of the fact they are more compact than a system with separate parts. Although in the majority of applications, such as solar farms, roof-top panels, and even charging stations for electric vehicles, the batteries are relatively much smaller than the panels and do not occupy any substantial space, there are some applications like out-door wireless sensors and wearable electronics for which the use of compact systems can make a significant difference in the final product and cost. The potential for niche markets can provide scientists and engineers the incentive to focus on hybrid devices for

specific applications. A great example is the wireless sensors for structural health monitoring systems (SHMS). For constant monitoring health status of a structure such as a bridge or a building, it is required to install several hundred sensors on the body of the structure to measure vibration, temperature, or corrosion rate of the structure and send data to a local hub [40]. Compact sensors can be designed with onboard solar cells and thin and flat energy storage devices. Since the size and mass of solar cells and energy storage cells are usually significantly larger compared to the actual electronic circuit, hybrid cells are potential solutions for making more compact and low-cost sensors. Of course, SHMS sensors are not the only examples and there are many other outdoor small electronics for IoTs (internet of things) and wearable electronics that can benefit from a hybrid device.

2.5 Circuit Topologies Using a Hybrid Cell for Powering Low-Voltage Electronics

Today, the majority of electronic circuits need 3.3 V-5.0 V as the supply voltage. Since no single solar cell can generate that level of voltage, several PV cells have to be connected in series to make miniaturized panels. In this scheme, as discussed, it is preferred to design a solar energy system (also known as power pack) with several discrete PV cells and an external battery. There are small integrated circuits designed for tracking the maximum power in small panels (e.g., CN3083 from Consonance Electronic) that serve as the smart charge control unit for miniaturized power packs. A small panel and a battery/SC (with or without the smart charger) can be integrated into a package for making a compact energy system [41], but the concept of hybrid devices is based on the integration of a single PV cell with an energy storage unit. Hence, this review focuses on the application of single hybrid cells, not the compact energy systems.

Recent developments in designing low-power electronics focus on low-voltage integrated circuits working with voltages less than 1.0 V that can be powered by a single solar cell [42, 43].

An Example of such integrated circuits is Si1000 from Silicon Labs (Figure 4). Si1000 is an ultra-low-power microcontroller unit with integrated RF transceiver that can operate with a voltage as low as 0.9 V. Potentially, the combination of low-power low-voltage electronics and hybrid devices for solar energy harvesting and energy storage can reduce the size of the final product and provide a solution for making more compact wireless sensors. However, the topology of using the hybrid cells, particularly three-terminal hybrid devices, and their connections to the electronic circuit is critical for practical applications.

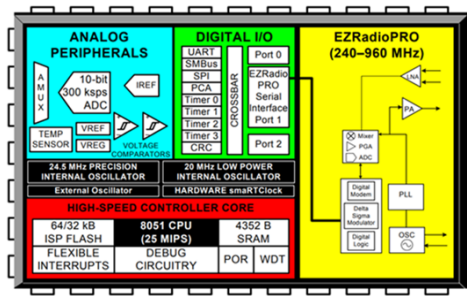


Figure 4: Block-diagram of Si1000 from Silicon Labs.

Potentially, a two-terminal device can be connected directly to low voltage electronics if the cell voltage is sufficient for running the circuit (Figure 5 (a)). As shown in Figure 5 (b), some reports suggest a direct parallel connection of a solar cell and an energy storage device for powering a load (e.g., wireless circuit) [44]. In this form, an inherently three-terminal hybrid cell is wired to perform as a two-terminal device by replacing the S1 switch in Figure 1 (a) with a short circuit path. However, this configuration is not practical, due to the nature of solar cells acting as a diode in the dark. There are various forms of solar cells, including pn-junctions, heterojunctions, thin-films, perovskites, organic (OPVs), and DSSCs. In all forms, a rectifying mechanism is employed in the structure (junction) of the PV cell for separating photogenerated electrons and holes. Therefore, as shown in Figure 5 (b), a solar cell can be modeled as a rectifier

(i.e., diode) being in parallel with a current source. The value of the current source is a function of light intensity. In the dark, when $I_{ph}=0$, the solar cell acts like a diode which quickly discharges the energy in the storage device. A simple solution is to use an external diode (instead of the S1 switch in Figure (1)) to block the discharge path. However, the voltage drop across the diode reduces the available voltage for the load. To minimize the voltage-drop, Schottky diodes with V_{diode} of 0.1-0.2 V are often used. As explained in this section, this solution implies a restriction in the choice of energy storage.

A type of charge storage used in some energy systems is a device called “redox flow-battery” [45, 46]. The approach is briefly explained in section 2.6.2.2. However, due to the requirements for pumping electrolyte from the PV cell to the flow-battery, the technology is not suitable for small electronic circuits. The two most common energy storage devices are batteries and SCs.

The mechanisms of charge storage in batteries and supercapacitors are explained in other sources [47-49]. The main difference, relative to this discussion, is the voltage range in batteries and SCs. While the energy density in rechargeable batteries (e.g. Li-ion batteries) is high enough for powering compact wireless sensors, the general problem is in their voltage range. At a fully discharged state, a Li-ion battery has a voltage of $V_{battery}=2.8$ V. Other rechargeable batteries including NiCd, NiMH, and Lead-acid all have voltages higher than 1.0 V even at their lowest value [50]. Hence, it is impossible to charge a battery directly with a single solar cell. Simply the diode in Figure 5 (c) will never be under forward bias if V_{oc} is not larger than the battery voltage. Realizing this problem, Qi et al have designed “photoassisted chargeable batteries” that still require an external power source in addition to the light but do not serve the purpose of hybrid cells for powering electronics [51, 52].

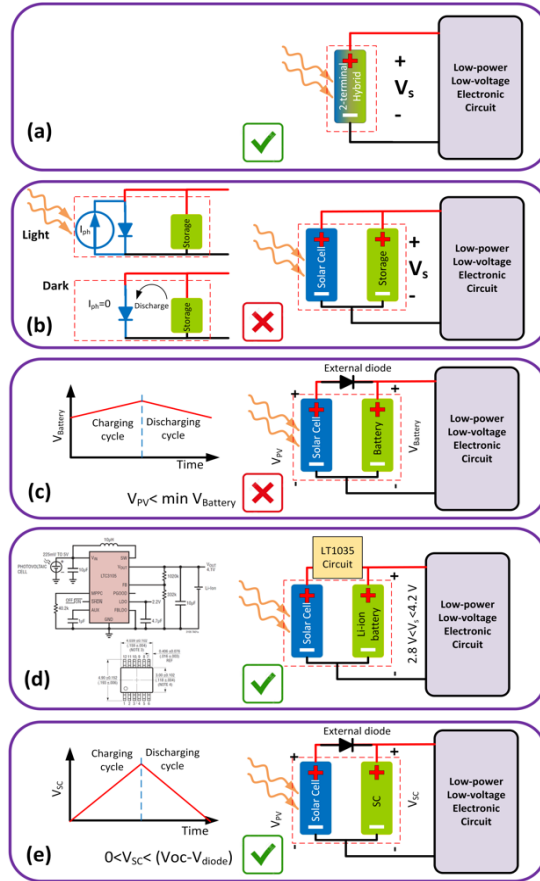


Figure 5: Various topologies where a hybrid single cell can be used for powering a circuit: (a) direct connection of a two-terminal cell, (b) impractical usage of a three-terminal as a two-terminal device, (c) impractical combination of a battery and a single PV, (d) using a DC-DC converter to charge a battery via a PV cell, and (e) a simple solution of using a diode in a three-terminal device with a SC storage. (✓ = Practical and X= impractical topologies).

Considering the voltage incompatibility between a battery and a PV cell, batteries are only useful in solar energy systems when the PV cells are connected in series (i.e., PV panel) [53, 54]. An alternative method to obtain higher V_{oc} is to use tandem PV cells [55, 56]. In tandem devices, two or more thin film solar cells are made in a stack structure using different semiconductors for each layer to absorb different wavelengths. Naturally being in a series connection, the overall voltage of a tandem cell will be the summation of the voltage of each cell. Also, tandem cells have shown higher efficiencies than single PV cells [57]. Agbo et al.

demonstrated a three-terminal hybrid cell with a lithium-ion accumulator and a triple-junction solar cell made from amorphous and microcrystalline silicon [58]. Although the tandem cell showed V_{oc} of 2.09 V, the voltage was still too low for efficiently charging the battery.

The most practical method of using a battery as the storage is to use commercially available integrated circuits that are designed as a DC-DC converter to boost the voltage of a solar cell to charge the batteries [59, 60]. Those integrated circuits consume a portion of the harvested power and are often designed for specific solar power and storage capacitance. An example is the LTC3105 from Linear Technology (now a part of Analog Devices Inc.) that can charge a Li-ion battery with a single solar cell with a voltage as low as 225 mV. A schematic of a circuit of the chip with the external elements is shown in Figure 5 (d). However, the chip consumes 24 μ A constantly and has a limitation of 6 mA current delivery to a wireless sensor. The constant current consumption requires using a larger solar cell to produce higher I_{ph} and also consumes the charge in the battery in the dark. Nevertheless, with the new technology of making low-power electronics operated at less than 1 V, another step-down regulator is needed to reduce the battery voltage to less than 1 V. This combination of stepping up the voltage to charge the battery and stepping down to power the low-voltage wireless sensor is more complicated and less energy efficient.

Due to the voltage incompatibility between a single solar cell and a battery, the majority of hybrid devices have used SCs as the energy storage element. As shown in Figure 5 (e), (a) fully discharged capacitor has a voltage near 0 V that increases gradually when it is charged by a solar cell. Yet, a switching mechanism, such as a Schottky diode, is needed in the three-terminal hybrid cell to stop the capacitor of being drained when the PV cell voltage drops below the capacitor voltage.

Although the combination of a supercapacitor and a single PV cell is the most practical arrangement for a hybrid device, it should be noted that in this combination, the supercapacitor is usually over-designed. The stored energy in a supercapacitor is equal to $0.5CV^2$ (where C is the device capacitance and V is the capacitor voltage). The nominal voltage of a supercapacitor with an organic-based electrolyte can reach almost 4.0 V. Hence, the stored energy in a supercapacitor charged with a single PV is always a fraction of the maximum energy that can be stored in the device. This makes the combination less efficient than the energy system shown in Figure 3 (a) where the storage element can be charged at higher voltages when a solar panel is used.

2.6 Review of Hybrid Cells

The majority of the reported hybrid devices are three-terminal cells that are technically a PV cell and a supercapacitor in one package with a terminal being shared. As explained, for practical applications, a switch such as a Schottky diode has to be added to avoid power loss through the solar cell. Although this combination is subject to energy loss and a voltage drop across the diode, designing and fabricating devices with three terminals allows researchers to characterize the solar cell and the storage unit separately and demonstrate the functionality of the hybrid device by controlling the switch. More importantly, due to the separated structures of the solar cell and the energy storage cell, generally, there is no material limitations for making a three-terminal hybrid device. Therefore, as discussed in section 2.6.1, various solar cell technologies have been used in developing hybrid cells. In contrast, two-terminal devices have innovative methods of combining both the energy harvesting and storage in a cell. Potentially, lack of the external switch can result in higher overall efficiency in two-terminal hybrid cells. However, optimizing the materials composition and structure design to have high energy conversion as well as efficient charge storage is a serious challenge, particularly for researchers

who cannot separate the energy harvesting effect from the storage in two-terminal devices. The material limitations in two-terminal cells are further discussed in section 2.6.2. Nevertheless, as of today, all two-terminal devices are inferior to three-terminal cells with an external switch/diode. In this section, both three and two terminal hybrid cells are critically reviewed for their applications in low-voltage electronics.

2.6.1 Three-Terminal Hybrid Cells

2.6.1.1 Si PV-SC Hybrid Cells

To achieve high energy conversion efficiency, some groups started with the fabrication of a silicon-based solar cell and then building a SC at the back side of the PV cell. The structure and mechanism of energy harvesting in silicon-based solar cells have been discussed in detail in other publications [61-63]. As examples, three different silicon-based solar cells used in hybrid devices are shown in Figure 6. Westover et al., etched the backside of a crystalline silicon-based solar cell to generate porous silicon acting as the shared electrode between the PV and the SC (Figure 6 (a)) [64]. Another piece of porous silicon was used as the second electrode of the capacitor with a gel electrolyte between them. An external wire was used as S1 switch to connect the front electrode on top of the solar cell to the SC electrode. Owing to the crystalline structure of the silicon, the energy conversion efficiency was 14.8% while a capacitance of 0.14 F/m² was obtained from the supercapacitor. Although the fabrication approach is compatible with the existing solar cell fabrication process, the storage capacitance was too low resulting in storage time less than a minute for a low power load of only 0.4 $\mu\text{A}/\text{cm}^2$. Figure 6 (b) shows a schematic of the device made by an Australian group integrating a graphene oxide-based SC of 0.01 F/m² on the back side of a crystalline silicon (c-Si) solar cell. The device demonstrated 15.69% conversion efficiency and a short storage time of ~ 10 s for a load of 0.33 $\mu\text{A}/\text{cm}^2$ [65].

Unlike the above two approaches, Liu et al. did not use a standard pn junction solar cell, but built a heterojunction solar cell made of n-type Si nanowires (NWs) and poly(3,4-ethylenedioxythiophene) polystyrene sulfonate (PEDOT:PSS) which is a conducting polymer (Figure 6 (c)). The capacitor was built on the back side with two layers of polypyrrole (Ppy) electrodes and a gel electrolyte. The solar cell alone had an efficiency higher than 13% but the combination of the solar cell and the SC resulted in 10.5% overall efficiency. Solar charging up to 0.55 V and a long charge storage stability of more than 11 hours under open circuit conditions was demonstrated [66].

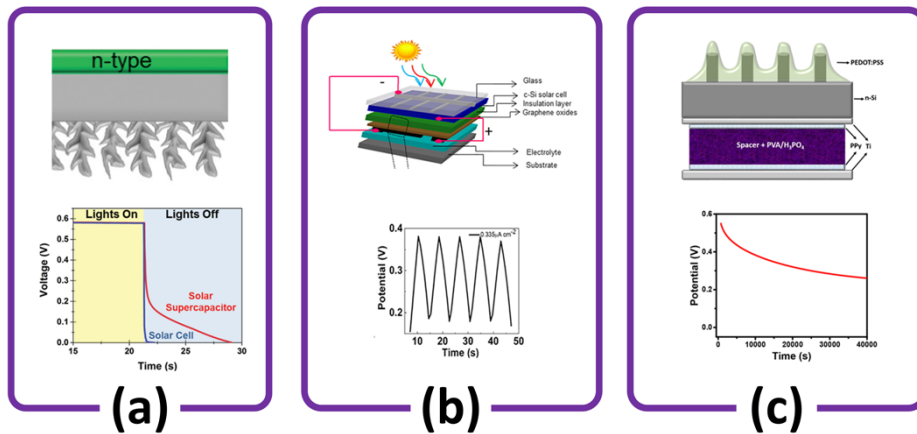


Figure 6: Three different Si PV-SC hybrid cells designed and reported by: (a) Westover et al., [64] (b) Thekkekara et al., [65] and (c) Liu et al. [66].

In all those designs, the experiments were carried out the hybrid device configuration by connecting the top electrode of the solar cell to the back electrode of the SC with a wire. As mentioned, in practice, a diode-like switch should be used between the solar cell and capacitor. With the low open-circuit voltage of less than 0.7 V in Si PVs, the voltage drop in the diode would be significant.

2.6.1.2 PSC-SC Hybrid Cells

With the recent progress in achieving high efficiency and improving stability, perovskite-based solar cells (PSCs) are already considered as one of the promising technologies for the widespread use of solar energy systems [67]. Efficiency as high as 25.2% has been verified by NREL for a PSC [68]. More importantly, PSCs are generally able to produce higher V_{oc} than silicon-based cells. V_{oc} higher than 1.0 V has been reported in several single PV cells [35, 69, 70]. Both the high efficiency and large V_{oc} are motivating for making hybrid devices with energy storage being built at the back of the cells. Liang et al. made a three-terminal device with a $CsPbBr_3$ based solar cell and a supercapacitor at its back. The PV cell had an excellent V_{oc} of 1.22 V [35]. The photocharging and the feasibility of delivering the stored energy in the capacitor under dark conditions with a discharge rate of 0.375 mA/cm^2 were demonstrated (Figure 7 (a)). Zhou et al. fabricated a PSC with a SC at its back side using all transparent electrodes that showed not only energy harvesting and storage, but also a photovoltachromic effect [71]. As a hybrid device, the photocharging voltage could reach 1.0 V. However, the storage part could keep the charge only for a few minutes (Figure 7 (b)) [72].

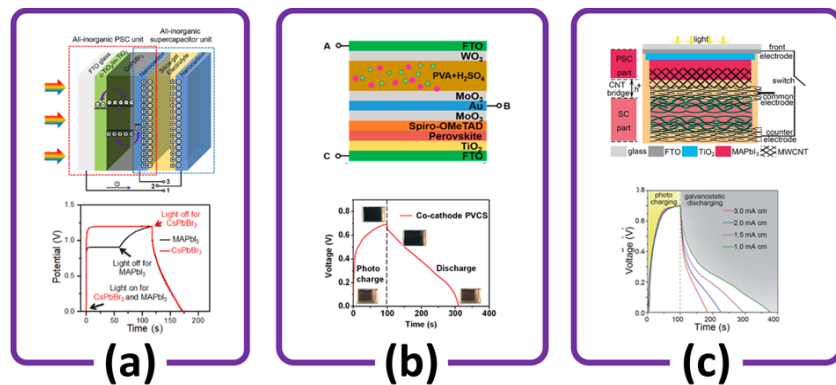


Figure 7: Three different PSC-SC hybrid cells designed and reported by: (a) Liang et al., [35] (b) Zhou et al., [71] and (c) Liu et al. [56].

There are other similar devices with a solid-state form of a perovskite cell and a SC at their back side [73]. Unlike most of the perovskite cells that use a compact layer of metal oxide as the electron transport layer, Xu et al. used a blend of perovskite with TiO₂ and ZrO₂ for making the solar cell. Their device showed a V_{oc} of 0.8 V and less than a minute of driving a 0.25 mA/cm² load from the charged supercapacitor [74]. Some of the hybrid devices were made on flexible substrates [53, 56]. Among them, Liu et al. demonstrated a wearable hybrid device with a solar cell on top of a supercapacitor embedded into a fabric structure (Figure 7 (c)). The solar cell could generate a V_{oc}=0.7 V and the stored energy was sufficient to run a 1 mA load for about 5 minutes [56].

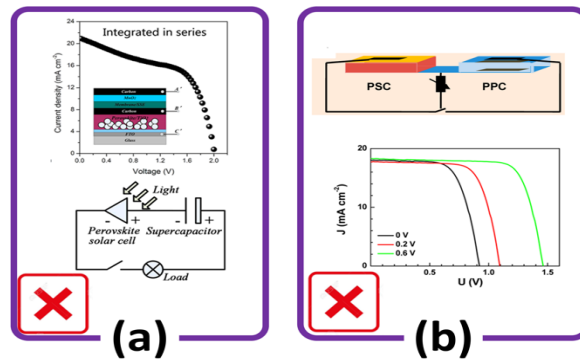


Figure 8: Examples of combination of a PV and a SC in series not acting as a hybrid cell reported by (a) Liu et al. [75] and (b) Xu et al. [76].

While one of the main advantages of using PSC is its high V_{oc} for charging SCs, some of the devices have been tested with a solar cell in series with the charged SC to obtain a high V_{oc} value (Figure 8) [75, 76]. Obviously, the voltage across two elements in a series connection is the summation of the two voltages, but the main point is that the series connection of a solar cell and a SC does not work as a hybrid device. Therefore, characterizing devices with this method generates false V_{oc} that, unfortunately, has been reported in several review papers [21, 23, 24, 26, 28]. Also, as shown in Figure 8 (a), the voltage of the SC can be added to the solar cell only

when the capacitor is charged by an external source (not the solar cell) with a polarity opposite of that of charging a solar cell.

2.6.1.3 OPV-SC Hybrid Cells

The mechanism of charge separation in OPVs is based on the molecular interface between materials with the tendency of electron acceptance and donation. There are many good references for teaching the structure and operational mechanism in OPVs [77-79]. Hybrid devices with organic photovoltaic (OPV) cells have been reported in several publications [80, 81]. Kim et al, fabricated two devices, one with a perovskite solar cell the other with an OPV [80]. The hybrid OPV device showed a V_{oc} of 0.79 V with an efficiency of 7.58% whereas the PSC had both higher V_{oc} and efficiency. As shown in Figure 9 (a), the OPV based hybrid device was able to run a load of 0.5 A/g for a few minutes after charging the SC for one minute with the OPV in front of the capacitor [80]. A similar design was implemented for making an OPV based hybrid device optimized for indoor light harvesting by a group at the University of California Berkeley [81]. Their devices showed an 11.5% efficiency and V_{oc} of 870 mV, with the ability to run a load for almost one minute after cessation of light (Figure 9 (b)). A group at Fudan University showed a novel design by fabricating an OPV and a SC with a Ti wire as the common electrode between the two devices [82]. Their design showed high enough mechanical flexibility for wearable applications with a V_{oc} of ~ 0.4 V and storage time higher than 5 min (Figure 9 (c)).

Since V_{oc} and efficiency in OPVs are both inferior to those in PSCs and Si PVs, OPV based hybrid devices can hardly compete with the other alternative technologies. To address the low voltage problem, Chien et al. designed a system with a series of OPVs on the same substrate used for the supercapacitor (Figure 10 (a)) [83]. As shown in Figure 10 (b), a group from Nanyang Technological University in Singapore suggested stacking two OPVs to obtain a V_{oc} of

~1.0 V [84]. With the recent progress in making low cost, flexible, and high energy conversion efficiency PSCs, connecting perovskite cells in series is a more efficient system for energy harvesting and storage (Figure 10 (c)) [53]. In this scheme, it is even possible to charge a Li-ion battery if the summation of the perovskite cells exceeds the voltage that one needs for charging a battery (Figure 10 (d)) [54].

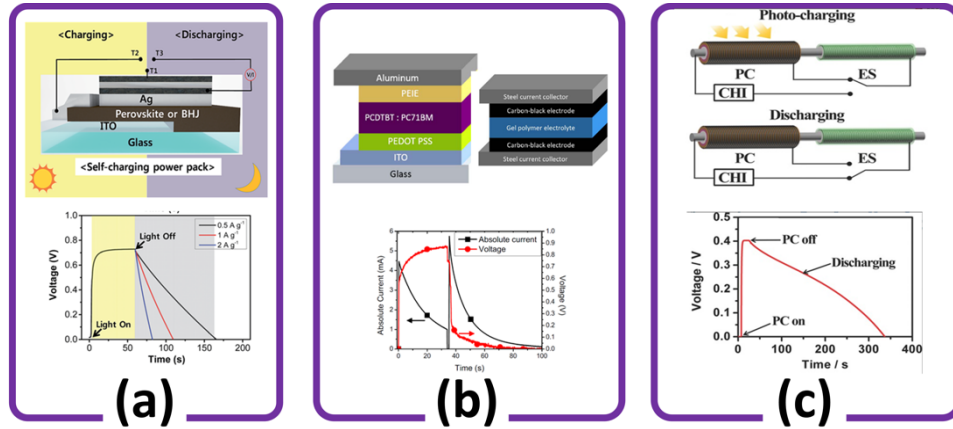


Figure 9: Three different OPV-SC hybrid cells reported by: (a) Kim et al., [80] (b) Lechêne et al., [81] and (c) Zhang et al. [82].

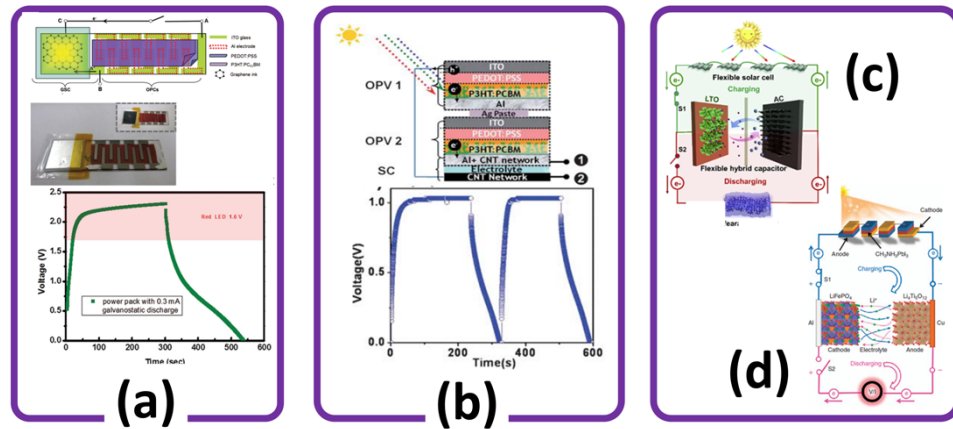


Figure 10: Four different examples of power packs with OPV or PSC cells in series and a supercapacitor reported by: (a) Chien et al., [83] (b) Wee et al., [84] (c) Li et al., [53] and (d) Xu et al. [54].

2.6.1.4 DSSC-SC Hybrid Cells

Although both silicon and perovskite-based solar cells have higher energy conversion efficiency than DSSCs, the majority of hybrid devices have used a DSSC like structure for energy harvesting. That is mainly because several of the fabrication steps in DSSCs and SCs are similar, as both are electrochemical cells. The structure of DSSC devices and the mechanism of charge circulation in them are explained in various sources [85-87]. The majority of the designs have proposed a hybrid structure with two separate electrolytes for the DSSC and SC parts, technically integrating a DSSC and an SC in one package. However, there are innovative designs with three electrodes being in one compartment and one electrolyte [88, 89]. It should be noted that cells with one electrolyte are easier to fabricate but any degradation of the electrolyte can decrease the device efficiency to levels lower than a cell with two separate electrolytes each optimized for their corresponding purpose.

In 2004, Nagai et al. showed a hybrid device with two compartments (Figure 11 (a)) [90]. The device was a standard DSSC with a mesoporous layer of TiO_2 and Ru-based dye as the photoactive electrode and sharing the Pt electrode with a supercapacitor made from polypyrrole, which resulted in a $V_{oc} = 0.6 \text{ V}$ [90]. A similar design was presented by Saito et al. using WO_3 for storing the charge in the supercapacitor compartment [91]. Their device showed $V_{oc} = \sim 0.6 \text{ V}$ under illumination, but the voltage dropped to 0.4 V almost instantly after the secession of light [91]. A higher voltage of $V_{oc} = 0.8 \text{ V}$ was reported in the work by Murakami et al. in 2005 [92]. A research group from Taiwan led by Dr. Ho fabricated the DSSC part on a flexible plastic substrate achieving a $V_{oc} = 0.77 \text{ V}$ [93]. In a different publication, Dr. Ho's group reported a three-terminal hybrid cell with PProDOt-Et₂ polymer for the supercapacitor part. Despite the improvement in the energy storage capacitance, V_{oc} was still limited to 0.75 V due to the DSSC

design [94]. Using TiO_2 nanotubes for making both the solar cell and supercapacitor, the voltage of the hybrid device made by Mini et al. reached only 0.3 V under illumination [95].

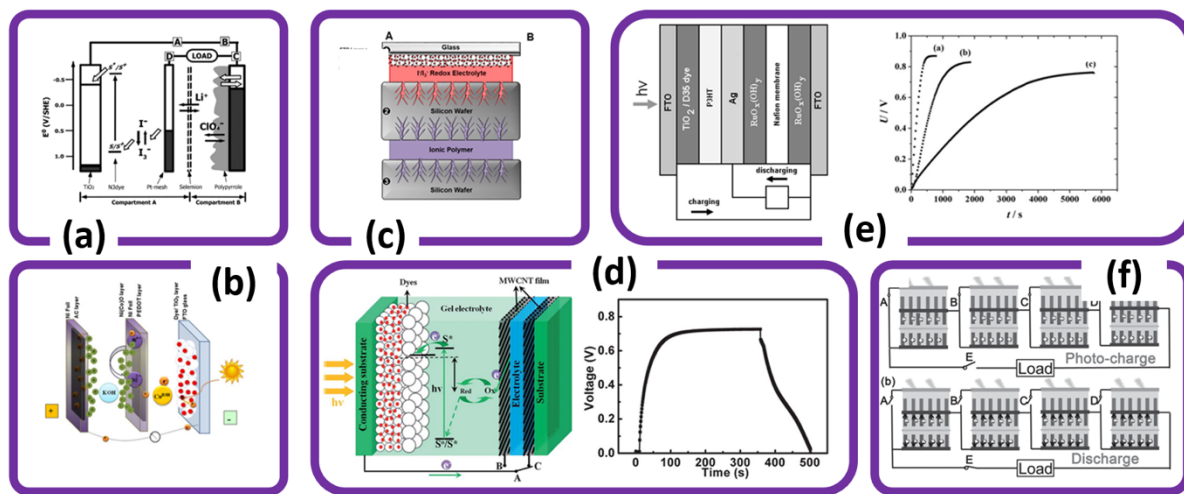


Figure 11: Examples of DSSC-SC hybrid device reported by: (a) Nagai et al., [90] (b) Bagheri et al., [96] (c) Cohn et al., [97] (d) Yang et al., [98] (e) Skunik-Nuckowska et al., [99] and (f) Xu et al. [100].

Bagheri et al. fabricated a hybrid device with an asymmetric supercapacitor (Figure 11 (b)). The redox electrolyte for the DSSC part used $\text{Co}^{2+}/\text{Co}^{3+}$ as the mediator while the supercapacitor electrolyte was an aqueous electrolyte containing KOH. The V_{oc} of the DSSC in their device reached 0.72 V [96]. Dr. Pint's group integrated a standard DSSC with a supercapacitor made of silicon nanostructure electrodes (Figure 11 (c)). Again the maximum charging voltage was limited by the DSSC to $V_{oc}=0.68$ V [97]. In an attempt to make liquid-free hybrid devices, some of the devices were made with either gel-based or polymer electrolytes [82, 98, 101]. However, generally, DSSCs with solid electrolytes have efficiencies lower than DSSCs with liquid electrolytes [102, 103]. Peng's group has developed a flexible three-terminal hybrid cell with two different gel electrolytes for the DSSC and supercapacitor (Figure 11 (d)). A solar conversion efficiency of 5.12% was achieved by the DSSC with a V_{oc} of 0.75 V [98]. As shown

in Figure 11 (e), another example is the device made with a layer of poly 3-hexylthiophene (P3HT) between the photoactive and the counter electrode in the DSSC. The device showed a maximum of 3% energy conversion efficiency with a V_{oc} of 0.898 V [99]. Scalia et. al fabricated a flexible hybrid device with a polymer electrolyte membrane. The V_{oc} in their device reached the maximum value of 0.67 V [104].

Recognizing the voltage limit in hybrid devices, some publications have reported connecting the cells in series [100, 105]. As shown in Figure 11 (f), Xu et al. used four three-terminal hybrid cells in series to generate sufficient voltage for powering an LED [100]. The technical challenge in connecting hybrid cells in series has already been explained in section 3 of this review.

2.6.1.5 Fabric-Base DSSC-SC Hybrid Cells

With the fast-growing market for wearable electronics [50, 106, 107], some designs have focused on developing fabric-based devices for energy harvesting and storage [108, 109]. A very essential feature for wearable electronics is the high flexibility of the devices and the ability to integrate them into fabrics. Many devised ideas have been practiced in recent years by fabricating solar cells and energy storage cells in the form of fibers [110-112]. As shown in Figure 12, some have used a coaxial structure [112] and some have made devices with parallel (or twisted) fibers [110]. Unlike flat hybrid cells, due to the flexibility requirement and complication in the fabrication, fiber-based hybrid cells are not made by stacking the two parts, instead, they have been made either by making the two devices on the same thread (Figure 12 (b) & (f)) [112, 113] or different threads being woven as a piece of fabric [114]. In such designs, the surface of the fabric is not efficiently used for optimum solar energy harvesting. However, it is much easier to fabricate an energy system made of several PVs in series for achieving high

enough voltage. Figures 12 (c-e) show schematics and the boosted voltage in some designs with series PVs [110, 114, 115]. The concept of fiber-based hybrid devices has also been applied to make a device with a fiber shape Li-ion battery as the storage element (Figure 12 (f)).

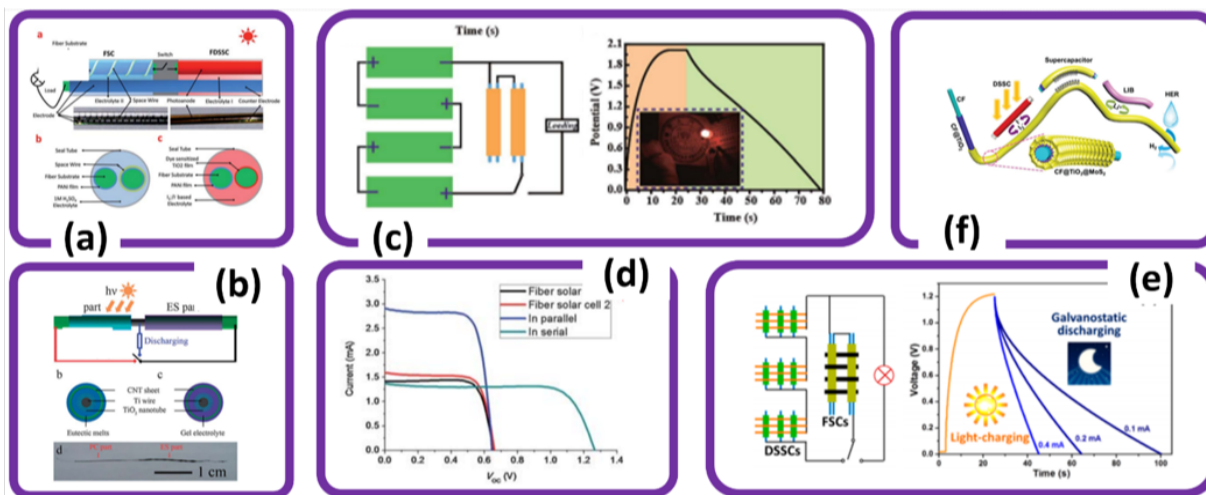


Figure 12: Example of fabric based hybrid cells reported by: (a) Fu et al., [110] (b) Chen et al., [112] (c) Zhang et al., [115] (d) Fu et al., [110] (e) Chai et al., [114] and (f) Liang et al. [113].

2.6.2 Two-Terminal Hybrid Cells

As discussed, the main advantage of three-electrode hybrid cells is the feasibility of optimizing the solar cell and SC. However, the voltage drop across the external Schottky diode is a drawback. To avoid using an external switch/diode, some novel ideas for making two-terminal devices have been reported that are reviewed in this section. It must be mentioned that devices made of two different compartments, with their terminals connected (internally or externally) are not considered in this part and have already been discussed in the previous section (see Figure 5 (b)). A general challenge in the two-terminal devices is the selection of the materials for the electrodes and the electrolyte. To achieve high solar energy conversion, the photoactive material has to have a wide absorption spectrum with the ability of generating separated electron-hole

pairs. At the same time, to achieve high capacitance, porous electrodes are needed. As discussed in details in this section, sometimes the material choice is needed to be compromised.

2.6.2.1 Photogalvanic Cells

The concept of designing a two-terminal device with the ability to harvest solar energy and store electric charge was first introduced by Rideal and Williams, when they studied the photogalvanic (PG) effect in 1925 [116]. Based on the PG effect, electrochemical devices were designed and studied by many scientists through the years [117-130]. As shown in Figure 13 (a), a conventional PG cell has an H-shape structure with two half electrochemical cells at the columns (i.e., chambers) and a bridge between them for the convenient circulation of ions between the half cells [117]. Unlike DSSCs, dye molecules (i.e., sensitizers) are freely floating in the electrolyte and are not attached to any electrode [131]. Therefore, the dye molecule does not need to have the carboxylic group for the surface attachment. Various forms of photosensitizers, including thionine, azur-B, and rhodamine have been reported for the PG cells [117]. The mechanism of operation is based on changing the concentration of oxidized/reduced mediators and sensitizers via the photoelectrochemical reactions in the electrolyte. Hence, the open-circuit voltage of the cell follows the Nernst equation [132]. Voltages as high as 1.235 V has been reported for PG cells [123]. However, due to the high rate of recombination in the electrolyte, the overall energy conversion efficiency in PG cells is far lower than those in other PV technologies [127]. More importantly, the storage mechanism in PG cells relies on the accumulation of charges in the electrolyte which makes their specific capacitance significantly lower than supercapacitors or batteries. Again, the recombination of the charges in the electrolyte is the major reason for their short charge storage stability in the dark [127].

Besides the low efficiency, the conventional H-shape cell is not suitable for powering a small electronic circuit. To address the form factor, in a recent work by Xiao et al., a carbon nitride nanotube membrane was used to separate the dark and light chambers (Figure 13 (b)) [129]. In their device, the maximum voltage difference across the cell was less than 0.5 V [129].

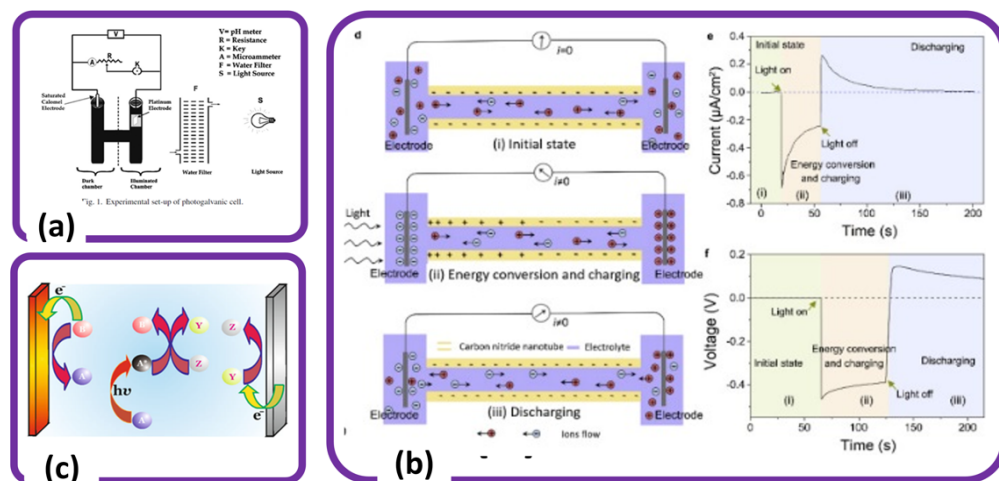


Figure 13: Examples of PG cells reported by: (a) Lal et al., [117] (b) Xiao et al., [129] and (c) Halls et al. [130].

Since the operation of PGs is based on the redox reaction rates at the anode, cathode and in the bulk of the electrolyte, another form of a PG device with a single chamber has been studied with semiconducting electrodes. In this form, the photoredox reaction occurs in the bulk electrolyte which pumps charges into the cell. However, the energy structure of the electrodes (i.e. conduction and valence bands) rectifies the charge transfer from the electrolyte to the electrodes. The mechanism of operation is shown in Figure 13 (c) [130]. Devices with different dye and semiconductor electrodes have been reported [123, 130]. In a novel approach, Aljafari et al. have developed a gel electrolyte with a conducting polymer as the sensitizer [133, 134]. In a simple form, there are only a dye material and a reductant in the electrolyte, but in some designs,

there is an oxidant material, as well. In this form, the reductant and oxidant materials act as mediators to transfer charges to the electrodes. The design with the two mediators was used for synthetic dyes and photosynthetic proteins. Takshi et al., have shown that the reaction centers from *Rhodobacter sphaeroides* alga can be used as the dye material with ferrocene and methyl viologen as the two mediators for transferring the photogenerated positive and negative charges to the electrodes. In this case, the storage time is limited by the reaction rates between the two mediators in the bulk electrolyte [135].

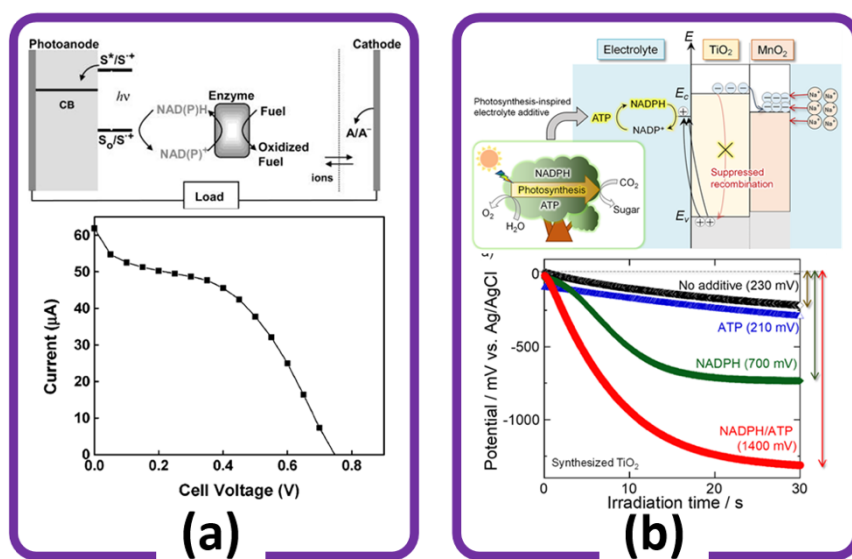


Figure 14: Examples of hybrid cells made from biomaterials reported by: (a) De La Garza et al. [136] and (b) Usui et al. [137].

The concept of employing biological materials in PG cells has been also applied for developing photoelectrochemical biofuel cells [121, 136, 138]. In 2003, de la Garza et al. reported the application of an enzyme in the electrolyte to generate V_{oc} of 0.75 V (Figure 14 (a)) [136]. In a recent work from Tottori University (Japan), nicotinamide adenine dinucleotide phosphate (NADPH) and adenosine triphosphate (ATP) were added to the electrolyte to achieve

a photovoltaic voltage of 1.4 V (Figure 14 (b)) [137]. Despite the high voltages in the bio-photoelectrochemical cells, the low overall efficiency and short lifetime of the biomaterials are the main challenges toward their applications.

2.6.2.2 DSSC-Redox Flow Battery Hybrid Cells

A system can be developed for solar energy harvesting and storage by integrating a DSSC-like solar cell and a redox flow battery (RFB). Generally, in an RFB there are two electrolytes each with a redox couple ions: O1-R1 and O2-R2. The electrolytes are separated by a membrane allowing certain ions being exchanged between the two electrolytes. Upon charging an RFB, O1 and R2 are produced at the anode and the cathode, respectively. The electrolytes with rich O1 and R2 can be stored in separate tanks/reservoirs via pumps or using the natural convection in the liquids. According to the Nernst equation, the change in the concentration of redox couples generates a voltage difference between the electrodes that can be used to derive a load in a discharge cycle. As shown in Figure 15 (a) [139], a solar flow battery (SFB) relies on the photoredox reaction in the DSSC-like cell that is coupled to an RFB.

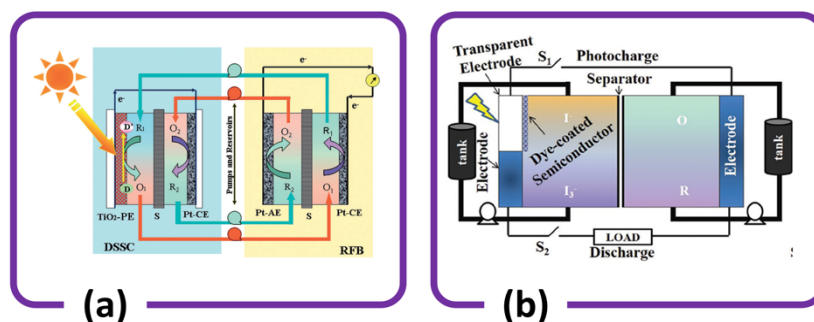


Figure 15: Examples of hybrid cells with flow batteries reported by: (a) Liu et al. [139] and (b) Cao et al. [140].

In another design shown in Figure 15 (b), the two electrochemical cells can be integrated. Since in both configurations, the storage in an SFB requires external tanks, SFBs are suitable for

power plants, not small electronics [140]. Hence, the details of different approaches are not discussed here, and we encourage enthusiastic readers to follow the related publications. Examples of review papers that include various approaches and list the performance of reported SFBs can be found in several publications [141-144].

2.6.2.3 Photoactive SCs

To integrate a supercapacitor and a DSSC, some have designed devices similar to a supercapacitor with one electrode being made from photoactive materials. Takshi et al. have made a photoactive supercapacitor with the photoanode made from a composite of a conducting polymer and a porphyrin dye and a porous carbon electrode as the cathode (Figure 16 (a)) [145]. The mechanism of operation is based on changing the redox state of the anode electrode with the photoexcited electrons. The electrode material at a different oxidation state stores the photogenerated charges like a pseudocapacitor. Using a porous cathode, the opposite charge is stored in the double layer. In this configuration, the open circuit voltage is determined from the potential difference between the electrochemical potential of the anode and the Fermi level of the cathode. The experimental results from Takshi's cell showed the cell voltage of 0.43 V under constant illumination. Photoactive supercapacitors with a composite of polyaniline and a dye showed much lower voltage change in the range of a few millivolts [146]. In a different approach (Figure 16 (b)), Takshi's group used a layer of a photoactive gel between two electrodes to make a two-terminal hybrid cell. Their device showed a photovoltage as high as 0.137 V [133]. Huang et al. used a composite containing WO_x at its counter electrode to convert a DSSC to a two-terminal hybrid cell (Figure 16 (c)). A voltage as high as 0.62 V was achieved but the voltage dropped sharply due to the small capacitance at the anode electrode [147]. As shown in Figure 16 (d), Cai et al. developed a micro-supercapacitor that could be charged up to 120 mV via

illumination [148]. A group in India have demonstrated a hybrid device with the photoactive electrode made of BiVO_4 and reduced graphene oxide with a max voltage of 340 mV [149].

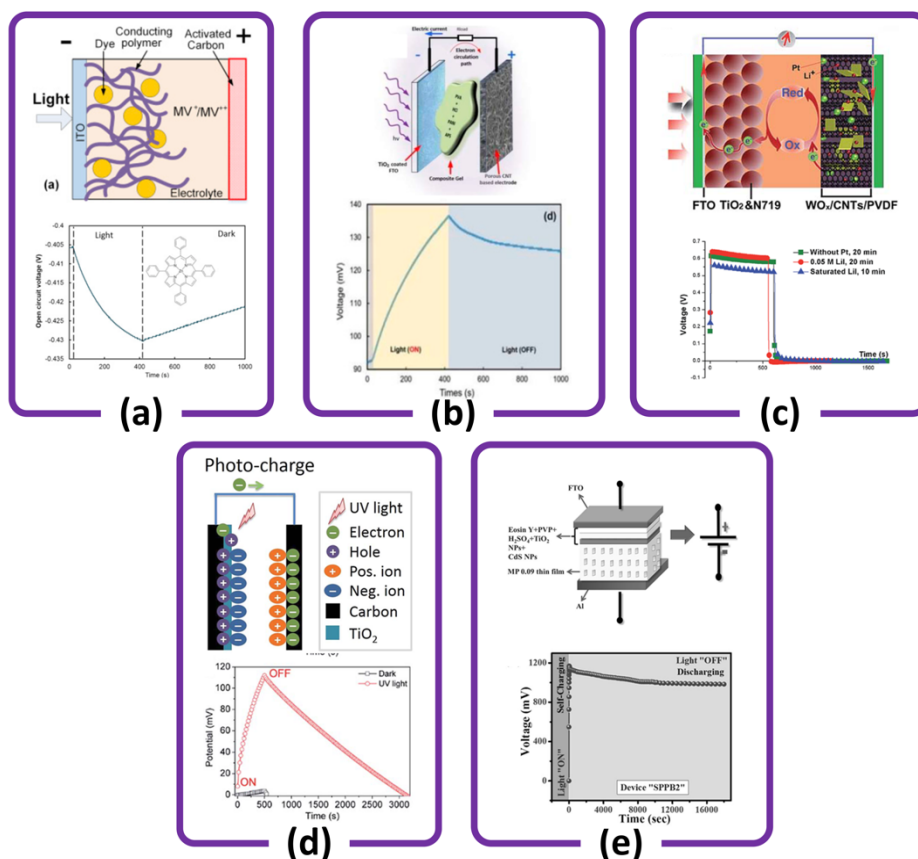


Figure 16: Examples of two-terminal photoactive supercapacitors reported by: (a) Takshi et al., [145] (b) Aljafari et al., [133] (c) Huang et al., [147] (d) Cai et al., [148] and (e) Roy et al. [150].

In a recent publication by Roy et al, a hybrid cell was made using a composite of TiO_2 and CdS nanoparticles (NPs). The device showed an incredibly high voltage of 1.17 V with an excellent charge storage stability exceeding 5 hours (Figure 16 (e)) [150]. Roy's work has brought promise to the field of two-terminal hybrid cells with high enough voltage to be used in real applications. However, the low energy conversion efficiency in the two-terminal hybrid cells

is still a serious challenge in using the devices for practical applications. Table 1 has summarized the different approaches discussed in this review.

Table 1: Summary of the reviewed works with their reported V_{oc} .

Type	Authors	Structure	V_{oc}	Comment	Ref
3-terminal					
Si PV-SC	Westover et al. (2014)	cSi PV+ Si based SC	0.58 V	Low capacitance-limited storage	[64]
	Thekkekar a et al. (2015)	cSi PV+GO SC	0.6 V	Low capacitance-limited storage	[65]
	Liu et al. (2017)	Si NW PV + PPy SC	0.55 V	long charge storage stability	[66]
	Ouyang et al. (2017)	cSi PV+MoOx Pseudo-SC	0.6 V		[151]
	Agbo et al. (2016)	a-Si and micro cSi+Li battery	2.09 V	Tandem PV	[58]
PSC-SC	Liang et al. (2018)	CsPbBr ₃ PV+SC	1.22 V		[35]
	Liang et al. (2018)	MAPbI ₃ PV+SC	0.9 V		[152]
	Zhou et al. (2016)	PSC+WO ₃ based SC	1.0 V	Photovotachromic+hybrid	[71, 72]
	Xu et al. (2016)	TiO ₂ /ZrO ₂ MAPbI ₃ +SC	0.8 V		[74]
	Liu et al. (2017)	Fabrics	0.7 V	On Fabrics	[56]
	Liu et al. (2017)		False V_{oc}	Series connection of PV and SC	[75]
	Xu et al.		False V_{oc}	Series connection of PV and SC	[76]
	Kim et al.(2017)	PSC+SC	0.91 V	$V_{oc} = 1.06$ V in the PV hybrid $V_{oc} = 0.91$ V	[80]
OPV-SC	Kim et al. (2017)	BHJ OPV+SC	0.71 V	V_{oc} of PV was 0.79 V but hybrid V_{oc} was only 0.71 V	[80]

Table 1: (Continued)

Type	Authors	Structure	V _{oc}	Comment	Ref
	Lechêne et al. (2016)	BHJ OPV+SC	0.87 V	Indoor light harvesting	[81]
	Zhang et al. (2014)	BHJ OPV+SC	0.4	Fiber shape hybrid cell	[82]
DSSC-SC	Lau et al.	DSSC with a Ppy/rGO counter electrode shared with the SC.	~0.65 V	V _{oc} =1.0 V is reported in the paper but the data shows Voc=~0.65 V	[153]
	Nagai et al. (2004)	DSSC+SC	0.6 V		[90]
	Saito et al. (2010)	WO ₃ for storing the charge in the supercapacitor	~0.6 V	V _{oc} dropped to 0.4 V instantly after the secession of light	[91]
	Murakami et al. (2005)	DSSC+SC	0.8 V		[92]
	Chen et al. (2010)	Flexible DSSC+SC	0.77 V	Flexible	[93]
	Hsu et al. (2010)	DSSC+PProDOt-Et ₂ based SC	0.75 V		[94]
	Mini et al. (2013)	TiO ₂ nanotubes	0.3 V		[95]
	Bagheri et al. (2014)	DSSC w Co ²⁺ /Co ³⁺ mediator+SC	0.72 V		[96]
	Cohn et al. (2015)	DSSC+Si nanostructure-based SC	0.68 V	Low cap./limited storage	[97]
	Yang et al. (2013)	DSSC+SC	0.75 V		[98]
	Skunik-Nuckowska et al. (2013)	P3HT as the electrolyte of DSSC	0.898 V		[99]
	Scalia et al. (2017)	flexible hybrid device with a polymer electrolyte membrane.	0.67 V		[104]
	Xu et al. (2014)	Anodic TiO ₂ nanotube arrays	0.6 V		[100].

Table 1: (Continued)

Type	Authors	Structure	V _{oc}	Comment	Ref
Wearable hybrid cells	Yang et al. (2013)	Nanowire forest structure	0.4 V	Mechanical, thermal, & solar harvest.	[108].
	Chen et al. (2014)	Same fiber	0.635 V		[112]
	Fu et al. (2013)	Parallel fibers	0.652 V	Power pack of 1.26 V	[110]
	Liang et al. (2017)	Coax same fiber DSSC+LIB	0.74 V		[113]
	Chai et al. (2016)	Coax and twisted	0.4 V	Power pack 2.6 V	[114]
	Zhang et al. (2017)	Flexible DSSC+SC	0.76 V	Power pack 4 PV in series	[115]
	Lee et al. (2013)	Flexible polymer PV +fabric-based LIB	2.01 V	Power pack with a LIB	[154]
Power packs	Li et al. (2015)	PSC+Li ion SC	1.05 V	Flexible (power pack)	[53]
	Xu et al. (2015)	PSC+LIB	3.84		[54]
	Chien et al. (2015)	OPV panel+SC	4.91 V		[83]
	Wee et al. (2011)	OPV panel+SC	1.0 V		[84]
	Xu et al (2014)	DSSC+SC	2.5 V	Series connections of hybrid cells	[100].
2-terminal					
PG	Lal et al. (2016)	H-shaped cell design not suitable for compact electronics.	1.235 V	Low conversion efficiency and low charge storage stability.	[123]
	Xiao et al. (2020)	Nanotube structure	~0.5 V	Low voltage low efficiency	[129]
	De La Garza et al. (2003)	Bio based hybrid	0.75 V	Low efficiency and short lifetime	[136]
	Usui et al. (2019)	Bio based hybrid	1.4 V	Low efficiency and short lifetime	[137]

Table 1: (Continued)

Type	Authors	Structure	V_{oc}	Comment	Ref
Photoactive SC	Takshi et al. (2015)	Photoanode CP+dye	0.43 V	Low efficiency	[145]
	Aljafari et al. (2019)	Photoactive gel	0.137 V	Low voltage	[133]
	Huang et al. (2016)	DSSC with the porous counter electrode	0.62 V	Poor charge storage stability	[147]
	Roy et al. (2020)	BiVO ₄ -RGO photoactive electrode	0.34 V		[149]
	Cai et al. (2017)	Micro Photoactive SC	110 mV	Long storage stability (5h)	[148]
	Roy et al. (2019)	Composite of TiO ₂ and CdS NPs	1.17 V	Excellent charge storage stability	[150]

*BHJ=Bulk Heterojunction; cSi=Crystalline Silicon; a-Si=Amorphous Silicon; MAPbI₃=methyl ammonium lead iodide; RGO=reduced graphene oxide; GO=Graphene oxide.

2.7 Suggestions and Outlook

Considering that the efficiency in solar energy harvesting is very critical, it is important to focus on solar cell technologies with high efficiencies. Also, knowing that the details of solar cell design and choice of materials directly impact the efficiency of the fabricated devices, it is suggested to develop more of three-terminal hybrid cells in which the solar cell part can be optimized independently from the storage part. The choice of solar cell technology has to be based on the open circuit voltage of the cell. In this regard, hybrid cells made from PSCs with V_{oc} of 1 V or higher are more promising than hybrid cells with OPVs or DSSCs with low voltages. Combining a thin film technology such as PSC with an electrochemical cell (i.e., SC), inevitably, a three-terminal design needs to be further developed. To operate the hybrid cell at its highest efficiency under various illumination conditions, it is recommended to equip a three-terminal cell with an integrated circuit such as CN3083 that is designed for tracking the maximum power in a miniaturized package. The combination of a single three-terminal hybrid

cell with V_{oc} of ~ 1 V and the smart miniaturized power tracker can be adequate for powering low-voltage integrated circuits such as Si1000. Although at this stage all two-terminal devices are inferior to the three-terminal devices, much better performances can be achieved from two-terminal cells first by developing theories explaining the mechanisms of concurrent energy harvesting and charge storage and then designing cells based on the theoretical studies. The lack of a comprehensive model, particularly for photoactive SCs, has resulted in trial and error approaches. Developing a model and using simulation tools perhaps can address some of the shortcomings particularly the low energy conversion efficiencies in two-terminal hybrid cells.

2.8 Conclusions

Due to the feasibility of using a smart charge controller unit between a separated solar panel and a battery, a conventional solar energy system is more efficient than connecting hybrid cells in series. Hence, the application of hybrid cells is justified mainly for small and low-voltage electronics that can run with a single hybrid cell. In addition, fiber shaped hybrid devices are potentially suitable for wearable electronics. Among different technologies, the three-terminal cells made from perovskite solar cells and integrated supercapacitors are promising due to their high energy conversion efficiency and high voltages exceeding 1.0 V. The main challenge in the two-terminal devices is the optimization of the efficiencies in both the energy conversion and charge storage. However, the two-terminal hybrid device introduced by Roy et al. made from a composite of CdS and TiO_2 NPs with V_{oc} of 1.17 V and 5 hours of charge storage is promising for the direct connection of a two-terminal cell to an electronic circuit. While each technology has its own advantages, focusing on the market need can merge efforts from different approaches to develop hybrid cells for practical applications.

Chapter 3: Impedance Spectroscopy Study of Hybrid Photovoltaic Supercapacitors²

3.1 Abstract

The integration of energy-harvesting and storage in a single device is considered to be one of the most demanding technologies for future wireless sensors. Photovoltaic supercapacitors are among promising solutions with the dual properties of photoelectric and electrochemical charge storage. In order to improve the efficiency in hybrid photovoltaic supercapacitors, most research has focused on studying electrode materials. In this work, we have studied the effect of polyaniline (PANI) concentration in a composite gel-based electrolyte on the impedance of the device. The photovoltaic supercapacitors were fabricated in a two-electrode configuration combining a titanium dioxide (TiO₂) coated on fluorine-doped tin oxide (FTO) glass as the working electrode, a multi-walled carbon nanotube (MWCNT) porous electrode as the counter electrode, and a composite gel-based electrolyte. The composite gel was made of polyvinyl alcohol (PVA), hydrochloric acid (HCl), ammonium persulfate (APS), and different concentrations of aniline (ANI). The impedance study of the gel with 0.5 mM concentration of PANI showed a two-stage charge storage mechanism associated to the double-layer at the electrode-electrolyte interface and a pseudo-capacitive charge storage mechanism in the bulk of the electrolyte. The absorption spectrum of the synthesized gel shows a strong absorption peak near 780 nm confirming the formation of the emeraldine salt of PANI in the gel. The current

² This chapter was published in SPIE proceeding (Kareri, T., Aljafari, B., & Takshi, A. (2020, August). Impedance spectroscopy study of hybrid photovoltaic supercapacitors. In *New Concepts in Solar and Thermal Radiation Conversion III* (Vol. 11496, pp. 8-14). International Society for Optics and Photonics). Permission is included in Appendix A.

results are inspiring the research for optimizing the composite material to improve both energy harvesting and the charge storage stability in photovoltaic supercapacitors.

3.2 Introduction

The need for using renewable energy sources is growing constantly due to the negative impacts of fossil fuels on the environment. The renewable energy sources, particularly solar and wind, are reliable and affordable for many applications. However, two main challenges in using them are their availability and conversion efficiency into electricity. In this regard, the development of energy storage devices contributes significantly and effectively to the exploitation of renewable energy resources and the evolution of their industry. Solar energy is one of the most promising alternatives to fossil fuels, and because of its intermittent nature, energy storage devices (i.e. battery or supercapacitor) are required in solar energy harvesting systems [31, 134, 145, 155, 156]. In an effort to store energy in a photovoltaic device, different hybrid devices have been fabricated and tested with various approaches [84, 94, 157-160]. The conventional method, reported by different groups, is to integrate a dye-sensitized solar cell (DSSC) with a supercapacitor in one package with a three-electrode configuration. In this configuration, an external switch is required to switch the operation mode of the device between the solar cell and the supercapacitor during the dark-light cycles [159-162].

Numerous studies have been carried out to enhance the efficiency and stability of the materials employed for electrodes and electrolyte of hybrid photovoltaic supercapacitors. Polyaniline (PANI)-based composite gels have elicited much consideration among researchers to be employed as the electrode material in supercapacitors due to their stability, conductivity, flexibility, ease of preparation, cost-efficient, and redox properties [163-166]. Besides, composite gels have gained a great deal of interest to be employed as an electrolyte in different

electrochemical devices because of their higher safety, flexibility, thermal stability, high ionic conductivity, and functionality. Our previous studies on a composite gel containing PANI have shown that a single layer of the composite gel can be worked as the redox-active electrode and electrolyte because of the capability of conducting ionic and electronic charges [133].

More focus has been given in this work to study the effect of PANI concentration in a composite gel-based electrolyte on the impedance of the hybrid device under both dark and light conditions. For this study, we have fabricated a hybrid device with a two-electrode configuration. Titanium dioxide (TiO_2) coated fluorine-doped tin oxide (FTO) glass electrode was used as a working electrode (solar cell), and a porous carbon nanotube (CNT) electrode was employed as a counter electrode (supercapacitor). The composite gel was employed as the photoactive electrolyte.

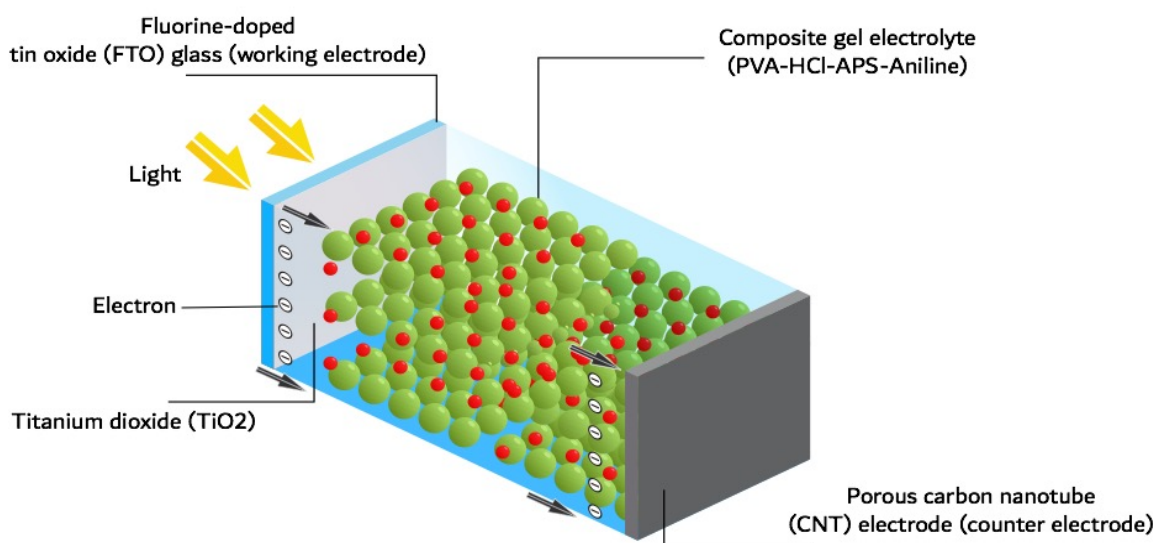


Figure 17: Schematic diagram of hybrid device based on composite gel electrolyte.

3.3 Experimental

3.3.1 Materials and Equipment

Multi-walled carbon nanotube (MWCNT), sodium dodecylbenzenesulfonate (SDBS), Poly(vinyl alcohol) (PVA), hydrochloric acid (HCl), ammonium persulfate (APS), and aniline were obtained from Sigma-Aldrich and used as received. TiO₂ coated fluorine-doped tin oxide (FTO) electrodes were obtained from Solaronix, the FTO substrate was (20 mm × 20 mm) with a TiO₂ coated area of (6.0 mm × 6.0 mm). Regular printing papers were used to make the porous carbon electrodes.

A VersaSTAT 4 Potentiostat/Galvanostat (Princeton Applied Research, AMETEK) was used to carry out all electrical and electrochemical experiments in a two-electrode configuration. Cyclic voltammetry (CV), open circuit voltage (OCV), short circuit current (SCC), and electrochemical impedance spectroscopy (EIS) experiments were conducted to test all devices after 48 hours (h) of fabrication at room temperature and under the same experimental conditions. To test the hybrid devices under dark and light modes, and to reduce the stray-light effects in the experiments, they were put in a dark box with an optical fiber connected to a solar simulator, from (RST, Inc), with a light intensity of 80 mW/cm² and AM 1.0 interior optical filter.

3.3.2 Electrode Fabrication

The porous carbon electrodes were fabricated using MWCNT-based ink and regular printing papers [167]. To prepare the ink, 300 mg of MWCNT and 150 mg of SDDBS were added into 30 mL of deionized DI water. Then, the ink was sonicated using a probe sonicator for 35 min at an average power of 30 W and an energy of 40 J to agitate nanoparticles in the solution and obtain a homogeneous mixture. The porous carbon electrodes were prepared by dispersing 1

mL of the ink on one side of a printing paper, (40 mm × 70 mm), then dried for 30 min at 120° C using a vacuum oven. The steps were repeated three times for both sides to improve the conductivity of the electrode. The apparent surface area of the porous carbon electrode was (40 mm × 8.0 mm) with a thickness of 130 μm and a surface resistivity of 71 Ω/sq.

3.3.3 Electrolytes Preparation

To prepare the composite gel electrolytes, as a first step, PVA-HCl gel electrolyte was synthesized by adding 5 g of PVA to 50 mL of 1 M HCl in DI water [168]. Then, the mixture was stirred adequately on a hot plate at 80° C for 4 h at a speed of 500 rpm. Then, 15 mL solution of 0.1 M APS in 1 M HCl was added to the PVA-HCl solution at room temperature and stirred for 1 h at 700 rpm. After that, the composite gel electrolytes were made by adding different concentrations (0.1, 0.2, 0.3, 0.4, and 0.5 mM) of aniline to the PVA-HCl-APS at room temperature and stirred for 2 h.

3.4 Results and Discussion

CV measurements were performed with the potential range between -1.0 V and +1.0 V at 50 mV/s scan rate. As an example, Figure 18 shows the CV results for the hybrid device with 0.3 mM of Aniline under dark and light conditions. The results show both solar energy harvesting and energy storage capabilities with a two-stage charge storage mechanism. The CV loops indicate the internal capacitance due to the double-layer charge storage mechanism at the electrode-electrolyte interface. As shown in our previous work, the redox peaks in the CV loops indicate a pseudo-capacitive charge storage mechanism in the bulk of the electrolyte, as an additional charge storage mechanism [133]. The specific capacitance of the device with 0.3 mM of Aniline was calculated to be 12.82 mF/g in the dark and increased to be 18.54 mF/g under the light mode based on the mass of the gel. The absorption spectrum of the composite gel exhibits

an absorption peak of 780 nm confirming the formation of the emeraldine salt of PANI in the gel, as shown in Figure 19 (a) [133].

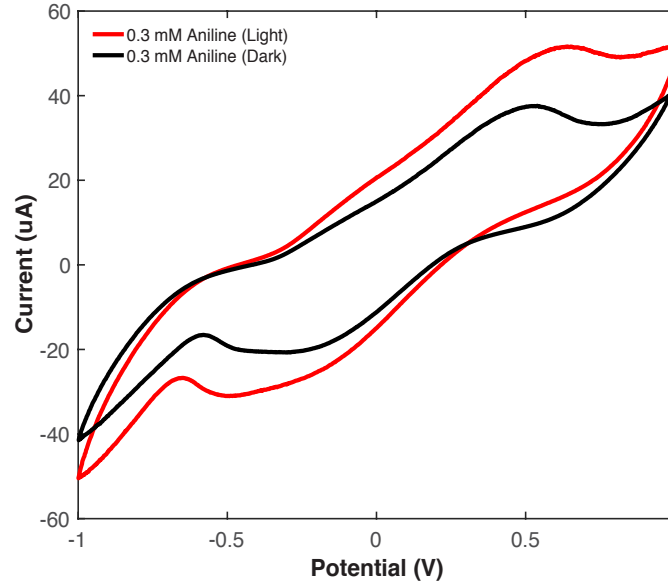


Figure 18: Cyclic voltammetry (CV) results of the hybrid device with PVA-PANI composite gel electrolyte, 0.3 mM of Aniline, under the dark and light conditions.

Further insights into the hybrid device characteristics were obtained by OCV and SCC tests under the dark and light conditions, as shown in Figure 19 (b) and Figure 20, respectively. The variation in the OCV during the dark and light conditions was monitored to study the photovoltaic effect on the devices. First, the OCV test was conducted in the dark until reaching a stable voltage. The OCV test was repeated under illumination for 400 s then in the dark for 600 s. As presented in Figure 19 (b), the change in the open circuit voltage (ΔV), for the device with 0.3 mM of Aniline, was reached to 58 mV in 400 s of illumination and then decreased to 35 mV in 600 s of the dark mode. Besides, the SCC in the device was studied by light pulses every 20 s. The results showed a slight increase in the current of 0.04 nA under the light pulses with a long-period transition between the dark and light, as shown in Figure 20. The transient response from

light to dark in the OCV result and the delay in the photocurrent response in Figure 20 suggest a delay mechanism likely due to the storage effect in the gel.

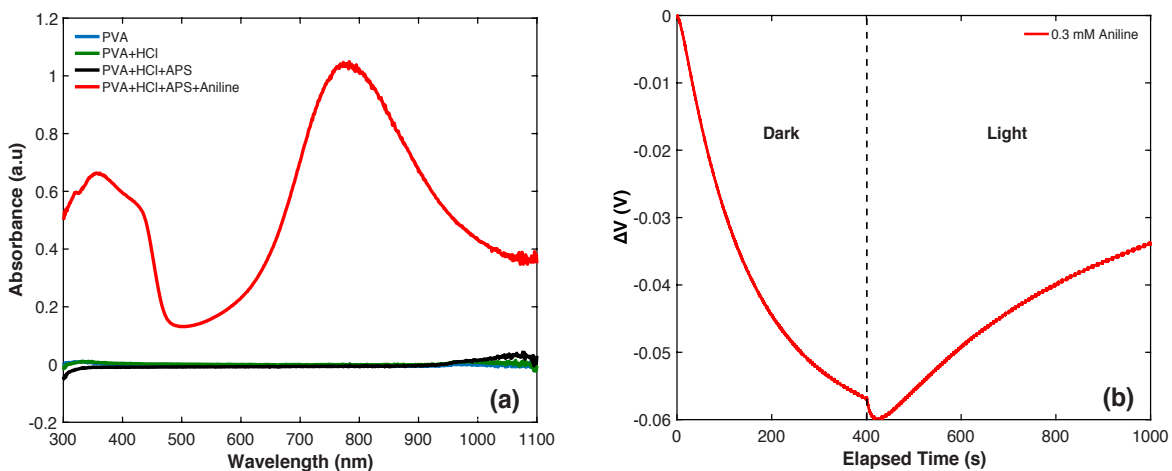


Figure 19: (a) UV-visible absorption spectrum, (b) open circuit voltage result of a hybrid photovoltaic supercapacitor with PVA-(0.3 mM)PANI composite gel electrolyte.

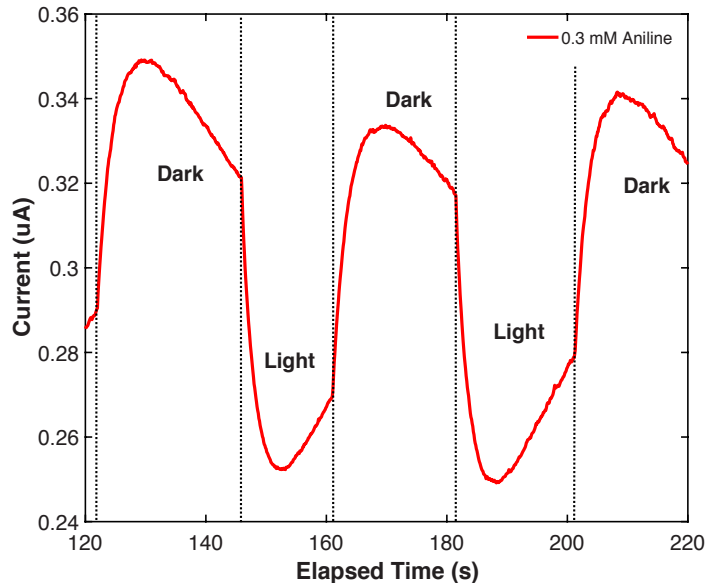


Figure 20: Short circuit current result of a hybrid photovoltaic supercapacitor with PVA-(0.3 mM)PANI composite gel electrolyte under dark and light pulses.

To understand the behavior of the electrode-electrolyte interface and the composite gel resistance in dark and light, electrochemical impedance spectroscopy (EIS) measurements were carried out with the frequency range between 100 mHz and 100 kHz with no DC bias potential and a sinusoidal signal of 20 mV. Figure 21 (a) shows the Nyquist plots for different concentrations of Aniline and Figure 21 (b) for 0.3 mM of Aniline. The impedance results at high frequencies exhibited a resistive behavior with a high series resistance due to low ionic conductivity caused by the water loss in the gel (caused after 48 hours of the device fabrication). Also, at the low frequencies, the slope of diffusion tail, for all concentrations, is almost 45°, suggesting a diffusion dominated mechanism of charge transport.

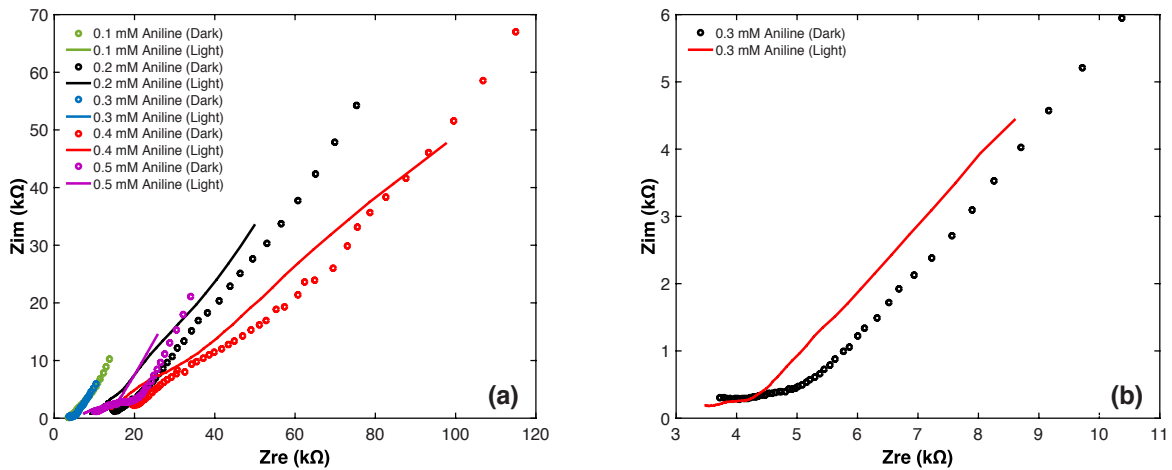


Figure 21: Nyquist impedance results of the hybrid devices with (a) different concentrations of Aniline, and (b) 0.3 mM of Aniline in dark and light.

For gaining a better understanding of the effect of Aniline concentration on the behavior of the cells, an equivalent circuit model has suggested for the device and simulation studies were conducted to find various parameters in each gel under the dark and light conditions. The suggested circuit model and the Bode plot of the measured impedance for the device with 0.3

mM concentration of PANI are shown in Figure 22. The plots show both the magnitude, Figure 22 (a), and phase, Figure 22 (b). The equivalent circuit model represents the two stages of charge storage. The first stage with the C_{dl} and CPE represents the charge storage at the electrode-electrolyte interface and the diffusion-limited response at the low frequencies, and the second stage with C_{gel} and R_{gel} is suggested to represent the charge storage in the bulk of the gel electrolyte which explains the redox peaks in the CV loops. EIS Spectrum Analyser software was used to find the values of the model elements, and the measured parameters of the hybrid devices, under the dark and light conditions, were listed in Table 2.

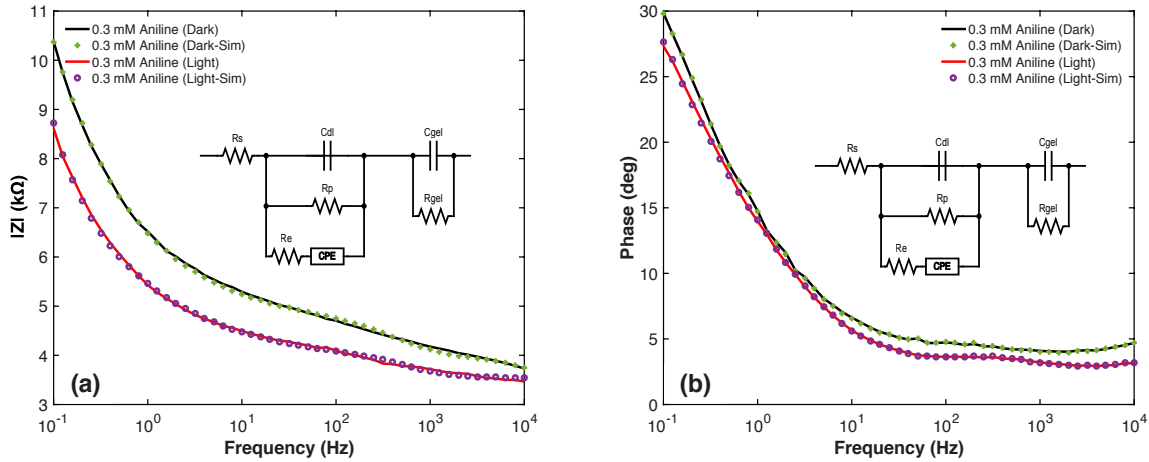


Figure 22: Experimental and simulation results for (a) Magnitude and (b) phase of impedance for the device with PVAPANI composite gel electrolyte containing of 0.3 mM of Aniline. (Inset) electrical equivalent circuit models.

The results show that the series resistance (R_s) of the device was lower for 0.1 mM and 0.3 mM of PANI, and the gel resistance (R_{gel}) was lower for 0.2 mM and 0.5 mM compared to the other concentrations of PANI. The decrease in the R_s and R_{gel} values under the light condition for all concentrations of PANI shows a clear correlation between R_s and light and supports the CV results. The variation in R_s value in the dark and light was high for 0.3 mM which indicates

the high light response in this concentration. There is no obvious effect on the capacitance at the electrode-electrolyte interface (C_{dl}) under the solar illumination. However, the capacitance of the gel (C_{gel}) for all concentrations of PANI increases in the light which explains the photoelectric and electrochemical charge storage properties of the gel. Also, the results show that C_{gel} of the device was the highest for 0.3 mM of PANI in both dark and light.

Table 2: Impedance parameters of different concentrations of Aniline in the dark and light.

Devices	R_s (k Ω)	R_p (k Ω)	C_{dl} (μ F)	C_{gel} (μ F)	R_{gel} (k Ω)	R_e (k Ω)	$0 < n < 1$	P (S.sec)
0.1 mM Dark	3.6904	19.386	0.5	247.93	70.377	0.60477	0.4945	6.8E-05
0.1 mM Light	3.5592	13.489	0.5	353.22	19.499	0.66997	0.49674	8.37E-05
0.2 mM Dark	15.931	9999	0.5028	0.51	2.4287	2.4881	0.47379	1.58E-05
0.2 mM Light	9.6368	6467.4	0.5	0.58	1.48	1.9693	0.45673	2.42E-05
0.3 mM Dark	3.9707	23.132	0.5	471.77	11.477	0.65015	0.4386	1.57E-04
0.3 mM Light	3.5353	9.4652	0.5	500	6.7153	0.46011	0.47563	1.77E-04
0.4 mM Dark	23.175	1440.5	0.4035	0.4	7.433	15.325	0.38925	1.20E-05
0.4 mM Light	13.121	10000	0.407	0.48	2.6694	3.8557	0.35951	1.32E-05
0.5 mM Dark	10.055	10000	0.46	50	2.842	5.1597	0.54346	5.09E-05
0.5 mM Light	7.2463	10000	0.46	96.4	2.0784	3.6296	0.51349	6.76E-05

The presented results in this work exhibit the capability of the PVA-PANI composite gel-based electrolyte with a dual property of the photoelectric and charge storage. The device with 0.3 mM of PANI showed the best electrochemical impedance spectroscopy results compared to the other concentrations. Practically, the internal resistance of the device was high in both dark

and light conditions. To enhance the performance of the device, reducing the internal resistance by keeping the gel electrolyte wet is needed.

3.5 Conclusion

The effect of PANI concentration in a gel-based electrolyte on the impedance of a hybrid photovoltaic supercapacitor based on a two-electrode configuration was studied. It was observed that the addition of 0.3 mM of PANI in the composite gel electrolyte enhances the charge storage and conductivity of the device compared to the other concentrations in this study. The internal resistance of the device decreases in the light for all concentrations of PANI which shows the photoelectric capability of the device. The energy harvesting and charge storage in hybrid photovoltaic supercapacitors can be improved by optimizing the composite materials.

Chapter 4: Hybrid Photovoltaic-Supercapacitors: Effect of the Counter Electrode on the Device Performance³

4.1 Abstract

In recent years, the interest in photovoltaic supercapacitors has been increasing in order to develop self-powered sensors for a sustainable system. Hence, significant research efforts are needed to enhance the photoelectric and electrochemical performances of hybrid devices. Herein, we have studied the effect of the porosity of different counter electrodes on the performance of the hybrid photovoltaic supercapacitors. The photovoltaic supercapacitors were fabricated in one package with a simple structure including a titanium dioxide (TiO₂) coated on fluorine-doped tin oxide (FTO) glass as a working electrode and polyaniline (PANI)-based gel electrolyte. The performance of the hybrid device was studied with four different counter electrodes: a multi-walled carbon nanotube (MWCNT) porous electrode, PEDOT:PSS coated on FTO glass, carbon monolithic electrode, and a carbon-based conductive fabric. The specific capacitance of the device with PEDOT:PSS coated FTO electrode was 255 mF/g in the dark and increased to be 274 mF/g under the light based on the mass of the gel. The hybrid device can be charged when the working electrode is illuminated. The variation in the open circuit voltage (ΔV) was reached 256 mV in 400 s under illumination, and the voltage drop was 4 mV (-4%) in 600 s of the dark.

³ This chapter was published in SPIE proceeding (Kareri, T., Aljafari, B., & Takshi, A. (2021, August). Hybrid photovoltaic-supercapacitors: effect of the counter electrode on the device performance. In *New Concepts in Solar and Thermal Radiation Conversion IV* (Vol. 11824, p. 1182407). International Society for Optics and Photonics). Permission is included in Appendix A.

The current results of the hybrid photovoltaic supercapacitor, with a simple fabrication process and basic structure, are boosting the study for the electrode materials selection to enhance the performance of the hybrid device.

4.2 Introduction

Over the past half-century, fossil fuel consumption has increased significantly due to the industrial revolution and global population growth, leading to climate change [1]. Recently, the interest in renewable energy has grown significantly to address climate change and ensure environmental sustainability [2, 3]. Therefore, the exploitation of renewable energy sources, such as solar energy, has attracted great interest, especially in industrial and scientific research for the applications in wearable electronics and self-powered devices such as wireless sensors [53, 169]. However, there are still major obstacles that limit the applications of renewable energy sources (e.g., solar energy), including their high cost, stability, availability, and challenges in the energy storage devices. Integrating solar energy systems with energy storage devices, such as batteries and supercapacitors, is a key factor in developing and implementing renewable energy applications. One of the solutions offered is the integration of a solar energy system with an external storage system, as a hybrid system [170]. Another approach is to combine a solar cell (i.e., dye-sensitized solar cell) with a supercapacitor in one package with three electrodes to switch between the two operating systems [31, 92, 171]. However, this approach is not practical in some applications like portable electronics that require low voltage and low power [172].

Our previous studies focused on fabricating and studying two-terminal hybrid devices with a photoactive gel electrolyte and simple structure (like asymmetric supercapacitors structure) [133, 173]. One of the most critical challenges in designing the hybrid device is optimizing photovoltaic conversion and energy storage performance. To improve the low energy

density in supercapacitors, developing new electrode materials with high porosity is needed [8]. Several approaches and electrode materials have been studied to enhance capacitance and energy density in supercapacitors [8, 9]. Among different materials used for supercapacitors, carbon-based materials are widely studied and utilized for manufacturing supercapacitors due to their large surface area and high chemical and thermally stability [174, 175]. Also, conducting polymers (e.g., PEDOT:PSS) and their composites are viable options due to their low cost with the high specific capacitance, which can be processed easily for mass production of supercapacitors [176, 177]. In this work, we have studied four different materials for the counter electrode (CE), which serves as a supercapacitor, to improve the energy storage performance of the hybrid device: A multi-walled carbon nanotube (MWCNT) porous electrode, poly(3,4-ethylene dioxythiophene):polystyrene sulfonate (PEDOT:PSS) coated film on fluorine-doped tin oxide (FTO) glass, carbon monolithic coated layer on FTO glass, and carbon-based conductive fabric electrode. As shown in Figure 23, poly(vinyl alcohol) (PVA)/PANI composite gel, which acts as an electrolyte and photoactive layer [133], was placed between two electrodes: titanium dioxide (TiO_2) coated layer on a transparent conductive substrate (FTO) glass as a working electrode (WE) and the four different porous materials for CE.

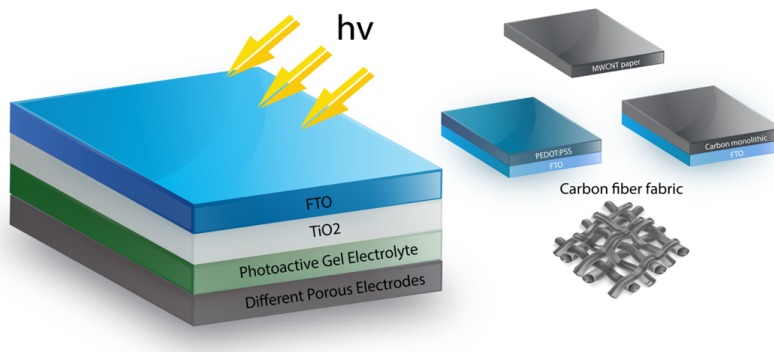


Figure 23: Schematic diagram of the hybrid device with different counter electrodes.

4.3 Experimental

4.3.1 Materials and Instrumentation

Multi-walled carbon nanotube (MWCNT), PEDOT:PSS, sodium dodecylbenzene-sulfonate (SDBS), ethylene glycol (EG), poly(vinyl alcohol) (PVA), ammonium persulfate (APS), aniline, and phosphoric acid (H_3PO_4) were purchased from Sigma-Aldrich. A regular printer paper was used for making the MWCNT paper electrode. TiO_2 coated FTO glass and carbon monolithic coated FTO glass were purchased from Solaronix, with a coated area of ($0.6 \text{ cm} \times 0.6 \text{ cm}$). A carbon-based conductive fabric was purchased from Easy Composites. A VersaSTAT 4.0 Potentiostat, connected with a solar simulator with a light intensity of 80 mW cm^{-2} and AM 1.0 interior optical filter, was used to conduct all electrochemical tests at room temperature and under the same experimental conditions. Evolution 201/220 UV-Visible Spectrophotometer was used to measure the optical absorbance peak of the composite gel.

4.3.2 Electrodes Fabrication

MWCNT solution was made by adding 300 mg of MWCNT and 150 mg of SDBS to 30 mL of deionized (DI) water. Then, the solution was sonicated using a probe sonicator for 30 minutes at 30 W to disperse nanoparticles. After preparing the solution, the MWCNT electrode was fabricated by coating 1 mL of MWCNT solution on a printer paper ($4.0 \text{ cm} \times 7.0 \text{ cm}$), followed by drying for 30 minutes at $120 \text{ }^\circ\text{C}$ using a vacuum oven. The coating and drying process was repeated three times for each side to increase the conductivity of the MWCNT electrode [167].

For the PEDOT:PSS electrode, a polymer solution was made by mixing PEDOT:PSS with 5.0 wt% of EG [177]. The mixed solution was then sonicated for 45 minutes using a bath sonicator to obtain a homogenous polymer solution. FTO glass substrate was cleaned by washing

with DI water and sonicating in DI water, methanol, and ethanol for 5 minutes, respectively. The PEDOT:PSS electrode was fabricated by dropping 15 μL of the solution onto ($0.6\text{ cm} \times 0.6\text{ cm}$) of the FTO glass using a drop-casting method, followed by drying on a hot plate for 15 minutes at $90\text{ }^\circ\text{C}$, treating in EG for 5 minutes at room temperature to increase the conductivity, and then annealing on a hot plate at $120\text{ }^\circ\text{C}$ for 60 minutes.

4.3.3 Electrolyte Preparation

The PVA/ H_3PO_4 gel electrolyte was synthesized by adding 3 g of PVA to 20 mL of DI water and 2 mL of H_3PO_4 , followed by stirring on a hot plate at $80\text{ }^\circ\text{C}$ and 400 rpm for 4 hours. A solution of 0.1 M APS and 0.5 mL of H_3PO_4 in 5 mL of DI water was added to the gel at room temperature and stirred for 30 minutes at 400 rpm. Then, the PVA/PANI gel electrolyte was made by adding 0.2 M of aniline to the gel at room temperature and stirred for 12 hours.

4.4 Results and Discussion

Cyclic voltammetry (CV) measurements were carried out in the potential window from -1.0 V to $+1.0\text{ V}$ at a scan rate of 50 mV s^{-1} to study the energy storage performance of the hybrid device with different counter electrodes. Figure 24 (a) exhibits the CV results of the hybrid device based on the MWCNT counter electrode. Redox peaks were observed in the CV curves due to the pseudocapacitive mechanism in the composite gel electrolyte. The results show that the storage part of the device increases drastically under light illumination. The device with the MWCNT counter electrode presents a specific capacitance of 121 mF g^{-1} in the dark and 181 mF g^{-1} under light illumination, based on the gel mass. The CV curves of the device with the PEDOT:PSS electrode shows strong redox peaks with increasing peak current density values, that emerged from the surface redox reactions of the PEDOT:PSS electrode and the gel electrolyte, as shown in Figure 24 (b). The device with the PEDOT:PSS electrode exhibits

specific capacitances of 255 mF g^{-1} and 274 mF g^{-1} in the dark and light, respectively. It was observed that the carbon monolithic-based counter electrode gives a low energy storage performance compared to the other counter electrode materials, likely due to the low mesoporosity of the carbon monolithic electrode, which limits the accessibility of electrolyte ions [178]. The specific capacitance of the device with the carbon monolithic electrode was calculated from the CV curve, Figure 24 (c), to be 77.5 mF g^{-1} in the dark and 92.2 mF g^{-1} under illumination. As shown in Figure 24 (d), compared to the other counter electrode materials, carbon-based conductive fiber shows the highest specific capacitance of 707 mF g^{-1} in the dark and 844 mF g^{-1} in the light, which is likely due to the high porosity of the fiber.

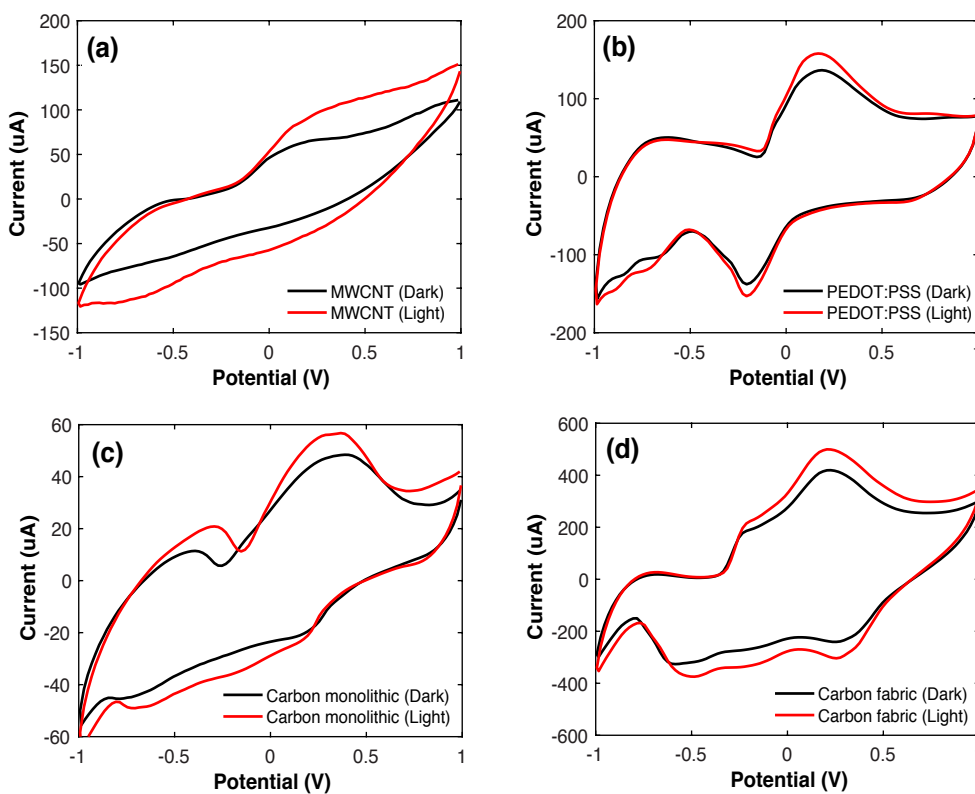


Figure 24: Cyclic voltammety results of the hybrid device with (a) MWCNT, (b) PEDOT:PSS, (c) carbon monolithic, and (d) carbon fiber fabric electrode.

Despite the importance of energy storage performance in hybrid cells, the photovoltaic effect of the devices must be considered to reach optimal performance. Due to the ability of the PVA/PANI gel electrolyte to absorb light and act as an active layer, as shown in Figure 25 (a), the photovoltaic performance of the device was studied in conventional methods of measuring dye-sensitized solar cells (DSSCs) performance. In order to investigate the photovoltaic effect of the hybrid device with different counter electrodes and the photoactive gel electrolyte, open circuit voltage (OCV) measurement was performed in two steps by testing the device under illumination for 400 s and then in the dark for 600 s, as depicted in Figure 25 (b).

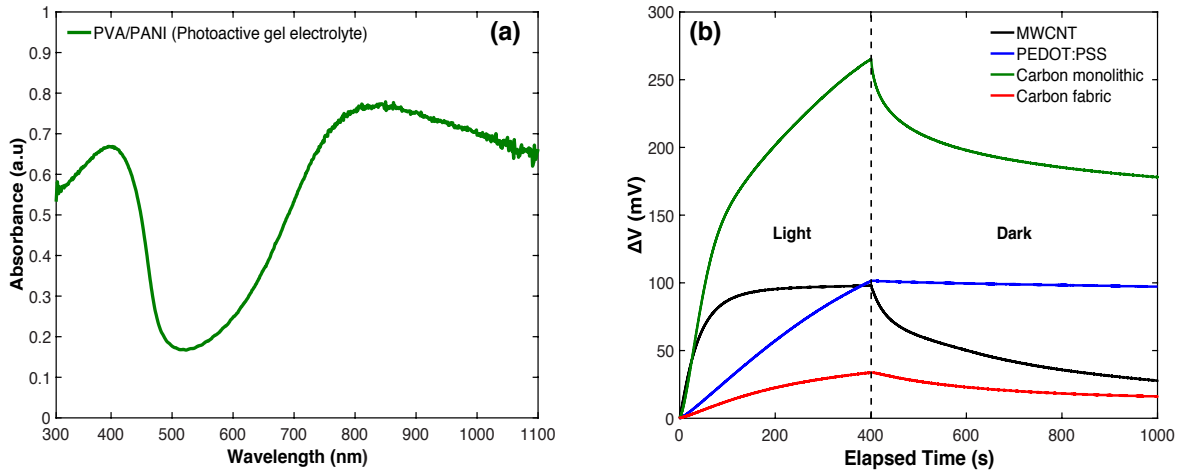


Figure 25: (a) UV-visible absorption spectrum of PVA/PANI gel, (b) open circuit voltage results of the hybrid device with different counter electrodes.

The voltage of the device based on the carbon monolithic electrode was significantly increased to reach 265 mV under illumination, while the other devices with MWCNT, PEDOT:PSS, and carbon fiber reached 97 mV, 101 mV, and 34 mV, respectively. However, after 600 s of the dark condition, the voltage drop (ΔV) of the devices with carbon monolithic, MWCNT, and carbon fiber electrodes were 87 mV (− 33%), 70 mV (− 72%), and 17 mV (− 50%), respectively, due to

the self-discharge in the hybrid devices. Unlike the other devices, the hybrid device based on the PEDOT:PSS electrode showed the lowest voltage drop (ΔV) of 4 mV (-4%), demonstrating its ability to store charges for a longer time.

Furthermore, to evaluate the photocurrent response in the hybrid device, short circuit current (SCC) measurement was performed under light pulses every 20 seconds. As shown in Figure 26, in the dark cycles, the hybrid device exhibited a current of $\sim 1.1 \mu\text{A}$, $\sim 0.55 \mu\text{A}$, $\sim 0.8 \mu\text{A}$, and $\sim 1.9 \mu\text{A}$ with the MWCNT, PEDOT:PSS, carbon monolithic, and carbon fiber, respectively, that is due to the charge storage mechanism in the hybrid devices. Under illumination cycles, the results showed an increase in the photocurrent (ΔI) about $0.61 \mu\text{A}$, $0.44 \mu\text{A}$, $0.62 \mu\text{A}$, and $0.58 \mu\text{A}$ with the MWCNT, PEDOT:PSS, carbon monolithic, and carbon fiber electrode, respectively.

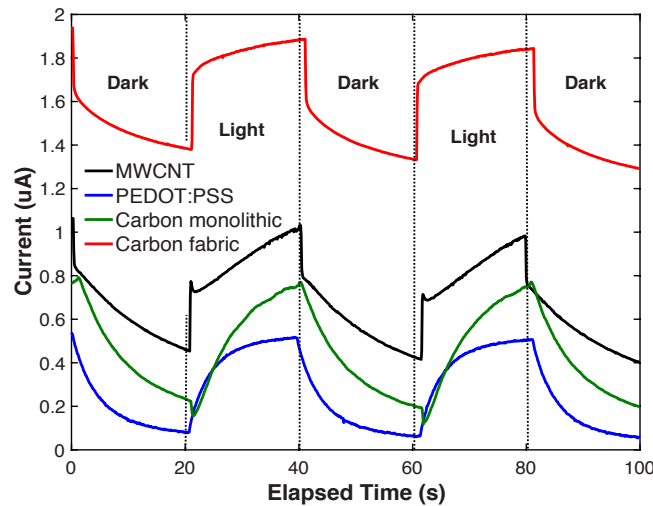


Figure 26: Short circuit current results of the hybrid device with different counter electrodes.

It is observed that all devices maintain good repeatability after several cycles of light pulses, indicating that the hybrid device has a good stability of the light response with all tested counter

electrodes. All the results of the presented hybrid devices with different counter electrodes are summarized in Table 3.

Table 3: Summary of the hybrid device characteristics with different counter electrodes.

Counter Electrode	Capacitance	ΔV (in 400s) Light	ΔV (in 600s) Dark	$\Delta J = \Delta I / (\text{area})$
MWCNT paper	121 mF g ⁻¹	97 mV	70 mV (- 72%)	1.69 $\mu\text{A cm}^{-2}$
FTO-PEDOT:PSS	255 mF g ⁻¹	101 mV	4 mV (- 4%)	1.22 $\mu\text{A cm}^{-2}$
FTO-Carbon monolithic	77.5 mF g ⁻¹	265 mV	87 mV (- 33%)	1.72 $\mu\text{A cm}^{-2}$
Carbon fiber fabric	707 mF g ⁻¹	34 mV	17 mV (- 50%)	1.61 $\mu\text{A cm}^{-2}$

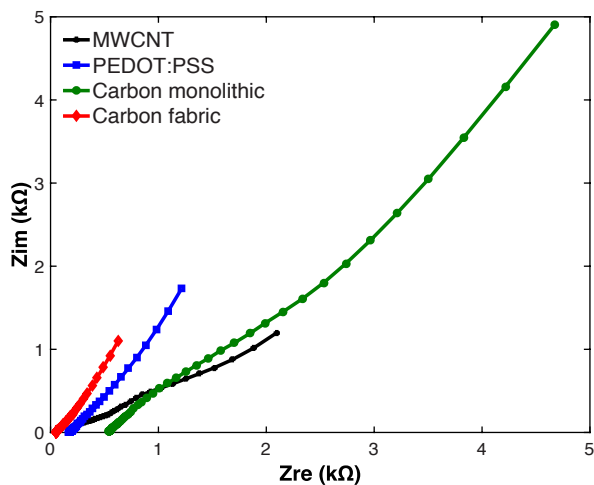


Figure 27: Nyquist plot of the hybrid device with MWCNT, PEDOT:PSS, carbon monolithic, and carbon fiber counter electrodes.

In order to study the electrode-electrolyte interface in the hybrid cells, electrochemical impedance spectroscopy (EIS) measurements were conducted at the same frequency range of (0.1 Hz - 10 kHz), DC bias of 0 V, and a sinusoidal signal of 20 mV. Figure 27 shows the

Nyquist diagram of the hybrid device. At low frequencies, the electrodes showed a nearly 45°, implying a diffusion-controlled reaction. Compared to the other counter electrodes, the devices with PEDOT:PSS and carbon fiber exhibited lower impedance, which supports the CV results.

The introduced results here demonstrate the two effects of energy storage and photovoltaic of hybrid devices based on different counter electrode materials. The hybrid device-based carbon conductive fiber presents the highest specific capacitance due to the high porosity of the carbon fiber electrode. On the other hand, monolithic as a counter electrode shows the demerit of energy storage part, which is expected due to the low penetration of the ions to the surface of the CE. However, the voltage under the photovoltaic effect is extremely high compared to the other counter electrode materials recording 265 mV. In terms of keeping photogeneration charges after cessation of the light, PEDOT:PSS based counter electrode for the hybrid device stands as the best material comparing to the others in this paper. Even though the voltage of the device based PEDOT:PSS-counter electrode under the light is not the highest, the ΔV is recorded to be the lowest for 600 s (4 mV).

4.5 Conclusion

Four different counter electrodes including MWCNT, PEDOT:PSS, carbon monolithic, and carbon fiber fabric were studied to improve the energy storage performance of a two-terminal hybrid device with a photoactive gel electrolyte. It was observed that the PEDOT:PSS coated FTO counter electrode provides good energy storage performance with high stability of the light response and low self-discharge rate compared to the other electrodes. Despite the remarkable improvement in the hybrid device performance through this study, there is still a great potential for further development.

Chapter 5: Image Processing Analysis of Supercapacitors with Twisted-Fiber Structures and a Gel Electrolyte⁴

5.1 Abstract

With the promising future of wearable electronics, a challenge is to find a suitable form of energy storage. Various forms of fiber-based batteries and supercapacitors, including parallel, coaxial and twisted fiber structures have been suggested. In this work, we have studied the electrical properties of three different twisted-fiber supercapacitors made of different commercially available conductive threads and a polyvinyl alcohol (PVA)-based gel electrolyte. The large signal capacitance and the electrochemical impedance of all three samples were studied for 1 to 6 turns of twists in 10 cm long threads. While the results showed a linear increase in the capacitance with the number of turns in a nylon-based thread, a stainless steel fiber-based device showed almost no change in its electrical properties with an increase in the number of turns. The image processing tool from MATLAB was used to study the structure of twisted threads. Analyzing the images showed that the change in the nylon-based capacitance was related to the length of the overlapped two threads. However, the hairy and intertwined structure of the threads containing stainless steel fibers had dominated the capacitive behavior of the devices. The applied image processing method not only is useful for analyzing fiber-based

⁴ This chapter was published in Journal of Applied Electrochemistry (Kareri, T., Yadav, R. L., & Takshi, A. (2022). Image processing analysis of supercapacitors with twisted fiber structures and a gel electrolyte. Journal of Applied Electrochemistry, 52(1), 139-148). Permission is included in Appendix A.

devices but also can be applied to design an optimum structure for high energy storage capacitances.

5.2 Introduction

Supercapacitors have been considered significant energy storage devices due to their high-power density and ability to fast charging and discharging compared to batteries [6]. Supercapacitors can be classified into three types based on their energy storage mechanism: electric double-layer capacitors (EDLCs), pseudocapacitors, and hybrid capacitors [10]. The electrical energy in EDLCs is stored based on charge accumulation at the electrode-electrolyte interface called the double layer [10, 179]. Additionally, electrical energy storage can be achieved by redox reactions in pseudocapacitors [10, 179]. Unlike batteries, supercapacitors have a low energy density, at least ten times lower than batteries [180].

To increase the energy density in supercapacitors, developing new conductive and porous electrode materials is demanded. Different techniques and electrode materials, such as carbon materials, metal oxides, and conducting polymers, have been developed to improve capacitance and energy density in supercapacitors [181-183]. With an increasing interest in using supercapacitors for wearable electronics, in addition to the capacitance density, mechanical properties, such as flexibility, mechanical stability, and weight of the devices, have become important. Recently, different studies have been published on various types of flexible supercapacitors, and among them flexible fiber supercapacitors [184-186].

The performance and functional properties of fiber supercapacitors depend on the electrode and electrolyte materials and the device structure. There are several basic structures of fiber supercapacitors, such as parallel [187], twisted [188-190], coaxial [191], and large-area woven structures [192]. Among them, twisted fibers or threads have the simplest structure that is

promising for low-cost fiber-based energy storage. Here, the performance of three thread-based symmetric supercapacitors with the twisted structure is studied. More focus has been given to study the effect of the number of turns of twisting on the devices' capacitance and electrochemical impedances. The devices were fabricated using commercially available conductive threads from Jameco, JL, and BCP as electrodes and polyvinyl alcohol (PVA)-based gel electrolyte between them, as shown in Figure 28. Then the structure of the twisted fibers was analyzed using an image processing tool to find a correlation between the twisted structure and the capacitance of the devices.

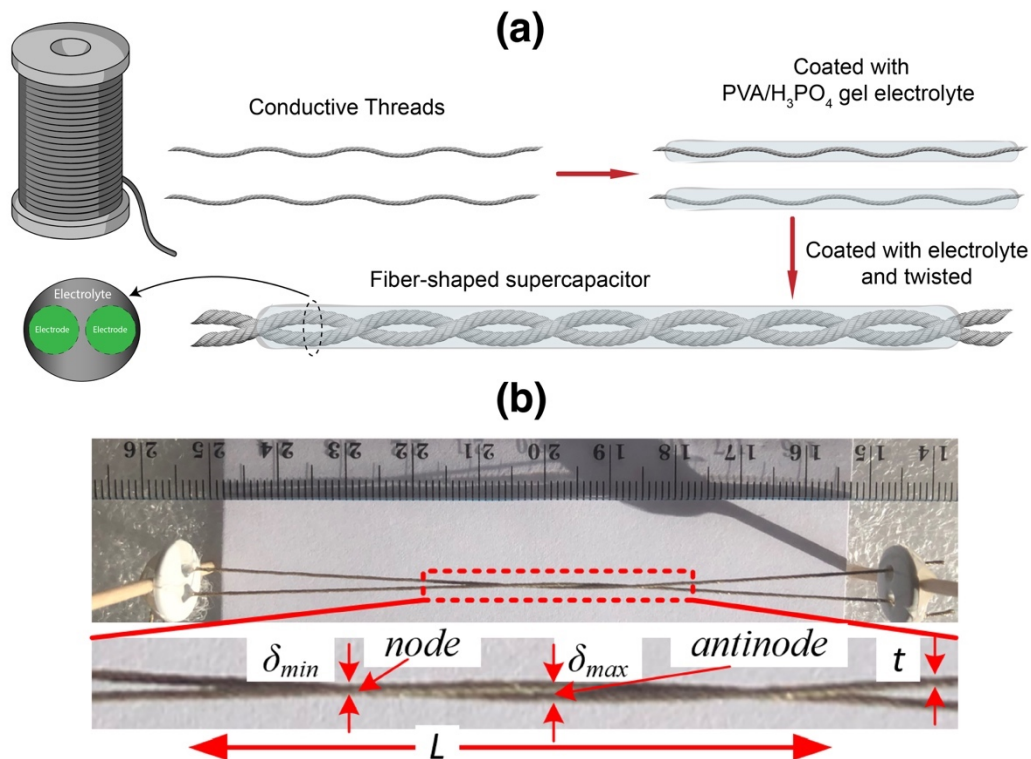


Figure 28: (a) Schematic and (b) the image of a twisted fiber supercapacitor, made by first coating a thin layer of the gel on two pieces of fibers. Then, twist and coat another layer of the gel. Features of a twisted structure, including the effective length, L , fiber thickness, t , and the thickness at nodes, δ_{min} , and antinodes, δ_{max} , are shown in the zoomed image of the twisted structure.

5.3 Experimental Section

5.3.1 Materials

Poly(vinyl alcohol) (PVA) and phosphoric acid (H_3PO_4) were purchased from Sigma-Aldrich. Jameco conductive thread (silver-coated nylon 66 fiber) with a lineal resistance of $50 \Omega \text{ m}^{-1}$ was purchased from Jameco Valuepro. JL conductive thread (stainless steel fiber) with a lineal resistance of $92 \Omega \text{ m}^{-1}$, and BCP conductive thread (stainless steel fiber blended with polyester) were purchased from SparkFun Electronics and BCP, respectively.

5.3.2 Preparation of Gel Electrolytes

The gel polymer electrolyte was prepared by adding 3 g of PVA to 2 mL of phosphoric acid (H_3PO_4) mixed with 20 ml of deionized water. Then, the mixture was stirred well on a hot plate at $90 \text{ }^\circ\text{C}$ for 4 h at a speed of 450 rpm until the PVA was completely solubilized. To prevent water loss, the gel container was covered by Parafilm and slowly brought to room temperature before use. The ionic conductivity of the gel electrolyte was measured to be $3.61 \times 10^{-4} \text{ S cm}^{-1}$ at room temperature using a four-point probe conductivity meter connected to a Keithley 2602 SourceMeter instrument.

5.3.3 Device Fabrication and Characterization

A few simple steps were followed to fabricate flexible fiber-shaped supercapacitors (Figure 28 (a)). First, using a glue gun, toothpicks were glued to two-holes round sewing buttons with the diameter of 1.2 cm and 2 mm spacing between the holes. A couple of the buttons were held at a distance of 10 cm by inserting the toothpicks into a piece of a Styrofoam. A parallel structure of two conductive threads was made by passing the threads through the buttons' holes and stretching the fibers before gluing them to the buttons (Figure 28 (b)). A piece of copper tape was used at the end of each thread for reliable electrical connection during the measurement. The

PVA-based gel electrolyte was uniformly coated on each fiber electrode separately and kept for 24 h to make it dry at room temperature. The dried coating was used instead of a separator to avoid short circuit when the fibers were twisted. Then, the fiber electrodes were coated with the gel electrolyte again and twisting them to make fiber supercapacitors with a twisted structure. The performance of the devices was studied for each device with 1 to 6 turns which are referred here as T1-T6. Since the lateral stress between the two fibers increases with the number of turns, some samples showed short circuit between the two fibers for $T > T_6$, where T is the number of turns.

Princeton Applied Research VersaSTAT 4 was used to carry out all electrical and electrochemical experiments in a two-electrode configuration. Cyclic voltammetry (CV), galvanostatic charge-discharge, and electrochemical impedance spectroscopy (EIS) experiments were performed to test the performance of the fiber supercapacitors at room temperature and under the same experimental conditions. Scanning electron microscopy method was applied to study the fiber structures. A 12 MP digital camera was used to take pictures of the samples at different twisting turns. The digital images were later analyzed using the image processing tool in MATLAB (R2017).

5.4 Results and Discussion

5.4.1 Device Characterization

CV measurements were conducted for all devices for six twisting turns in the potential range between -0.5 V and $+0.5$ V at a scan rate of 50 mV s^{-1} . The voltage range was deliberately limited to 0.5 V to avoid water electrolysis. Figure 29 (a) shows the CV results of the fiber supercapacitor based on Jameco threads with 1 to 6 twisting turns. For devices with one and two turns (T_1 and T_2), two pairs of redox peaks were observed in the CV curve: one pair around 0.0

V and the other near 0.35 V. With the larger peak current near 0.0 V the second peak was not visible as the device was tested for 3 to 6 turns of twists. The strong redox peaks near 0.0 V suggest a pseudocapacitive behavior that emerged from the surface redox reactions, due to the presence of silver in the structure of the fibers. The redox reaction is a reversible reaction between Ag and Ag⁺ ($\text{Ag}^+ + e \leftrightarrow \text{Ag}$). Considering the symmetrical structure of the device with Jameco working and counter electrodes, a very small over potential is required for the redox reaction. A similar redox peak has been observed in other supercapacitors with the electrodes containing Ag nanoparticles [193, 194]. The weaker peaks (also were observed in Figure 29 (c)) are likely due to the redox active behavior of the gel electrolyte [195]. In our earlier publication [195], we have studied this effect in the PVA gels and we have realized that PO₄³⁻ anion can make or break bonds with the PVA molecules and that results in a weak redox peak in the gel. It should be noted that compare to the redox current through the silver reaction the contribution of the electrolyte redox current is limited. Hence, as the redox current gets stronger in the Jameco device, the second peak vanishes (not visible anymore). A noticeable aspect in the CV curves in Figure 29 (a) is the increase of the redox peak amplitude with increasing the twisting turns, which led to an increase in the capacitance of the device. Since the surface of the threads were covered with the gel even before twisting, the increase in the capacitance with the increase in the number of turns can be explained by the penetration of gel into the dense structure of the Jameco fibers as the threads were twisted. Such effect was not observed in the other threads with a looser structure that the gel was already penetrated deep into them, even before twisting. The CV results of the device based on JL threads showed nearly symmetrical rectangular shapes, as shown in Figure 29 (b). While the capacitance loop increased with the second twisting turn (*T2*), there is no noticeable increase with an increment in number of turns after that, indicating the

device's capacitance limitation. Figure 29c shows a narrow CV loop in the BCP fiber-based supercapacitor with one twisting ($T1$). For $T2$ to $T6$, weak redox peaks were observed with a significant increase in the capacitance area compared to the first twisting turn.

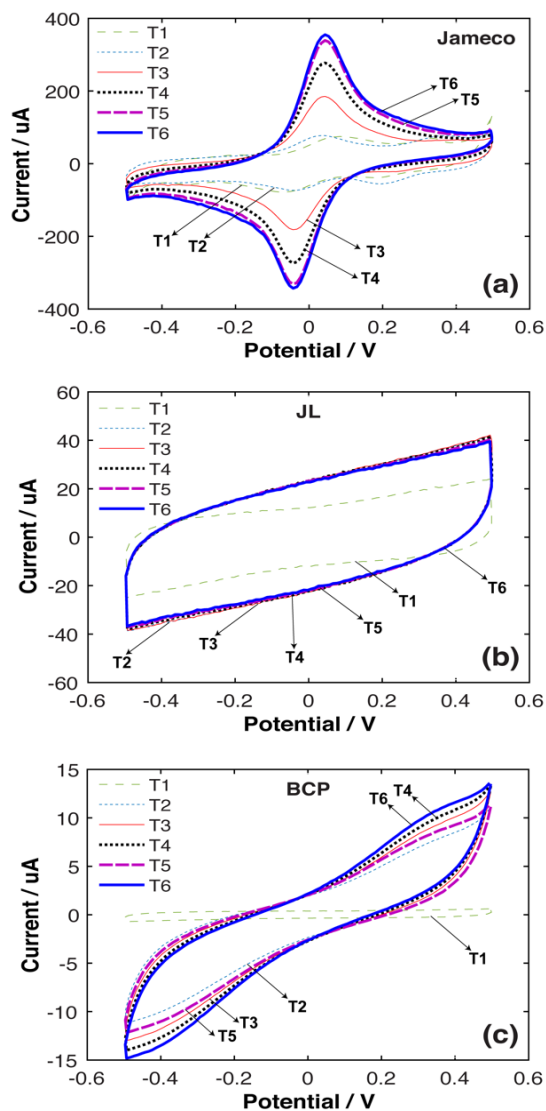


Figure 29: CV curves of the supercapacitors with (a) Jameco, (b) JL, and (c) BCP fibers at different twisting turns.

The specific capacitance values of the supercapacitors with Jameco, JL, and BCP fibers at their highest value (i.e., $T6$) were 15.1 mF g^{-1} , 3.55 mF g^{-1} , and 0.5 mF g^{-1} , respectively. The

significantly larger capacitance in the Jameco device was due to the pseudocapacitive effect because of the redox reaction of the silver coating on the thread, whereas the dominate storage effect in the other two devices (i.e., JL and BCP) was the double layer charges at the electrode-electrolyte interfaces.

The galvanostatic charge/discharge measurements of the fiber supercapacitors made of the Jameco and JL were tested by chronopotentiometry (CP) technique with a constant current of 0.5 mA during the charge cycle and -0.5 mA for the discharge cycle. Due to the smaller capacitance in the BCP devices, the current pulses were reduced to ± 0.05 mA. The results of the galvanostatic tests are presented in the supporting information in Appendix B (Figure S1). The Jameco device exhibited an almost linear voltage profile with a slight distortion during the charging and discharging cycles for one twisting turn ($T1$). Due to strong Faradaic reaction in Jameco fiber at higher turns, the voltage profile was changed to a nonlinear curve. However, JL and BCP fibers gave nearly linear curves during the charging and discharging cycles, as shown in Figure. S1 (b) and (c).

Additionally, electrochemical impedance spectroscopy (EIS) analyses were conducted for studying the electrical behavior of the devices at different twisting turns. A frequency range of 0.1 Hz to 10 kHz was used for the impedance studies at 0.0 V DC bias and a sinusoidal signal of 20 mV. Figure S2 (a-c) show the Nyquist plots of the supercapacitors with Jameco, JL and BCP fibers at different number of turns. The impedance spectra at the high frequency exhibited small series resistance, especially for Jameco and JL fibers. At the low frequency, the diffusion tail slope for ($T1$) is nearly 45° , suggesting a diffusion-controlled reaction represented as a constant phase element (CPE). For better understanding the difference between the samples at different twisting turns, the Bode plot of the impedances for each sample at $T1$ and $T6$ are shown in Figure

30. An equivalent circuit model consisting of two stages was suggested to represent the charge storage at the electrode-electrolyte interface (C_{dl}) and in the bulk of the gel electrolyte (C_{gel}) [195].

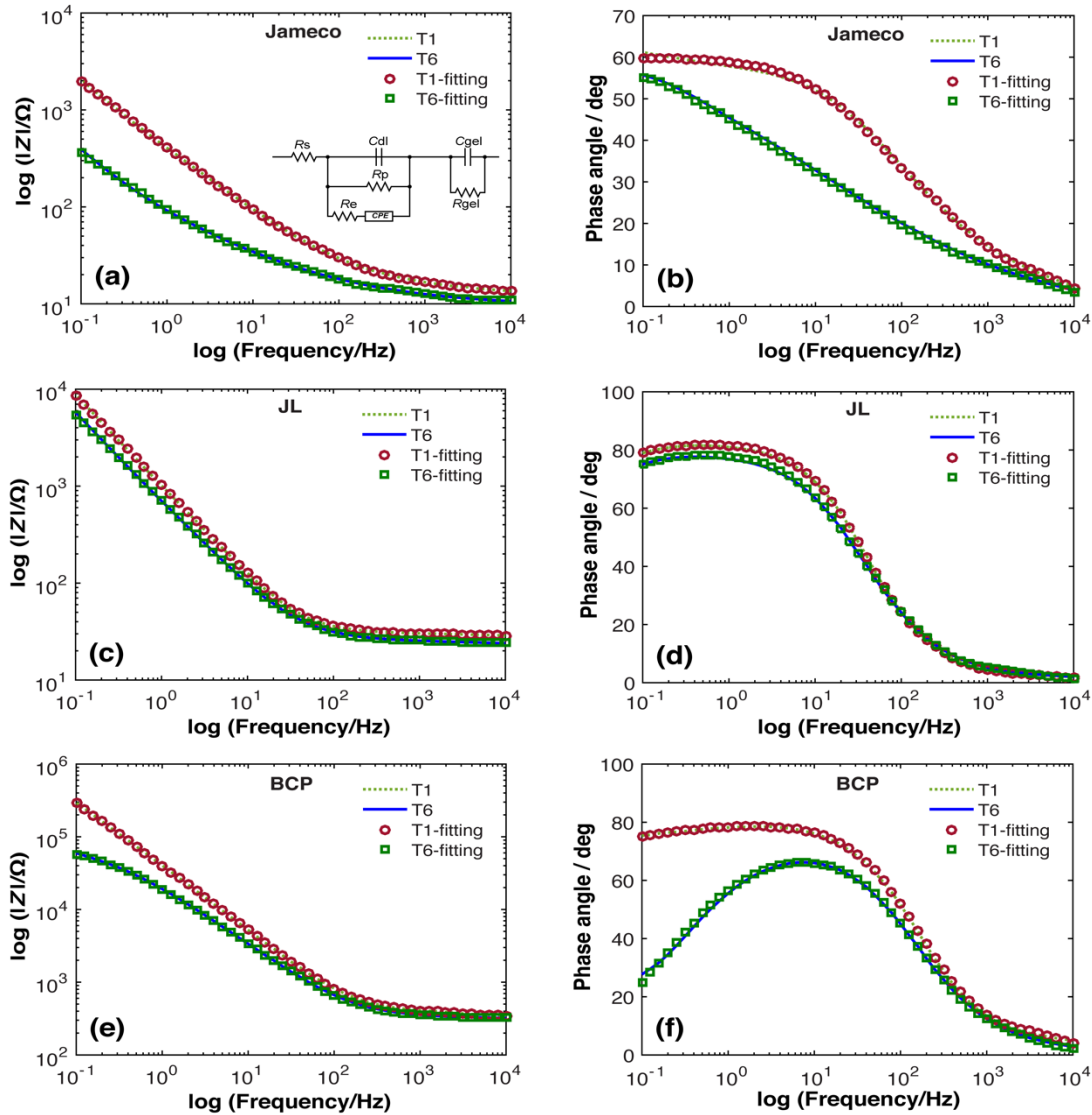


Figure 30: Experimental and fitted results of the impedance magnitude and phase for the supercapacitors with (a,b) Jameco, (c,d) JL, and (e,f) BCP fibers at T1 and T6. (Inset) the equivalent circuit model.

Using EIS Spectrum Analyzer (version 1.0) free software, the impedance results were analyzed. Table 4 shows the suggested values for the capacitances, resistors and the constant phase element (*CPE*) in each case. As shown in Figure 30, the simulated results from the small-signal equivalent model are in perfect match with the experimental data. A noticeable feature in the results is the small changes in the EIS response of JL from *T1* to *T6*. However, the behavior of Jameco and BCP devices are very different at *T1* and *T6*. The differences are well reflected in the values of the elements of the circuit model as presented in Table 4.

Table 4: Impedance parameters of different fiber supercapacitors based on the number of twists per length.

Devices	R_s (Ω)	R_p (Ω)	C_{dl} (μF)	C_{gel} (μF)	R_{gel} (Ω)	R_e (Ω)	$0 < n < 1$	Q ($S s^n$)
Jameco <i>T1</i>	13.31	1000000	39.36	21.38	2.13	11.86	0.655	68.11×10^{-5}
Jameco <i>T6</i>	10.81	997500	151.54	49.75	3.29	12.58	0.626	370.5×10^{-5}
JL <i>T1</i>	28.49	141380	82.72	21.99	1.74	28.52	0.855	9.65×10^{-5}
JL <i>T6</i>	23.93	69523	102.76	40.27	1.97	40.13	0.825	17.13×10^{-5}
BCP <i>T1</i>	341.89	8172600	1.86	0.88	54.57	796.23	0.784	3.24×10^{-6}
BCP <i>T6</i>	320.7	77917	2.33	2.88	30.37	417.14	0.402	9.36×10^{-6}

Most of the values in JL *T1* and JL *T2* are almost the same or at least in the same range. However, R_p has changed significantly in the BCP sample from *T1* to *T6*. Also, as it is evident in Figure 30 (e) and (f) that the nature of *CPE* changed from *T1* to *T6* when n was decreased from 0.784 to 0.402. It should be noted that although the resistance in Jameco and JL are at the same range, the capacitance from the Jameco device was significantly higher because of two reasons: (1) the packed structure of Jameco (providing much higher internal surface area) and (2) the

pseudocapacitive effect due to the presence of Ag in the composition of Jameco. Overall, the results show that, in comparison to the other two, the JL based capacitor had a more consistent electrical behavior at different turns. Since the conductive material in JL and BCP is the same (i.e., stainless steel), we have studied the effect of the thread structures on the structure of the devices when two threads were twisted.

5.4.2 Image Processing

To better understand the structure of each fiber, SEM images were taken. While Figure 31 (b), (d), and (f) show that the micro-fibers of each sample were uniform (Jameco with $\sim 30\ \mu\text{m}$, JL and BCP with $\sim 10\ \mu\text{m}$ in diameter), their thread structure in Figure 31 (a), (c), and (e) are very different.

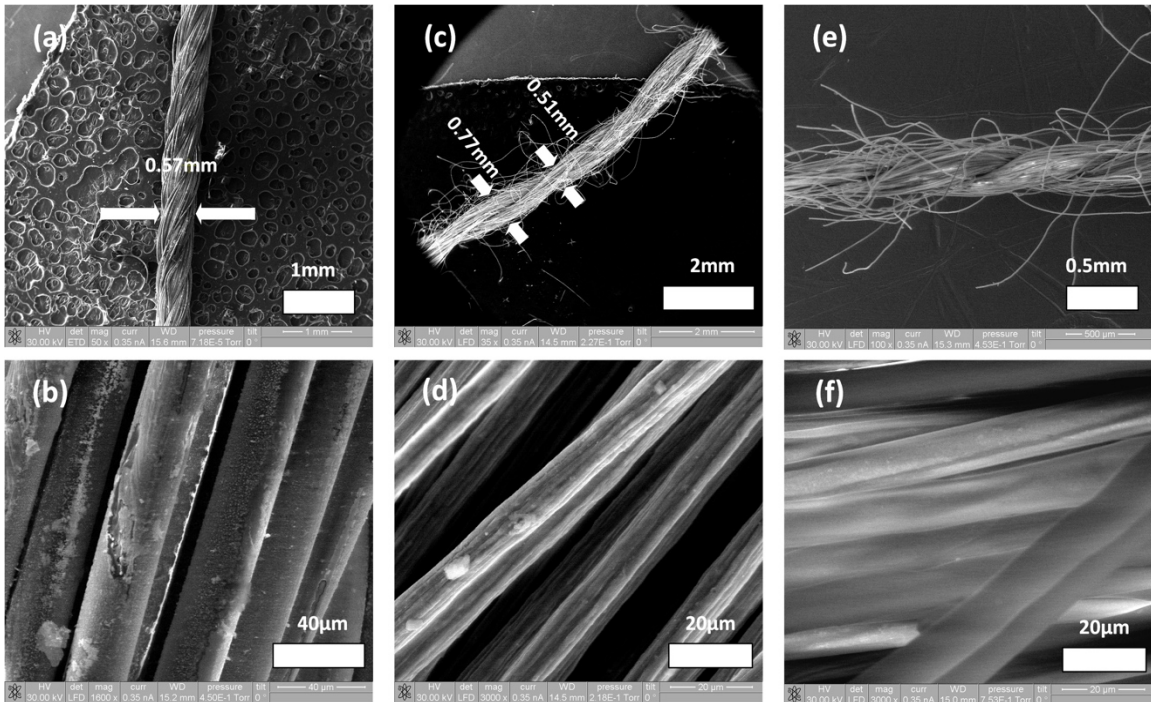


Figure 31: SEM images of (a,b) Jameco, (c,d) JL, and (e,f) BCP threads.

Jameco with the nylon fibers had a packed and uniform thread diameter of ~ 0.57 mm. The purchased stainless steel thread from JL had a structure of a twisted pair with the node and antinode diameters of ~ 0.51 mm and ~ 0.77 mm, respectively. The stainless steel mixed with polyester thread (i.e., BCP) had the finest diameter of 0.42 mm. A notable feature of the JL and BCP threads was their fuzzy (hairy) structure. The initial gel coating on each fiber (before twisting) apparently is effective to reduce their fuzzy surface for not short circuiting the devices (Figure S3).

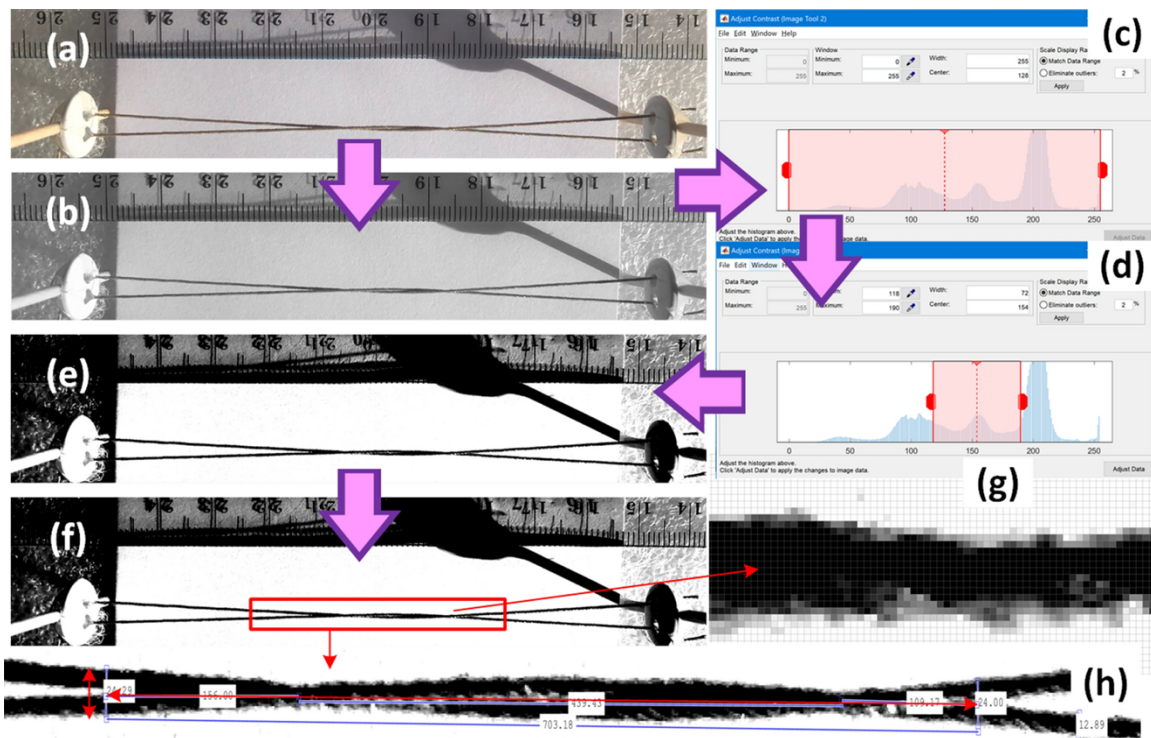


Figure 32: Image processing steps: (a) reading the image files, (b) converting to the black and white, (c) opening the adjust contrast tool, (d) adjusting the minimum and maximum of the contrast range to get (e) the images with high contrasts. (f) Analyzing the image with (g) the inspect pixel values and (h) the measure distance tools. (The image is from the Jameco device at T_2 turns).

To understand the reason for the change in the capacitance when the threads were twisted, digital images were taken from the devices with $T1$ to $T6$ turns. Before processing, the images were cropped to reduce the size of the digital files from 3024×4032 pixels to 3024×627 (Figure S4). Each image was opened in MATLAB, using `imread()` and `imshow()` instructions (Figure 32 (a)). Then, the pictures were converted to black and white using `rgb2gray()` function and opened with `imtool()` in MATLAB (Figure 32 (b)). Using the Adjust contrast tool with the consideration of the contrast map, the minimum and maximum of the contrasts were set at 118 and 190 values, respectively (Figure 32 (c-e)). The high contrast images were further analyzed using the Inspect pixel values and the Measure distance tools (Figure 32 (f-h)). To measure different features, simply pixels with a value less than 175 (gray and black pixels) were counted, assuming to be the image of the fibers. Measuring the number of pixels between two marks on the ruler in the picture, number of the pixels were converted to the mm scale. The average diameter of each thread (t), the effective length of the twisted structure (L), the thickness of the twisted structure at nodes (δ_{\min}) and antinodes (δ_{\max}) were measured and are reported in Table 5. The concept of each feature is shown in the schematic in Figure 28 (b). The processed images showed large differences from $T1$ to $T2$ in all the samples, particularly the effective length was increased more than twice between $T1$ and $T2$. However, incremental changes in L were observed from $T2$ to $T6$. The measured data shows that at each turning state, L in BCP was the shortest due to its low thread diameter, t . Another noticeable feature was the variation in the thicknesses at the nodes and antinodes. In Jameco, δ_{\max} was almost equal to $2 \times t$, but $\delta_{\max} < (2 \times t)$ in the JL and BCP devices for all cases from $T1$ to $T6$. To study the uniformity of the twisted structures, normalized $\Delta\delta = (\delta_{\max} - \delta_{\min})$ to the thickness of the threads ($\Delta\delta/t$) were calculated and reported as the uniformity factor in Table 5. While the variation in the thickness of the structure

was near or higher than 100% of the thickness in the Jameco devices, JL showed much more uniform structure. Specifically, at T_6 Jameco had 160% variation in the thickness while the uniformity factor was only 21% in the JL sample. This is mainly due to the structure of JL thread being made of a twisted pair in each thread. As shown in Figure 31 (c), the JL thread has a non-uniform thickness along its length ($0.54 \text{ mm} \leq t \leq 0.71 \text{ mm}$) which has affected on how the two threads were entangled when twisted in a device (Figure S5).

Table 5: Measured dimensions of the samples using the image processing tool in MATLAB and calculated the uniformity factor in the twisted structures.

Devices	Jameco (Nylon+Ag coating) (mm)	JL (SS fibers) (mm)	BCP (Polyester+SS) (mm)
Thread diameters	$t = 0.52$	$t = 0.54-0.71$ $t_{ave} = 0.625$	$t = 0.38$
T_1	$\delta_{min} = 0.53$ $\delta_{max} = 1.07$ $L = 13.6$ $\Delta\delta/t \times 100 = 104\%$	$\delta_{min} = 0.65$ $\delta_{max} = 1.04$ $L = 14.5$ $\Delta\delta/t_{ave} \times 100 = 63\%$	$\delta_{min} = 0.38$ $\delta_{max} = 0.56$ $L = 11.9$ $\Delta\delta/t \times 100 = 47\%$
T_2	$\delta_{min} = 0.61$ $\delta_{max} = 1.07$ $L = 31.7$ $\Delta\delta/t \times 100 = 88\%$	$\delta_{min} = 0.74$ $\delta_{max} = 1.04$ $L = 31.8$ $\Delta\delta/t_{ave} \times 100 = 49\%$	$\delta_{min} = 0.34$ $\delta_{max} = 0.56$ $L = 23.4$ $\Delta\delta/t \times 100 = 57\%$
T_3	$\delta_{min} = 0.52$ $\delta_{max} = 1.00$ $L = 40.1$ $\Delta\delta/t \times 100 = 92\%$	$\delta_{min} = 0.69$ $\delta_{max} = 1.03$ $L = 43.8$ $\Delta\delta/t_{ave} \times 100 = 55\%$	$\delta_{min} = 0.25$ $\delta_{max} = 0.55$ $L = 28.6$ $\Delta\delta/t \times 100 = 79\%$
T_4	$\delta_{min} = 0.44$ $\delta_{max} = 1.10$ $L = 53.9$ $\Delta\delta/t \times 100 = 127\%$	$\delta_{min} = 0.69$ $\delta_{max} = 0.95$ $L = 48.1$ $\Delta\delta/t_{ave} \times 100 = 42\%$	$\delta_{min} = 0.30$ $\delta_{max} = 0.55$ $L = 36.8$ $\Delta\delta/t \times 100 = 65\%$
T_5	$\delta_{min} = 0.53$ $\delta_{max} = 1.10$ $L = 59.0$ $\Delta\delta/t \times 100 = 109\%$	$\delta_{min} = 0.84$ $\delta_{max} = 1.07$ $L = 60.3$ $\Delta\delta/t_{ave} \times 100 = 37\%$	$\delta_{min} = 0.30$ $\delta_{max} = 0.55$ $L = 40.7$ $\Delta\delta/t \times 100 = 65\%$
T_6	$\delta_{min} = 0.39$ $\delta_{max} = 1.22$ $L = 64.9$ $\Delta\delta/t \times 100 = 160\%$	$\delta_{min} = 0.88$ $\delta_{max} = 1.01$ $L = 68.0$ $\Delta\delta/t_{ave} \times 100 = 21\%$	$\delta_{min} = 0.25$ $\delta_{max} = 0.51$ $L = 47.1$ $\Delta\delta/t \times 100 = 68\%$

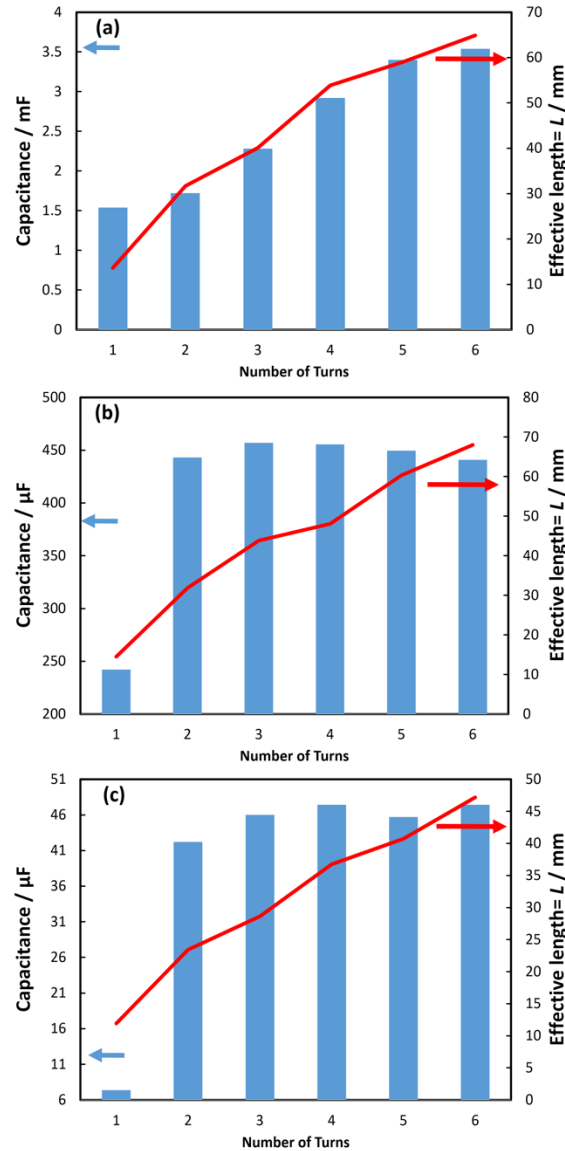


Figure 33: The magnitude of the capacitances and the effective length of the twisted structures vs. number of the twisting turns in the (a) Jameco, (b) JL, and (c) BCP devices.

The JL thread structure had also an effect on the stress between the two threads. As the reported values in Table 5 shows, in the Jameco and BCP samples, the lowest amount of δ_{\min} occurred at T_6 reflecting the effect of the lateral stress between the fibers at the larger number of turns. In contrast, at T_6 , δ_{\min} in JL was not the lowest. Again, this can be explained through the JL thread structure. Because of the twisting structure of the JL threads (Figure 31 (c)), when two

threads were twisted in a device, the threads intertwined along each other with relatively a lower level of lateral stress compared to the solid structure of Jameco threads.

The correlation between the effective length of the twisted-fiber structure and their capacitances was further studied in Figure 33. The change in the capacitance in the Jameco device showed a gradual increase with the number of turns. The capacitance increase from *T2* to *T6* was 2.05 times which is in good agreement with the increase in the effective length from 31.7 mm in *T2* to 64.9 mm in *T6* (2.04 times increase). However, the capacitance variation in the JL and BCP devices does not show any correlation with the effective length. As observed, the capacitance value increased after *T1* in BCP and JL devices and stayed almost at its maximum value. A reason could be the hairy structure of the stainless steel based threads that dominates the capacitance when the fibers are close enough to have the gel bridging between them. Since the entire fiber length is coated with the gel electrolyte, a part of the structure that fibers are not twisted but extended along each other can participate in the charge storage.

The results suggest that the structure of threads is important when designing a twisted-fiber supercapacitor. Specifically, the dual-fiber structure of JL and its non-redox active material of the threads (stainless steel, in contrast to Ag in Jameco) result in fabrication of devices with consistent and predictable electrical properties. Although the structure of threads plays a vital role in the storage performance of fiber-based supercapacitors, the performance can be further optimized by studying the concentration, conductivity, viscosity, tensile, and aging effect of the gel electrolyte. In particular, the effect of losing water from the gel electrolyte under ambient conditions (and even absorbing water if the supercapacitor devices are used in washable wearable electronics) need to be studied to find the potential applications of the twisted fiber supercapacitors.

5.5 Conclusion

In conclusion, using the image processing tools in MATLAB, the structure of twisted fibers from different thread materials was analyzed to find the effective length and study the uniformity of the twisted structures at different number of turns. The measured capacitances from various twisted fiber structures revealed that when the conductive threads are made of smooth and uniform threads (e.g., Ag-coated nylon fibers in the Jameco threads), the capacitance is directly related to the effective length of the device. However, a more uniform twisted structure can be achieved from stainless steel threads with dual-twisted fiber thread structure. The results can be used in the future for designing more efficient wearable energy storage devices.

Chapter 6: A Flexible Fiber-Shaped Hybrid Cell with a Photoactive Gel Electrolyte for Concurrent Solar Energy Harvesting and Charge Storage⁵

6.1 Abstract

Fiber-shaped solar energy harvesting and storage devices are promising flexible hybrid systems for next-generation wearable electronics. Here, three flexible fiber-shaped hybrid devices were designed and fabricated by twisting two different conductive threads as electrodes and a photoactive gel-based electrolyte. In all three devices, the electrolyte was a composite gel of polyaniline (PANI), polyvinyl alcohol (PVA), and an acid (H_3PO_4) and the cathode electrode was a piece of a commercially available stainless steel-based thread. However, for two of the devices, conductive threads, one coated with Ag and another coated with carbon nanotube (CNT), were used as the anode electrodes with different work functions. In the third device, ZnO nanowires (NWs) were grown on the CNT coated threads as the electron transport layer (ETL) on the anode. The capacitance, photovoltage, and photocurrent of all three devices were measured. The highest capacitance was found to be 10.1 mF cm^{-1} in device with the anode made of Ny66-Ag/CNT, while a photovoltage of 37 mV was measured in the device with the ETL when exposed to light for 400 s. The current results provide a new design strategy with a flexible structure and simple fabrication process for the fiber-shaped hybrid devices with the dual properties of energy harvesting and storage.

⁵ This chapter has been submitted to journal of Advanced Functional Materials. (T. Kareri, M. Hossain, M. K. Ram, and A. Takshi. (2022). A Flexible Fiber-Shaped Hybrid Cell with a Photoactive Gel Electrolyte for Concurrent Solar Energy Harvesting and Charge Storage. Submission confirmation letter is included in Appendix A.

6.2 Introduction

Science is making rapid steps towards the era of artificial intelligence and the internet of things to provide an intelligent future that can enhance the speed, accuracy, and effectiveness of research, human, and industrial efforts. In this process, the new generation of electronics must keep pace with this development and comply with the requirements in terms of shape, flexibility, functionality, and performance for the new applications. Currently, majority of the wearable electronics are made of circuits being fabricated on a flexible substrate and glued/sewn to fabrics.[15] Such structures lack the required flexibility for convenient wearable electronics. Hence, the focus is drifting toward fiber-based devices and systems that can be integrated into fabrics. Considering the required powers for such electronics, fiber-shaped supercapacitors and fiber-shaped solar cells have attracted increasing scientific attention [17, 196]. Various types of fiber-shaped supercapacitors have been reported in recent years with parallel [197, 198], twisted [188], and coaxial fiber structures [191, 199] fabricated with different methods using various types of the electrode materials (i.e., carbon-based [191], metallic [197], and composite materials [188, 198, 200]). Some of the devices have presented relatively high power densities, fast charging/discharging, and long cycle life. However, the low energy density and high self-discharge in such devices are among challenges that require more scientific studies [16]. Also, energy harvesting devices (e.g., solar cells) can be fabricated using fibers and threads. Different types of fiber-shaped solar cells have been reported recently, such as dye-sensitized solar cells [201-203], perovskite [204, 205], and organic solar cells [206].

Integrating electrochemical energy storage and harvesting in a single fiber-based hybrid device presents unique features and potential for wearable applications and self-powered systems. However, some issues and challenges need to be overcome, such as low efficiency and

performance, low mechanical and electrochemical stability, and cost of fabrication [17]. Although the majority of the reported hybrid devices for wearable electronics were made with flat structures stacking solar cells and supercapacitors being attached to textile [207], some devices used conductive threads as the electrodes to make fiber shape supercapacitors and solar cells connected together to make a hybrid system [208]. Dye-sensitized solar cells are widely used as an energy conversion unit in most fiber-shaped hybrid devices due to their low cost, reasonable efficiency, and ease of fabrication, and they can be fabricated with the energy storage unit on the same thread (electrode) [112, 113] or different threads separately, which can be woven into textiles [114]. However, the complexity in fabricating solar cells and supercapacitors on threads is a major concern for their applications in wearable electronics.

In the attempt for developing two-terminal hybrid solar cell-supercapacitor devices, previously, we have reported a new class of hybrid devices made from a photoredox active gel electrolyte being placed between two electrodes [133]. The gel was a composite material consisting of polyvinyl alcohol (PVA), polyaniline (PANI), ammonium persulfate (APS), and an acid. The fabrication process of the flat devices was as simple as placing the photoredox active gel electrolyte between two electrodes [133, 173, 209]. In this work, the approach has been transformed for making thin, lightweight, and flexible fiber-shaped hybrid energy storage and harvesting devices with a twisted structure and simple fabrication processes using two conductive threads and the photoactive composite gel electrolyte. Although the gel electrolyte functionality, which can serve both as a redox-active layer and electrolyte, is critical to develop a hybrid device, the work function and structure of the electrodes are also important for efficient charge storage and electron transfer. Hence, we have studied the effect of the different anode thread shape electrodes in devices made with a stainless steel (SS) fiber shape cathode and the

composite gel electrolyte. Three devices were fabricated and compared. The first device was made using a silver-coated nylon 66 (Ny66-Ag) thread and a CNT coated Ny66-Ag thread was used as the anode in the second device. To improve the electron transfer rate from the gel to the anode, the third device had an anode made from a CNT coated thread with a grown layer of ZnO NWs (Ny66-Ag/CNT/ZnO-NWs) as the electron transport layer. Figure 34 shows the simple steps used for fabricating a device and pictures of hybrid devices tested in the lab.

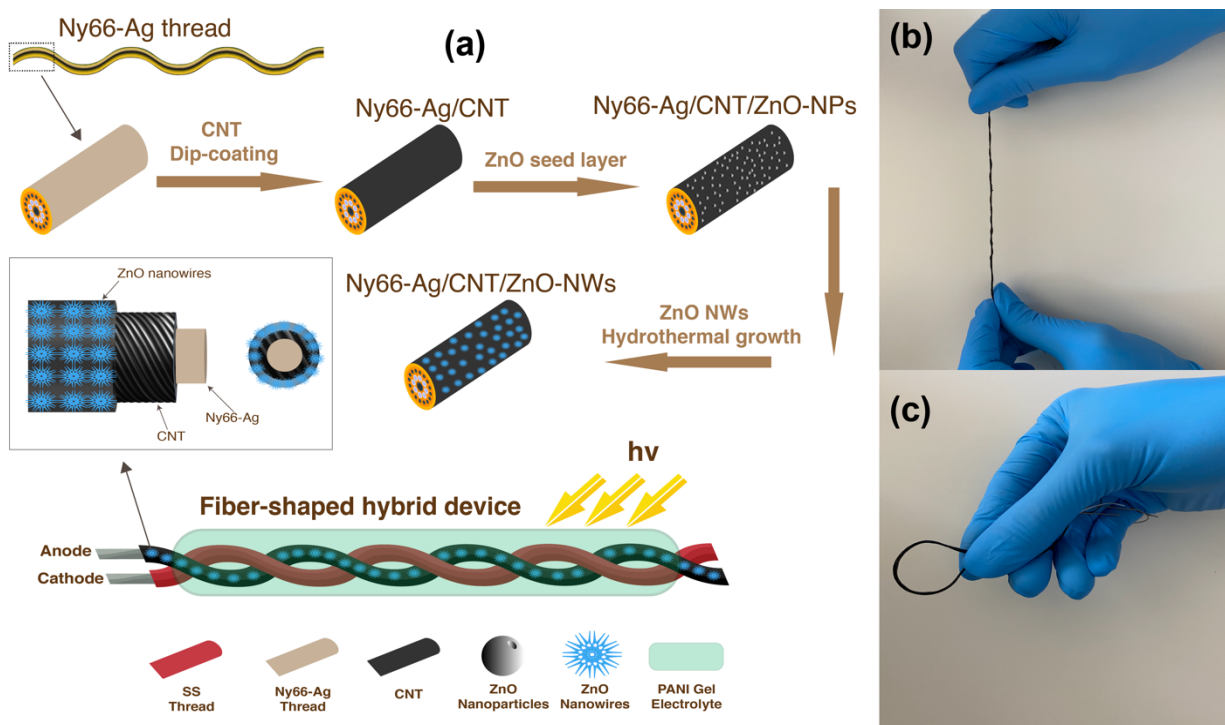


Figure 34: (a) Schematic illustration of the fabrication steps of the Ny66-Ag/CNT/ZnO-NWs anode electrode and the final device structure, (b,c) photographs of the fiber-shaped hybrid devices.

6.3 Experimental Section

6.3.1 Materials

The required chemical materials, including PVA and phosphoric acid (H_3PO_4), ammonium persulfate ($(NH_4)_2S_2O_8$) (APS), aniline (ANI), sodium dodecylbenzenesulfonate

(SDBS), zinc acetate dihydrate (ZAD), sodium hydroxide (NaOH), ethanol, hexamethylenetetramine (HMTA), and ammonium hydroxide (NH₄OH) were purchased from Sigma-Aldrich. Multi-walled CNTs and zinc nitrate hexahydrate (ZNH) were purchased from Alfa Aesar. Silver-coated nylon 66 (Ny66-Ag) conductive thread with a lineal resistance of 50 Ω m⁻¹ and SS-based threads were purchased from Jameco Electronics and Electronics123, respectively.

6.3.2 Preparation of the Gel Electrolyte and the CNT Ink

The composite gel electrolyte was prepared as was described in our earlier work [133]. The process included three steps starting with adding (3 g) of PVA to (2 mL) of H₃PO₄ mixed with (20 mL) of DI water and stirring well on a hot plate at 90° C over a period of 5 h at a speed of 400 rpm until the PVA was completely solubilized. In the second step, (5 mL) solution of (0.1 M) APS in (0.5 mL) of H₃PO₄ was added to the PVA/H₃PO₄ solution at room temperature with continuous stirring for 30 min at 500 rpm. After that, the PVA/PANI composite gel electrolyte was made by adding (0.2 M) of aniline to the PVA/H₃PO₄/APS at room temperature with continuous stirring for 12 h. The CNT ink was made as explained before by dispersing (300 mg) of MWCNT and (150 mg) of SDBS in (30 mL) of deionized (DI) water under probe sonication for 40 min at a power of 30 W and an energy of 40 J [210].

6.3.3 Preparation of Electrodes

Three different anode electrodes were fabricated using Ny66-Ag conductive thread as the base: a) as-purchased Ny66-Ag, b) CNT coated Ny66-Ag thread (Ny66-Ag/CNT), and c) ZnO NWs grown on the CNT coated Ny66-Ag (Ny66-Ag/CNT/ZnO-NWs). The Ny66-Ag/CNT electrode was made through repeated, 10 times, dip-coating of Ny66-Ag threads into the CNT ink followed by drying at room temperature.

For the Ny66-Ag/CNT/ZnO-NWs electrode, the growth of ZnO nanowires on the Ny66-Ag/CNT thread was carried out through a hydrothermal process that depends on the reactions of zinc acetate dihydrate, zinc nitrate hexahydrate, and hexamethylenetetramine [211]. In brief, the seeding solution (ZnO nanoparticles) was first prepared by dissolving (18 mg) of ZAD and (5 mg) of NaOH separately into (20 mL) of ethanol, followed by adequate stirring on a hotplate at 65° C for 25 min. Then, (20 mL) of ethanol was added into the ZAD solution to dilute it, followed by slow stirring at 65° C for 35 min. After the two solutions were brought to the ambient temperature for 30 min, the NaOH solution was slowly added to the ZAD solution using a burette with slow stirring; then, the seeding solution was put into an oven for two hours to crystallize the ZnO nanoparticles. After the crystallization process, a white precipitate was observed, indicating the existence of ZnO nanoparticles in the seeding solution. In order to provide nucleation sites for the growth process, the Ny66-Ag/CNT thread was dipped into the ZnO seeding solution for 5 min and dried for 5 min at 85° C with repeating the process three times to obtain a uniform layer of ZnO nanoparticles.

After the seeding process was done, the growth solution was prepared by dissolving (3 g) of ZNH and (0.7 g) of HMTA separately into (190 mL) of DI water and mixed at room temperature, followed by adding (10 mL) of ammonium hydroxide (NH₄OH) to the final mixture to increase the growth efficiency [212]. The Ny66-Ag/CNT/ZnO nanoparticles thread was immersed in the growth solution and put into an oven at 85° C for 8 hours, then washed and dried at room temperature. A 3D printed holder was designed and used to set the thread horizontally inside the middle of the growth solution to make the growth rate of the ZnO nanowires uniform around the fibers and reduce unwanted deposits during the hydrothermal process (Figure S6) in Appendix C.

6.3.4 Device Fabrication and Characterization

The fiber-shaped hybrid devices were fabricated by cutting 10 cm long pieces of the prepared anode electrodes (Ny66-Ag, Ny66-Ag/CNT, or Ny66-Ag/CNT/ZnO-NWs threads) and a similar size cathode electrode (SS-based conductive thread), covering separately by a uniform thin layer of the PVA/PANI composite gel electrolyte, and drying for 24 hours at room temperature. Then, devices were made by putting the anode and cathode electrodes in parallel with a few millimeters spacing, applying a layer of the gel electrode between them and then twisting the threads for 10 turns (~1 turn per cm).

Surface morphologies and structures of the anode electrodes were characterized via scanning electron microscopy (SEM) and energy-dispersive X-ray spectroscopy (EDS) (HITACHI S-800). VersaSTAT 4 Potentiostat/Galvanostat was used to conduct the electrical and electrochemical experiments in a two-electrode configuration. Different experiments were executed to characterize the electrochemical properties and test the performance of the fiber-shaped hybrid device, including cyclic voltammetry (CV), galvanostatic charge-discharge, open circuit potential (OCP), short circuit current (SCC), and electrochemical impedance spectroscopy (EIS) experiments. To test the fiber-shaped hybrid device under two operation modes (dark and light) and minimize stray light effects in the experiments, the devices were placed in a dark box with an optical fiber connected to a solar simulator (Radiant Source Technology Inc.) with a light intensity of 80 mW cm^{-2} and AM 1.0 interior optical filter.

6.4 Results and Discussion

6.4.1 Characterization

To understand the surface morphology of the fiber-shaped electrodes, scanning electron microscopy (SEM) images were taken before coating with the gel and the device fabrication.

Figure 35a shows an SEM micrograph of the commercial conductive Ny66-Ag thread with an estimated diameter of 560 μm . Also, it can be seen that the microfibers have a uniform structure with $\sim 29 \mu\text{m}$ in diameter for each fiber (Figure 35 (b)). The diameter of the Ny66-Ag/CNT thread remained uniform after coating the Ny66-Ag thread with a layer of CNT, as shown in Figures 35 (c) and 35 (d). Figures 35 (e) and 35 (f) exhibit the surface of the Ny66-Ag/CNT/ZnO-NWs electrode after the hydrothermal growth of ZnO nanowires. The thread was uniformly covered with radially aligned ZnO nanowires with an estimated nanowire length of 2 μm and diameter of 330 nm. For the cathode electrode, SS thread with a diameter of $\sim 490 \mu\text{m}$ (Figure 35 (g)) and $\sim 8.5 \mu\text{m}$ for each fiber (Figure 35 (h)) was used.

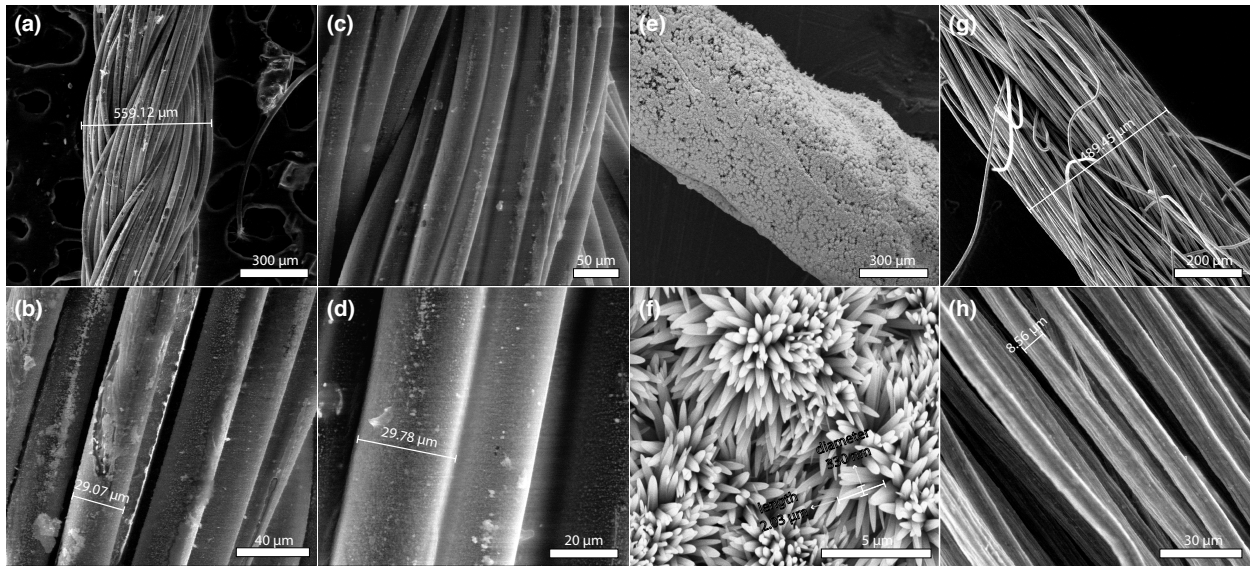


Figure 35: SEM images of (a,b) Ny66-Ag conductive thread at different magnifications, (c,d) Ny66-Ag/CNT electrode surface, (e,f) ZnO nanowires growth on Ny66-Ag/CNT/ZnO-NWs electrode, and (g,h) SS conductive thread at different magnifications.

Furthermore, energy-dispersive X-ray spectroscopy (EDS) analysis was conducted to identify chemical elements on the anode electrodes. The result in Figure 36 (a) confirms the presence of a high percentage of Ag element ($\sim 75 \text{ wt}\%$) in the Ny66-Ag conductive thread. After

adding a CNT layer uniformly on the surface of the Ny66-Ag, carbon and Ag elements appeared in the spectrum with percentages of 48.8 and 50.1 wt%, respectively (Figure 36 (b)). Meanwhile, the elements sodium (Na) and sulfur (S) also appeared due to adding sodium dodecylbenzene-sulfonate (SDBS) surfactant with the CNT ink. The EDS analysis of the Ny66-Ag/CNT/ZnO-NWs electrode indicates a high percentage of Zn, about 92.3 wt%, confirming the homogeneous coverage of the thread surface with the ZnO nanowires (Figure 36 (c)).

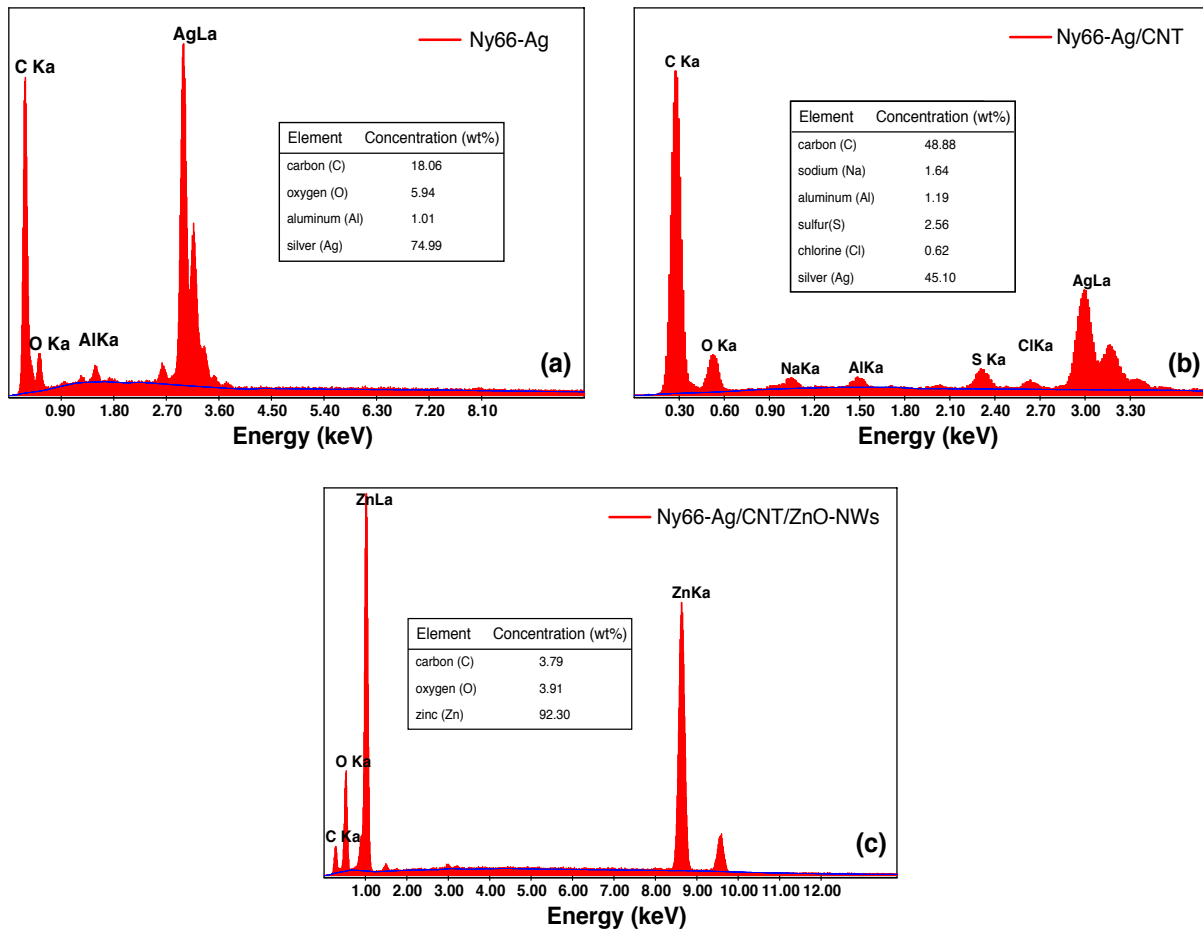


Figure 36: EDS analysis of (a) Ny66-Ag conductive thread, (b) Ny66-Ag/CNT, and (c) Ny66-Ag/CNT/ZnO-NWs electrodes.

6.4.2 Electrochemical Properties of Fiber-Shaped Hybrid Devices

The fabricated devices were characterized using various electrochemical experiments. Cyclic Voltammetry (CV) measurements were executed with the potential range between -0.5 V and 0.5 V at 50 mV s^{-1} scan rate to investigate the energy storage performance of the fiber-shaped hybrid devices. As shown in Figure 37 (a), the CV curve from the first device with the anode of Ny66-Ag showed energy storage capability with both double-layer and pseudocapacitive charge storage mechanisms with redox peaks at 0.2 and 0.4 V. A similar effect of pseudocapacitive storage was observed in our previous work when twisted-fiber supercapacitors were made from a PVA-based gel and two Ny66-Ag electrodes with the strong redox peaks associated to silver [213]. The capacitance of the fiber-shaped hybrid device with the Ny66-Ag electrode was calculated to be 2.9 mF cm^{-1} (or 20.2 mF g^{-1} based on the gel mass) in the dark. As expected, after coating the threads with CNTs, the capacitance in the Ny66-Ag/CNT device was increased to 10.1 mF cm^{-1} likely due to the much larger surface area that CNTs have provided. The CV curves of Ny66-Ag/CNT electrode also show a two-stage charge storage mechanism with shifting the anodic peak to 0.1 V and the cathodic peak to a voltage higher than 0.5 V. Since MWCNTs and stainless steel are not redox active materials, the strong peaks can be due to the redox reactions inside the gel as reported before [133]. However, the change in the cell resistance after coating with CNTs can be the reason for shifting the redox peaks in the two-terminal electrochemical cell. After ZnO nanowires growth on the Ny66-Ag/CNT/ZnO-NWs electrode, the device showed a dominated double-layer charge storage of 6.8 mF cm^{-1} with no redox peaks which is likely due to the thick layer of ZnO NWs and their semiconducting property suppressing reversible redox reactions at the anode [214]. As the results

suggest, the Ny66-Ag/CNT fiber delivers the highest capacitance of 10.1 mF cm^{-1} , compared to the other electrodes.

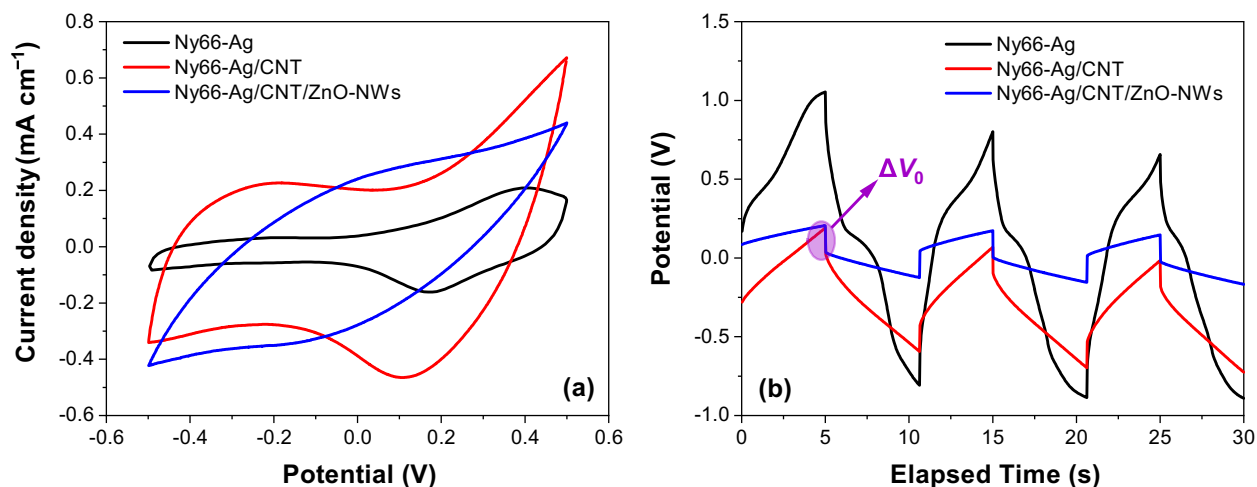


Figure 37: Comparative (a) CV and (b) galvanostatic charge-discharge curves of the fiber-shaped hybrid device with Ny66-Ag, Ny66-Ag/CNT, and Ny66-Ag/CNT/ZnO-NWs anode electrodes tested in dark. The CV scan rate was 50 mV s^{-1} .

Also, each device was tested once in the dark and once under solar simulated illumination. All three devices showed a slight increase in the capacitance under illumination, indicating the solar energy harvesting and energy storage capabilities of the gel electrolyte (Figure S7). However, due to the domination of the capacitive effect, the current-voltage characteristic in the devices are almost the same with a small increase in the voltage and current in the light, due to the generated photovoltage and photocurrent.

To understand the effect of different coatings on the series resistance (R_s), the galvanostatic charge-discharge profiles of the fiber-shaped hybrid devices were studied by chronopotentiometry (CP) method at a constant current of $\pm 500 \mu\text{A}$ for Ny66-Ag and Ny66-Ag/CNT, and $\pm 50 \mu\text{A}$ for Ny66-Ag/CNT/ZnO-NWs. The charge-discharge curves shown in Figure 37 (b) exhibit non-linear shapes for Ny66-Ag and Ny66-Ag/CNT electrodes during the

charging and discharging cycles due to the faradaic reaction [213]. However, the Ny66-Ag/CNT/ZnO-NWs electrode shows an almost linear voltage profile during the charging and discharging cycles, confirming the observed double-layer charge storage mechanism in the CV results [215]. Considering the voltage drop (ΔV_0) at the transition between the charging and discharging cycles, the equivalent series resistance (ESR) of the devices were found to be 102.46 Ω , 111.68 Ω , and 1733.3 Ω for the devices with the anode of Ny66-Ag, Ny66-Ag/CNT, and Ny66-Ag/CNT/ZnO-NWs, respectively.

As shown in Figure S8, in Appendix C, due to the domination of the capacitive effect, the standard I-V characterization for solar cells does not reflect the ability of the hybrid 2-terminal devices [172]. Therefore, the open circuit potential (OCP) and short circuit current (SCC) measurements were conducted to gain further insights into the photovoltaic (PV) performance of the fiber-shaped hybrid devices. As illustrated in Figure 38 (a), OCP of the fiber-shaped hybrid devices was tested with the different anode electrodes in two steps, under illumination for 400 s and in the dark for 600 s. In all devices, the magnitude of the OCP increased during the illumination, confirming the ability of harvesting energy. The negative photovoltage implies electron collections by the anode. For the Ny66-Ag electrode, the magnitude of the photovoltaic potential (ΔV_{ph}) was increased around 30 mV under illumination and slightly decreased to ~28 mV in the dark mode. However, after adding a porous layer of CNT on the electrode (Ny66-Ag/CNT), the voltage of the hybrid device only reached 17 mV in light with a high self-discharge rate in the dark. As expected, the highest OCP was achieved after adding the electron transport layer (ZnO NWs) on the electrode. The photovoltage was improved significantly and reached 37 mV in 400 s of illumination in the device with the Ny66-Ag/CNT/ZnO-NWs electrode.

Besides, SCC measurements were executed under light pulses to evaluate the photocurrent response in the fiber-shaped hybrid device. Since the thickness of the twisted structures were almost the same in all three different devices (~ 1 mm), the current density is reported as the normalized current to the device length, as depicted in Figure 38 (b). Under illumination cycles, the fiber-shaped hybrid device exhibited a photocurrent (ΔI) response around 3.5 nA cm^{-1} , 6.3 nA cm^{-1} , and 15.1 nA cm^{-1} with the Ny66-Ag, Ny66-Ag/CNT, and Ny66-Ag/CNT/ZnO-NWs electrode, respectively. The good repeatability after several cycles of light pulses suggests the stability of the light response. The results clearly show that after adding the ETL of ZnO NWs, the photocurrent was improved significantly. It should be noted that the negative OCP and positive photocurrent implies the generation mode in all devices [145].

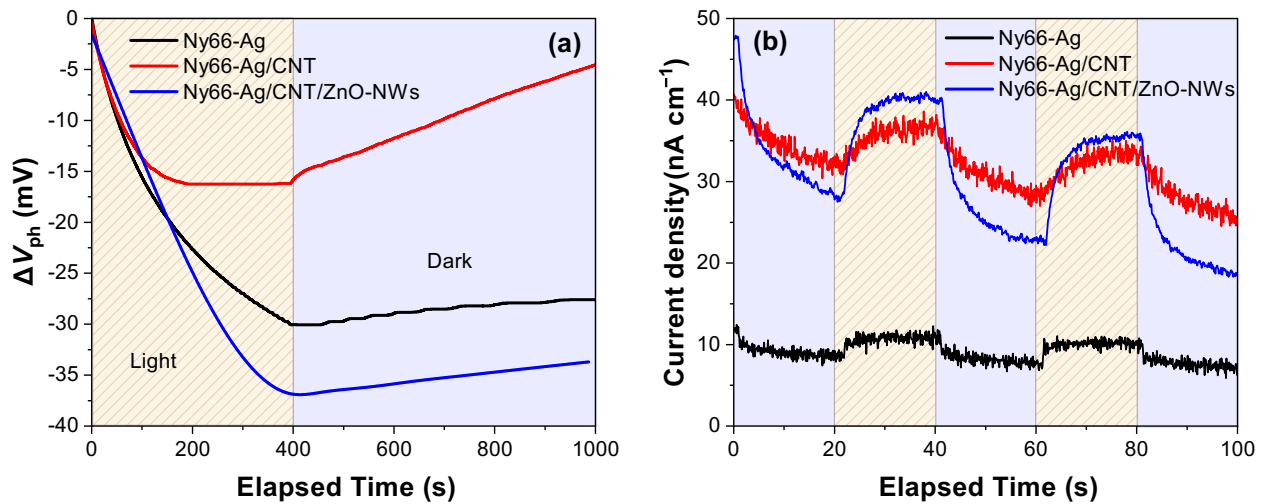


Figure 38: Comparative measurements of (a) open circuit potential of the fiber-shaped hybrid devices with Ny66-Ag, Ny66-Ag/CNT, and Ny66-Ag/CNT/ZnO-NWs anode electrodes and (b) short circuit current under light pulses.

Electrochemical impedance spectroscopy (EIS) measurements were conducted to study the behavior of the interface between the electrodes and the electrolyte in the devices. The EIS experiments were conducted in a frequency range of 10 kHz to 0.1 Hz at 0 V DC bias and a

sinusoidal signal of 15 mV. Figure 39 exhibits the Nyquist plots of the fiber-shaped hybrid devices under the dark and light conditions.

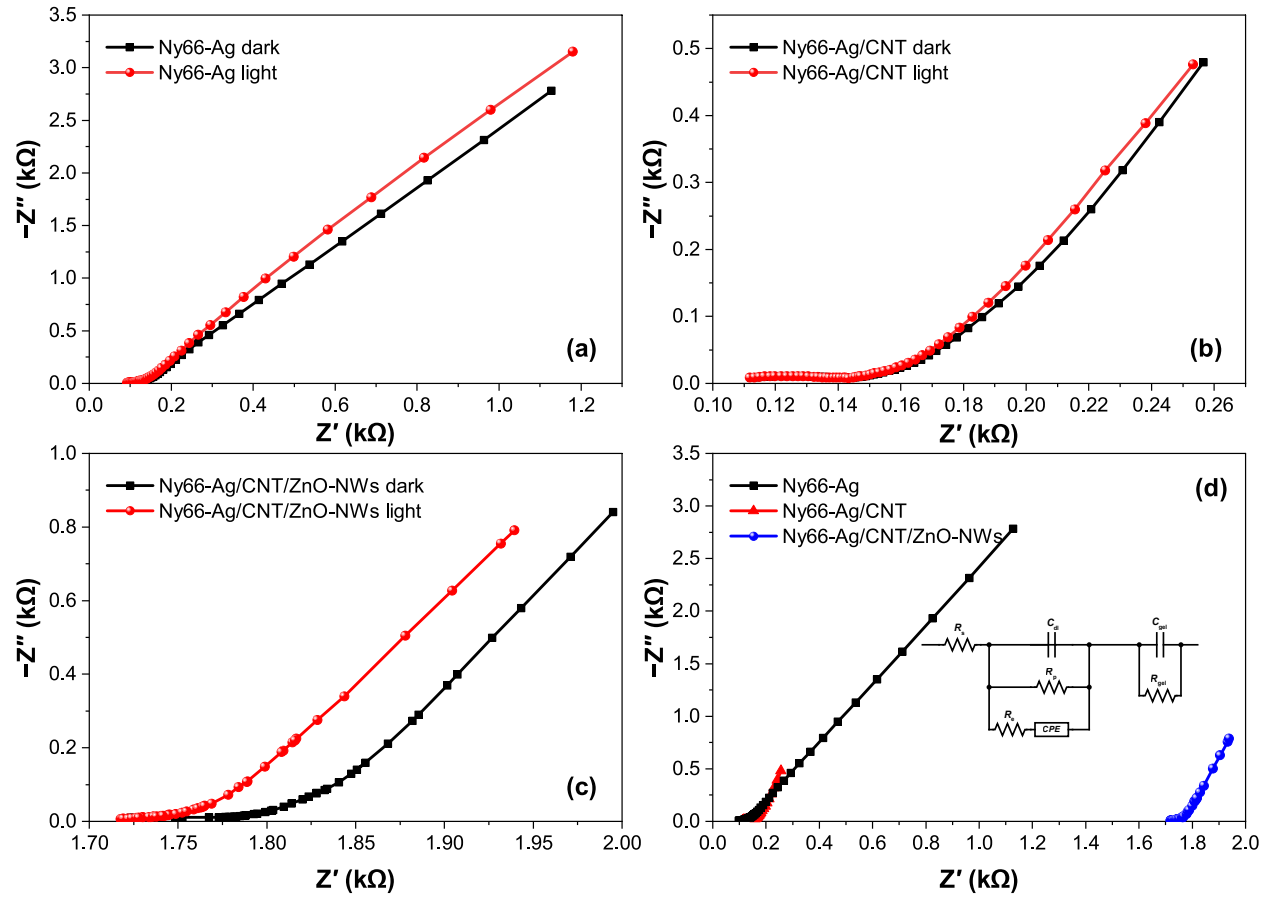


Figure 39: Nyquist plots of the fiber-shaped hybrid device with (a) Ny66-Ag, (b) Ny66-Ag/CNT, and (c) Ny66-Ag/CNT/ZnO-NWs anode electrodes in the dark and under illumination; (d) comparative Nyquist plots of the devices in the dark condition. (Inset) the electrical equivalent circuit model.

The impedance results of the devices with the Ny66-Ag and Ny66-Ag/CNT electrodes showed relatively small series resistances at the high frequency compared to R_s in the Ny66-Ag/CNT/ZnO-NWs electrode. At lower frequencies, the diffusion tail slope for all electrodes revealed an inclination of almost 45°. To compare the differences in different electrodes under the dark and light conditions, a simple electrochemical equivalent circuit was suggested. The

measured EIS spectra were fitted to the simulated model using EIS Spectrum Analyser software based on the proposed equivalent circuit in Figure 39 (d), representing the two-stage charge storage mechanism at the electrode-electrolyte interface (C_{dl}) and in the bulk of the gel electrolyte (C_g) [173]. The equivalent circuit model is also described by the series resistance of the device (R_s), the resistance of the photoactive gel electrolyte (R_g), and the constant phase element (CPE). The fitting parameters are listed in Table S1 (Supporting Information), in Appendix C. Comparing the results in Figure 39 (a-c), it was observed that the effect of illumination on the impedance in the devices with the Ny66-Ag and Ny66-Ag/CNT electrodes was not significant, while a noticeable change was found in R_s with the Ny66-Ag/CNT/ZnO-NWs electrode under illumination. In that device, R_s dropped from 1733.3 Ω in the dark to 1713.4 Ω under simulated solar illumination.

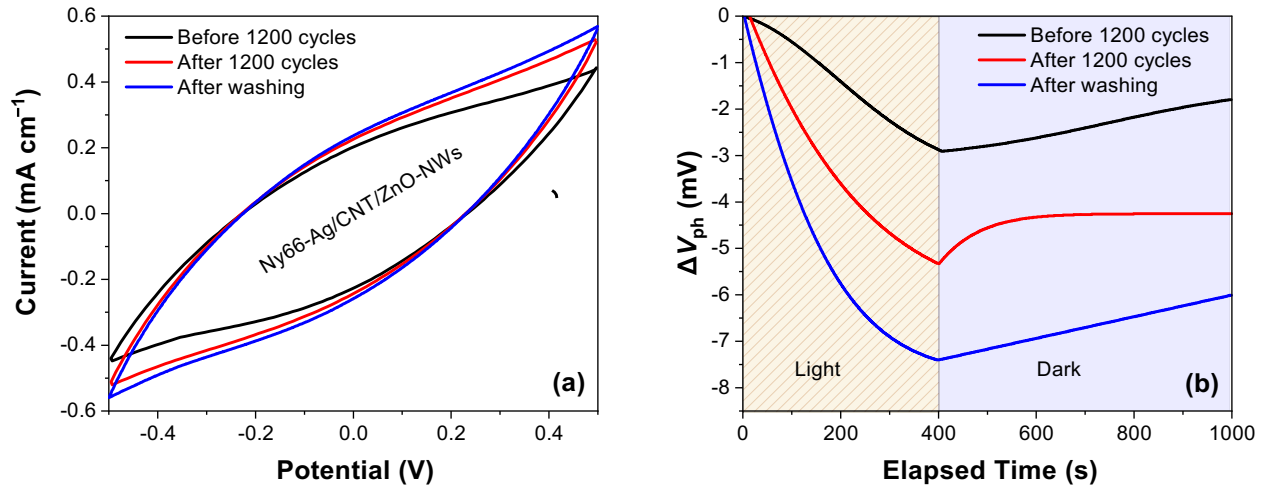


Figure 40: Stability measurements of the device with the Ny66-Ag/CNT/ZnO-NWs electrode. (a) CV curves before/after 1200 cycles at 50 mV s⁻¹ and after washing process. (b) Photovoltaic performance during the stability measurements.

The stability of the device with ZnO NWs was further studied by testing it 4 months after the fabrication while being stored in the lab. Following the test, the device was charged and

discharged for 1200 cycles with a scan rate of 50 mV s^{-1} . The performance of the device was tested again after the cycles. The results of the CV and the OCP measurements are presented in Figure 40. While the capacitance was 6.8 mF cm^{-1} (Figure 37 (a)), the CV result in Figure 40 (a) shows a drop in the capacitance to 5.6 mF cm^{-1} after being stored for 4 months. However, after 1200 cycles of charging and discharging, the capacitance was increased to 6.3 mF cm^{-1} encouraging frequent use of the device to maintain the original energy storage capability. Since the device was not sealed, there was a question if the degradation in the device performance was due to the loss of water in the composite gel over the storage time. Therefore, after the cycling test, the device was soaked in water and left for a day to dry before testing. The process mimics washing wearable electronics. The CV results showed an increase of the capacitance to 6.7 mF cm^{-1} which was almost as high as the original capacitance of 6.8 mF cm^{-1} . The effect of aging, cycling, and washing on the photovoltaic performance of the cell was studied through the OCP measurement in Figure 40 (b). Unfortunately, the photovoltaic response was significantly weaker after 4 months storage resulting in only $\Delta V_{\text{ph}} = \sim 2.8 \text{ mV}$. Similarly, after 1200 cycles of charging and discharging (CV in dark), the performance was slightly improved to achieve an OCP of 5.4 mV . Further increase (by 37%) was observed after the washing process. However, the overall photovoltaic effect was much weaker than the original performance.

In order to understand the operation of the hybrid device, the energy levels of the cathode, PANI, APS, and the anode before and after adding the CNT layer and ZnO NWs were considered. Figure 41 illustrates the comprehensive energy diagram of the devices. The gel is a composite material. However, since PVA is not a conductive material and H_3PO_4 is acting as the supporting electrolyte, we have considered the energy levels in PANI and the electrochemical potential of APS. Chemical polymerization of aniline in presence of APS and an acid produces

PANI in its emeraldine salt (ES) state [216]. Based on the two peaks in the UV-vis absorption spectrum of the gel (Figure S9), the energy levels in the PANI is expected to have a polaron state 2.8 eV lower than the lowest unoccupied molecular orbital (LUMO) [133].

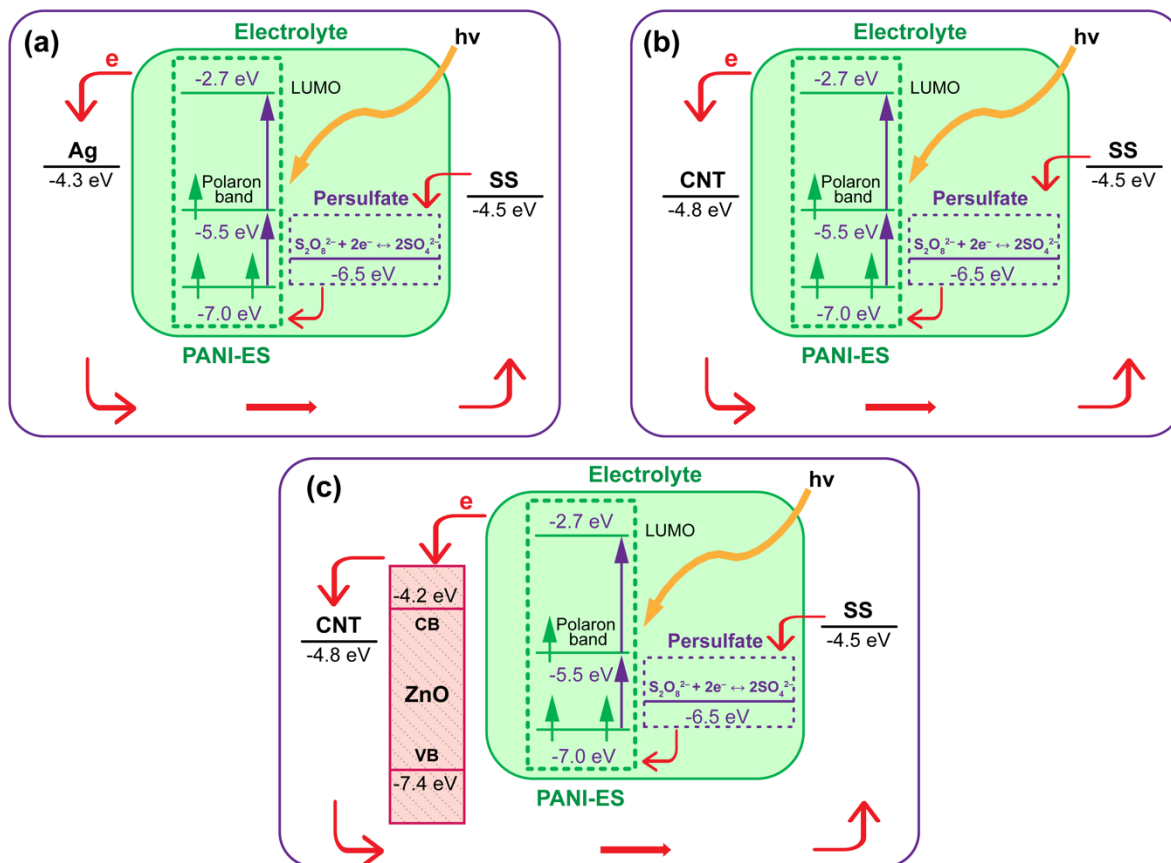


Figure 41: Energy diagram of the fiber-shaped hybrid device with (a) the Ny66-Ag, (b) Ny66-Ag/CNT, and (c) the Ny66-Ag/CNT/ZnO-NWs electrode.

As shown in Figure 41, absorption of photons can promote electrons from lower states to the LUMO level. Persulfate anion acts as a mediator between PANI and the cathode by interacting with the lost electrons in the lower states in PANI and receiving electrons from the cathode (work function of -4.5 eV [217]) in a reversible reaction ($S_2O_8^{2-} + 2e^- \leftrightarrow 2SO_4^{2-}$). While the transfer of electrons from the cathode to the PANI is expected to be the same in all three devices,

it is expected that the electron transfer from the gel to the anode to be different for different anodes. Considering both Ny66-Ag and Ny66-Ag/CNT as conductors, the energy structure of them are shown with their work function (Φ_{WF}) at -4.3 eV for Ag [218] and -4.8 eV for CNT [219-221]. In the absence of any electron transport layer between the photoactive materials (i.e., the gel) and anode in the first two devices, the electron transfer to the anode is expected to be inefficient. However, considering the work function of the cathode electrode ($\Phi_{WF, SS} = -4.5$ eV), shifting the work function of the anode to a lower energy level, after deposition of CNT, leads to a decrease in the photovoltaic performance, which can be observed in the open circuit voltage results. In order to improve the light harvesting and electron extraction efficiency in the hybrid device, ZnO nanowires were grown on the CNT layer as an electron transport layer (ETL). Due to the semiconducting properties of ZnO with the conduction band edge at $E_{CB} = -4.2$ eV and the valence band edge at $E_{VB} = -4.7$ eV [222, 223], a rectifying mechanism is established for transferring the excited electrons from the gel to the anode and block the recombination of the holes at the anode surface. [224, 225]. The presence of the ETL clearly led into boosting the photovoltaic performance with higher OCP and photocurrent (Figure 38). Considering the gel as a conductor for both electronic (through PANI) and ionic charges (through anions and cations), optimizing the performance of a hybrid device is challenging. However, improving the performance after washing the device indicates the importance of the ionic charge transportation through the gel.

The results clearly show the feasibility of fabricating simple thread-shaped hybrid devices using photo-redox active gels with comparable energy storage capacitances to the conventional supercapacitors. However, significant improvement in the photovoltaic performance of the device is required before using them in practical applications.

6.5 Conclusion

In conclusion, a fiber-based hybrid device design consisted of two conductive threads and a photoactive gel electrolyte with the photoelectric and energy storage properties has been demonstrated. The experimental results indicate that the PANI-based photoactive gel electrolyte can be used for fiber-shaped hybrid devices with a simple fabrication process. The energy storage of the device can be enhanced by adding the CNT layer on the Ny66-Ag thread; however, that could reduce the photovoltaic performance remarkably due to shifting the work function of the coated electrode. Moreover, the fabricated device showed significant improvement in the photovoltaic performance after adding the ZnO NWs. The test results after washing the sample proved the advantages of using such device structure in wearable electronics. Further studies on the stability and photovoltaic performance of the device are suggested prior to the practical applications.

Chapter 7: Conclusion and Recommendations for Future Work

7.1 Conclusion

In this dissertation work, several studies have been addressed, including investigating the effect of aniline percentage in the gel electrolyte on the electrochemical and photovoltaic performance of the two-electrode hybrid devices and studying different porous materials for the counter electrodes of such hybrid devices. The experimental results indicated that optimizing aniline percentage in the composite gel electrolyte plays a vital role in improving the energy harvesting and charge storage of the two-terminal hybrid cells.

Furthermore, the configuration effect of the twisted fiber-shaped supercapacitors on the electrochemical properties has been examined and analyzed. The study was taken with the purpose of finding a suitable thread and design for the thread-based devices. The results demonstrated that the capacitance is directly related to the effective length of the twisted fiber-shaped devices when the surface of thread-based electrodes is smooth and uniform.

Also, the approach used in the two-electrode hybrid device, which relies on the photoactive gel electrolyte to absorb light, has been adopted and successfully used for fabricating a fiber-shaped hybrid device for wearable electronics. The energy storage of the device was improved by coating CNT ink on the surface of the anode electrode made of silver-coated nylon66. Also, the experimental results revealed notable enhancement in the photovoltaic response after adding the electron transport layer (i.e., ZnO nanowires) on the anode; however, in order to be suitable for practical applications, further improvements are needed.

7.2 Recommendations for Future Work

Employing a photoactive gel electrolyte in two-terminal hybrid devices, whether fiber-shaped or flat hybrid devices, is promising and encouraging based on the current results. However, further investigations and improvements are needed. Some suggestions for the hybrid device are as follows.

- (1) The energy storage can be improved by introducing Ti_3C_2 MXene to the gel.
- (2) Sealing the device after the fabrication to reduce the internal resistance and aging effects and improve the device stability.
- (3) Using different ETL for the fiber-shaped hybrid device, for example, adding a layer of TiO_2 instead of ZnO .
- (4) Study the effect of adding dye sensitizers in the photoactive gel electrolyte on the photovoltaic response.
- (5) The possibility of using a fabric-based hybrid device with the photoactive electrolyte can also be investigated, which could increase the PV response of the device due to the large surface area of the electrode.

References

- [1] O. Edenhofer *et al.*, "Contribution of Working Group III to the Fifth Assessment Report of the Intergovernmental Panel on Climate Change," *Climate change*, pp. 1-11, 2014.
- [2] U. E. I. Administration, *Annual Energy Outlook 2011: With Projections to 2035*. Government Printing Office, 2011.
- [3] B. P. Center, "Annual Energy Outlook 2020," *Energy Information Administration, Washington, DC*, 2020.
- [4] B. Ricketts and C. Ton-That, "Self-discharge of carbon-based supercapacitors with organic electrolytes," *Journal of Power Sources*, vol. 89, no. 1, pp. 64-69, 2000.
- [5] C. Largeot, C. Portet, J. Chmiola, P.-L. Taberna, Y. Gogotsi, and P. Simon, "Relation between the ion size and pore size for an electric double-layer capacitor," *Journal of the American Chemical Society*, vol. 130, no. 9, pp. 2730-2731, 2008.
- [6] M. Winter and R. J. Brodd, "What are batteries, fuel cells, and supercapacitors?," ed: ACS Publications, 2004.
- [7] S. Kandalkar, D. Dhawale, C.-K. Kim, and C. Lokhande, "Chemical synthesis of cobalt oxide thin film electrode for supercapacitor application," *Synthetic Metals*, vol. 160, no. 11-12, pp. 1299-1302, 2010.
- [8] G. Wang, L. Zhang, and J. Zhang, "A review of electrode materials for electrochemical supercapacitors," *Chemical Society Reviews*, vol. 41, no. 2, pp. 797-828, 2012.
- [9] P. Simon and Y. Gogotsi, "Materials for electrochemical capacitors," in *Nanoscience And Technology: A Collection of Reviews from Nature Journals*: World Scientific, 2010, pp. 320-329.
- [10] A. González, E. Goikolea, J. A. Barrena, and R. Mysyk, "Review on supercapacitors: technologies and materials," *Renewable and Sustainable Energy Reviews*, vol. 58, pp. 1189-1206, 2016.
- [11] A. K. Yetisen, J. L. Martinez-Hurtado, B. Ünal, A. Khademhosseini, and H. Butt, "Wearables in medicine," *Advanced Materials*, vol. 30, no. 33, p. 1706910, 2018.
- [12] R. Pailes-Friedman, "Electronics and Fabrics: The Development of Garment-Based Wearables," *Advanced Materials Technologies*, vol. 3, no. 10, p. 1700307, 2018.
- [13] P. Dominique and P. Crégo, *Wearables, Smart Textiles & Smart Apparel*. Elsevier, 2018.
- [14] Grand View Research. "Wearable Technology Market Size, Industry Report, 2020-2027." <https://www.grandviewresearch.com/industry-analysis/wearable-technology-market> (accessed April 5, 2021).
- [15] J. S. Heo, J. Eom, Y. H. Kim, and S. K. Park, "Recent progress of textile-based wearable electronics: a comprehensive review of materials, devices, and applications," *Small*, vol. 14, no. 3, p. 1703034, 2018.
- [16] D. Yu *et al.*, "Emergence of fiber supercapacitors," *Chemical Society Reviews*, vol. 44, no. 3, pp. 647-662, 2015.

- [17] D. Chen, K. Jiang, T. Huang, and G. Shen, "Recent advances in fiber supercapacitors: materials, device configurations, and applications," *Advanced Materials*, vol. 32, no. 5, p. 1901806, 2020.
- [18] H. Ryu, H. J. Yoon, and S. W. Kim, "Hybrid energy harvesters: toward sustainable energy harvesting," *Advanced Materials*, vol. 31, no. 34, p. 1802898, 2019.
- [19] Y. Hu, S. Ding, P. Chen, T. Seaby, J. Hou, and L. Wang, "Flexible solar-rechargeable energy system," *Energy Storage Materials*, 2020.
- [20] M. Pagliaro, R. Ciriminna, and G. Palmisano, "Flexible solar cells," *ChemSusChem: Chemistry & Sustainability Energy & Materials*, vol. 1, no. 11, pp. 880-891, 2008.
- [21] B. Luo, D. Ye, and L. Wang, "Recent progress on integrated energy conversion and storage systems," *Advanced Science*, vol. 4, no. 9, p. 1700104, 2017.
- [22] Y. Sun and X. Yan, "Recent advances in dual-functional devices integrating solar cells and supercapacitors," *Solar RRL*, vol. 1, no. 3-4, p. 1700002, 2017.
- [23] H. Meng, S. Pang, and G. Cui, "Photo-Supercapacitors Based on Third-Generation Solar Cells," *ChemSusChem*, vol. 12, no. 15, pp. 3431-3447, 2019.
- [24] D. Lau *et al.*, "Hybrid solar energy harvesting and storage devices: the promises and challenges," *Materials Today Energy*, vol. 13, pp. 22-44, 2019.
- [25] M. Falk and S. Shleev, "Hybrid dual-functioning electrodes for combined ambient energy harvesting and charge storage: Towards self-powered systems," *Biosensors and Bioelectronics*, vol. 126, pp. 275-291, 2019.
- [26] S. Yun *et al.*, "New-generation integrated devices based on dye-sensitized and perovskite solar cells," *Energy & Environmental Science*, vol. 11, no. 3, pp. 476-526, 2018.
- [27] H. Wei *et al.*, "Energy conversion technologies towards self-powered electrochemical energy storage systems: the state of the art and perspectives," *Journal of Materials Chemistry A*, vol. 5, no. 5, pp. 1873-1894, 2017.
- [28] S. Yun, Y. Zhang, Q. Xu, J. Liu, and Y. Qin, "Recent advance in new-generation integrated devices for energy harvesting and storage," *Nano Energy*, 2019.
- [29] A. Gurung and Q. Qiao, "Solar charging batteries: advances, challenges, and opportunities," *Joule*, vol. 2, no. 7, pp. 1217-1230, 2018.
- [30] Q. Zeng *et al.*, "Integrated Photorechargeable Energy Storage System: Next-Generation Power Source Driving the Future," *Advanced Energy Materials*, p. 1903930, 2020.
- [31] C. Ng, H. Lim, S. Hayase, I. Harrison, A. Pandikumar, and N. Huang, "Potential active materials for photo-supercapacitor: a review," *Journal of Power Sources*, vol. 296, pp. 169-185, 2015.
- [32] V. Vega-Garita, L. Ramirez-Elizondo, N. Narayan, and P. Bauer, "Integrating a photovoltaic storage system in one device: A critical review," *Progress in Photovoltaics: research and applications*, vol. 27, no. 4, pp. 346-370, 2019.
- [33] W. Shockley and H. J. Queisser, "Detailed balance limit of efficiency of p-n junction solar cells," *Journal of applied physics*, vol. 32, no. 3, pp. 510-519, 1961.
- [34] A. Polman, M. Knight, E. C. Garnett, B. Ehrler, and W. C. Sinke, "Photovoltaic materials: Present efficiencies and future challenges," *Science*, vol. 352, no. 6283, 2016.
- [35] J. Liang *et al.*, "An all-inorganic perovskite solar capacitor for efficient and stable spontaneous photocharging," *Nano Energy*, vol. 52, pp. 239-245, 2018.

- [36] S. A. Mohammed and E. T. Hashim, "Designing a maximum power point tracking system for a monocrystalline silicon solar module using the Arduino microcontroller and synchronous Buck converter," *FME Transactions*, vol. 47, no. 3, pp. 524-533, 2019.
- [37] S. Salman, A. Xin, and W. Zhouyang, "Design of a P-&O algorithm based MPPT charge controller for a stand-alone 200W PV system," *Protection and Control of Modern Power Systems*, vol. 3, no. 1, pp. 1-8, 2018.
- [38] K. Ş. Parlak, "PV array reconfiguration method under partial shading conditions," *International Journal of Electrical Power & Energy Systems*, vol. 63, pp. 713-721, 2014.
- [39] P. S. Rao, G. S. Ilango, and C. Nagamani, "Maximum power from PV arrays using a fixed configuration under different shading conditions," *IEEE journal of Photovoltaics*, vol. 4, no. 2, pp. 679-686, 2014.
- [40] S. Jang *et al.*, "Structural health monitoring of a cable-stayed bridge using smart sensor technology: deployment and evaluation," *Smart Structures and Systems*, vol. 6, no. 5_6, pp. 439-459, 2010.
- [41] H.-D. Um, K.-H. Choi, I. Hwang, S.-H. Kim, K. Seo, and S.-Y. Lee, "Monolithically integrated, photo-rechargeable portable power sources based on miniaturized Si solar cells and printed solid-state lithium-ion batteries," *Energy & Environmental Science*, vol. 10, no. 4, pp. 931-940, 2017.
- [42] M. A. Eldeeb, Y. H. Ghallab, Y. Ismail, and H. Elghitani, "Low-voltage subthreshold CMOS current mode circuits: Design and applications," *AEU-International Journal of Electronics and Communications*, vol. 82, pp. 251-264, 2017.
- [43] Y. Bastan, A. Nejati, S. Radfar, P. Amiri, M. Nasrollahpour, and S. Hamed-Hagh, "An Ultra-Low-Voltage Sub-Threshold Pseudo-Differential CMOS Schmitt Trigger," in *2018 31st IEEE International System-on-Chip Conference (SOCC)*, 2018: IEEE, pp. 1-5.
- [44] S. Intermite *et al.*, "Perovskite solar cell–electrochemical double layer capacitor interplay," *Electrochimica Acta*, vol. 258, pp. 825-833, 2017.
- [45] Y. Y. Lai, X. Li, and Y. Zhu, "Polymeric Active Materials for Redox Flow Battery Application," *ACS Applied Polymer Materials*, vol. 2, no. 2, pp. 113-128, 2020.
- [46] W. Li, H. C. Fu, L. Li, M. Cabán-Acevedo, J. H. He, and S. Jin, "Integrated photoelectrochemical solar energy conversion and organic redox flow battery devices," *Angewandte Chemie*, vol. 128, no. 42, pp. 13298-13302, 2016.
- [47] M. Salanne *et al.*, "Efficient storage mechanisms for building better supercapacitors," *Nature Energy*, vol. 1, no. 6, pp. 1-10, 2016.
- [48] Y. Hong *et al.*, "Highly selective ZnO gas sensor based on MOSFET having a horizontal floating-gate," *Sensors and Actuators B: Chemical*, vol. 232, pp. 653-659, 2016.
- [49] Y. Gogotsi and R. M. Penner, "Energy storage in nanomaterials—capacitive, pseudocapacitive, or battery-like?," ed: ACS Publications, 2018.
- [50] Y. Liang *et al.*, "A review of rechargeable batteries for portable electronic devices," *InfoMat*, vol. 1, no. 1, pp. 6-32, 2019.
- [51] Q. Li, N. Li, Y. Liu, Y. Wang, and H. Zhou, "High-Safety and Low-Cost Photoassisted Chargeable Aqueous Sodium-Ion Batteries with 90% Input Electric Energy Savings," *Advanced Energy Materials*, vol. 6, no. 18, p. 1600632, 2016.
- [52] Q. Li, N. Li, M. Ishida, and H. Zhou, "Saving electric energy by integrating a photoelectrode into a Li-ion battery," *Journal of Materials Chemistry A*, vol. 3, no. 42, pp. 20903-20907, 2015.

- [53] C. Li *et al.*, "Flexible perovskite solar cell-driven photo-rechargeable lithium-ion capacitor for self-powered wearable strain sensors," *Nano Energy*, vol. 60, pp. 247-256, 2019.
- [54] J. Xu, Y. Chen, and L. Dai, "Efficiently photo-charging lithium-ion battery by perovskite solar cell," *Nature communications*, vol. 6, no. 1, pp. 1-7, 2015.
- [55] G. Dennler *et al.*, "Design Rules for Donors in Bulk-Heterojunction Tandem Solar Cells Towards 15% Energy-Conversion Efficiency," *Advanced Materials*, vol. 20, no. 3, pp. 579-583, 2008.
- [56] R. Liu, C. Liu, and S. Fan, "A photocapacitor based on organometal halide perovskite and PANI/CNT composites integrated using a CNT bridge," *Journal of Materials Chemistry A*, vol. 5, no. 44, pp. 23078-23084, 2017.
- [57] L. Meng *et al.*, "Organic and solution-processed tandem solar cells with 17.3% efficiency," *Science*, vol. 361, no. 6407, pp. 1094-1098, 2018.
- [58] S. N. Agbo *et al.*, "Development towards cell-to-cell monolithic integration of a thin-film solar cell and lithium-ion accumulator," *Journal of Power Sources*, vol. 327, pp. 340-344, 2016.
- [59] A. Gurung *et al.*, "Highly efficient perovskite solar cell photocharging of lithium ion battery using DC–DC booster," *Advanced Energy Materials*, vol. 7, no. 11, p. 1602105, 2017.
- [60] A. Gurung *et al.*, "Rear-Illuminated Perovskite Photorechargeable Lithium Battery," *Advanced Functional Materials*, p. 2001865, 2020.
- [61] G. Conibeer *et al.*, "Silicon nanostructures for third generation photovoltaic solar cells," *Thin solid films*, vol. 511, pp. 654-662, 2006.
- [62] L. Mangolini, "Synthesis, properties, and applications of silicon nanocrystals," *Journal of Vacuum Science & Technology B, Nanotechnology and Microelectronics: Materials, Processing, Measurement, and Phenomena*, vol. 31, no. 2, p. 020801, 2013.
- [63] S. Bhattacharya and S. John, "Beyond 30% conversion efficiency in silicon solar cells: a numerical demonstration," *Scientific reports*, vol. 9, no. 1, pp. 1-15, 2019.
- [64] A. S. Westover, K. Share, R. Carter, A. P. Cohn, L. Oakes, and C. L. Pint, "Direct integration of a supercapacitor into the backside of a silicon photovoltaic device," *Applied Physics Letters*, vol. 104, no. 21, p. 213905, 2014.
- [65] L. V. Thekkekara, B. Jia, Y. Zhang, L. Qiu, D. Li, and M. Gu, "On-chip energy storage integrated with solar cells using a laser scribed graphene oxide film," *Applied Physics Letters*, vol. 107, no. 3, p. 031105, 2015.
- [66] R. Liu *et al.*, "Silicon nanowire/polymer hybrid solar cell-supercapacitor: a self-charging power unit with a total efficiency of 10.5%," *Nano letters*, vol. 17, no. 7, pp. 4240-4247, 2017.
- [67] "Best research-cell efficiency chart," *NREL.gov*. [Online]. Available: <https://www.nrel.gov/pv/cell-efficiency.html>. [Accessed: 22-Mar-2022].
- [68] F. Zhang and K. Zhu, "Additive engineering for efficient and stable perovskite solar cells," *Advanced Energy Materials*, p. 1902579, 2019.
- [69] X. Li *et al.*, "A vacuum flash–assisted solution process for high-efficiency large-area perovskite solar cells," *Science*, vol. 353, no. 6294, pp. 58-62, 2016.

- [70] S. Nair and J. V. Gohel, "A Review on Contemporary Hole Transport Materials for Perovskite Solar Cells," in *Nanotechnology for Energy and Environmental Engineering*, L. Ledwani and J. S. Sangwai Eds. Cham: Springer International Publishing, 2020, pp. 145-168.
- [71] F. Zhou *et al.*, "Perovskite photovoltachromic supercapacitor with all-transparent electrodes," *ACS nano*, vol. 10, no. 6, pp. 5900-5908, 2016.
- [72] F. Zhou, Y. Zhao, X. Shen, Y. Chai, and Q. Ma, "Multifunctional perovskite photovoltachromic supercapacitor," in *2016 IEEE International Nanoelectronics Conference (INEC)*, 2016: IEEE, pp. 1-2.
- [73] F. Meng *et al.*, "Current progress in interfacial engineering of carbon-based perovskite solar cells," *Journal of Materials Chemistry A*, vol. 7, no. 15, pp. 8690-8699, 2019.
- [74] J. Xu, Z. Ku, Y. Zhang, D. Chao, and H. J. Fan, "Integrated photo-supercapacitor based on PEDOT modified printable perovskite solar cell," *Advanced Materials Technologies*, vol. 1, no. 5, p. 1600074, 2016.
- [75] Z. Liu *et al.*, "Novel integration of perovskite solar cell and supercapacitor based on carbon electrode for hybridizing energy conversion and storage," *ACS applied materials & interfaces*, vol. 9, no. 27, pp. 22361-22368, 2017.
- [76] X. Xu *et al.*, "A power pack based on organometallic perovskite solar cell and supercapacitor," *ACS nano*, vol. 9, no. 2, pp. 1782-1787, 2015.
- [77] Y. Cui, L. Hong, and J. Hou, "Organic Photovoltaic Cells for Indoor Applications: Opportunities and Challenges," *ACS Applied Materials & Interfaces*, 2020.
- [78] N. Kaur, M. Singh, D. Pathak, T. Wagner, and J. Nunzi, "Organic materials for photovoltaic applications: Review and mechanism," *Synthetic Metals*, vol. 190, pp. 20-26, 2014.
- [79] J. Yu, Y. Zheng, and J. Huang, "Towards high performance organic photovoltaic cells: A review of recent development in organic photovoltaics," *Polymers*, vol. 6, no. 9, pp. 2473-2509, 2014.
- [80] J. Kim *et al.*, "A highly efficient self-power pack system integrating supercapacitors and photovoltaics with an area-saving monolithic architecture," *Journal of Materials Chemistry A*, vol. 5, no. 5, pp. 1906-1912, 2017.
- [81] B. P. Lechêne, M. Cowell, A. Pierre, J. W. Evans, P. K. Wright, and A. C. Arias, "Organic solar cells and fully printed super-capacitors optimized for indoor light energy harvesting," *Nano Energy*, vol. 26, pp. 631-640, 2016.
- [82] Z. Zhang *et al.*, "Integrated polymer solar cell and electrochemical supercapacitor in a flexible and stable fiber format," *Advanced Materials*, vol. 26, no. 3, pp. 466-470, 2014.
- [83] C. T. Chien *et al.*, "Graphene-based integrated photovoltaic energy harvesting/storage device," *Small*, vol. 11, no. 24, pp. 2929-2937, 2015.
- [84] G. Wee, T. Salim, Y. M. Lam, S. G. Mhaisalkar, and M. Srinivasan, "Printable photo-supercapacitor using single-walled carbon nanotubes," *Energy & Environmental Science*, vol. 4, no. 2, pp. 413-416, 2011.
- [85] B. Lee, J. He, R. P. Chang, and M. G. Kanatzidis, "All-solid-state dye-sensitized solar cells with high efficiency," *Nature*, vol. 485, no. 7399, pp. 486-489, 2012.
- [86] M. K. Nazeeruddin, E. Baranoff, and M. Grätzel, "Dye-sensitized solar cells: a brief overview," *Solar energy*, vol. 85, no. 6, pp. 1172-1178, 2011.

- [87] M. Grätzel, "Dye-sensitized solar cells," *Journal of photochemistry and photobiology C: Photochemistry Reviews*, vol. 4, no. 2, pp. 145-153, 2003.
- [88] Y. Saito, A. Ogawa, S. Uchida, T. Kubo, and H. Segawa, "Energy-storable dye-sensitized solar cells with interdigitated nafion/polypyrrole–Pt comb-like electrodes," *Chemistry letters*, vol. 39, no. 5, pp. 488-489, 2010.
- [89] W. Zhao, X.-F. Wang, E. Zheng, Y. Wei, Y. Sanehira, and G. Chen, "High capacity WO₃ film as efficient charge collection electrode for solar rechargeable batteries," *Journal of Power Sources*, vol. 350, pp. 28-34, 2017.
- [90] H. Nagai and H. Segawa, "Energy-storable dye-sensitized solar cell with a polypyrrole electrode," *Chemical communications*, no. 8, pp. 974-975, 2004.
- [91] Y. Saito, S. Uchida, T. Kubo, and H. Segawa, "Surface-oxidized tungsten for energy-storable dye-sensitized solar cells," *Thin Solid Films*, vol. 518, no. 11, pp. 3033-3036, 2010.
- [92] T. N. Murakami, N. Kawashima, and T. Miyasaka, "A high-voltage dye-sensitized photocapacitor of a three-electrode system," *Chemical communications*, no. 26, pp. 3346-3348, 2005.
- [93] H.-W. Chen *et al.*, "Plastic dye-sensitized photo-supercapacitor using electrophoretic deposition and compression methods," *Journal of Power Sources*, vol. 195, no. 18, pp. 6225-6231, 2010.
- [94] C.-Y. Hsu, H.-W. Chen, K.-M. Lee, C.-W. Hu, and K.-C. Ho, "A dye-sensitized photo-supercapacitor based on PProDOT-Et₂ thick films," *Journal of Power Sources*, vol. 195, no. 18, pp. 6232-6238, 2010.
- [95] P. A. Mini, S. V. Nair, and K. R. Subramanian, "Design and development of an integrated device consisting of an independent solar cell with electrical storage capacity," *Progress in Photovoltaics: Research and Applications*, vol. 21, no. 5, pp. 1153-1157, 2013.
- [96] N. Bagheri *et al.*, "Combination of asymmetric supercapacitor utilizing activated carbon and nickel oxide with cobalt polypyridyl-based dye-sensitized solar cell," *Electrochimica Acta*, vol. 143, pp. 390-397, 2014.
- [97] A. P. Cohn *et al.*, "All silicon electrode photocapacitor for integrated energy storage and conversion," *Nano letters*, vol. 15, no. 4, pp. 2727-2731, 2015.
- [98] Z. Yang *et al.*, "An integrated device for both photoelectric conversion and energy storage based on free-standing and aligned carbon nanotube film," *Journal of Materials Chemistry A*, vol. 1, no. 3, pp. 954-958, 2013.
- [99] M. Skunik-Nuckowska *et al.*, "Integration of solid-state dye-sensitized solar cell with metal oxide charge storage material into photoelectrochemical capacitor," *Journal of power sources*, vol. 234, pp. 91-99, 2013.
- [100] J. Xu *et al.*, "Integrated Photo-supercapacitor Based on Bi-polar TiO₂ Nanotube Arrays with Selective One-Side Plasma-Assisted Hydrogenation," *Advanced Functional Materials*, vol. 24, no. 13, pp. 1840-1846, 2014.
- [101] N. Harankahawa, K. Perera, and K. Vidanapathirana, "Use of gel polymer electrolytes to integrate photoelectric conversion and energy storage," *Journal of Energy Storage*, vol. 13, pp. 96-102, 2017.

- [102] H. M. Upadhyaya, S. Senthilarasu, M.-H. Hsu, and D. K. Kumar, "Recent progress and the status of dye-sensitized solar cell (DSSC) technology with state-of-the-art conversion efficiencies," *Solar Energy Materials and Solar Cells*, vol. 119, pp. 291-295, 2013.
- [103] B. Li, L. Wang, B. Kang, P. Wang, and Y. Qiu, "Review of recent progress in solid-state dye-sensitized solar cells," *Solar energy materials and solar cells*, vol. 90, no. 5, pp. 549-573, 2006.
- [104] A. Scalia *et al.*, "A flexible and portable powerpack by solid-state supercapacitor and dye-sensitized solar cell integration," *Journal of Power Sources*, vol. 359, pp. 311-321, 2017.
- [105] F.-W. Lee, C.-W. Ma, Y.-H. Lin, P.-C. Huang, Y.-L. Su, and Y.-J. Yang, "A micromachined photo-supercapacitor integrated with CdS-sensitized solar cells and buckypaper," *Sens. Mater.*, vol. 28, pp. 749-756, 2016.
- [106] P. C. Chow and T. Someya, "Organic Photodetectors for Next-Generation Wearable Electronics," *Advanced Materials*, vol. 32, no. 15, p. 1902045, 2020.
- [107] Y. Cho *et al.*, "Hybrid Smart Fiber with Spontaneous Self-Charging Mechanism for Sustainable Wearable Electronics," *Advanced Functional Materials*, vol. 30, no. 13, p. 1908479, 2020.
- [108] Y. Yang, H. Zhang, G. Zhu, S. Lee, Z.-H. Lin, and Z. L. Wang, "Flexible hybrid energy cell for simultaneously harvesting thermal, mechanical, and solar energies," *ACS nano*, vol. 7, no. 1, pp. 785-790, 2013.
- [109] J.-H. Lee, J. Kim, T. Y. Kim, M. S. Al Hossain, S.-W. Kim, and J. H. Kim, "All-in-one energy harvesting and storage devices," *Journal of Materials Chemistry A*, vol. 4, no. 21, pp. 7983-7999, 2016.
- [110] Y. Fu *et al.*, "Integrated power fiber for energy conversion and storage," *Energy & environmental science*, vol. 6, no. 3, pp. 805-812, 2013.
- [111] X. Pu, W. Hu, and Z. L. Wang, "Toward wearable self-charging power systems: the integration of energy-harvesting and storage devices," *Small*, vol. 14, no. 1, p. 1702817, 2018.
- [112] X. Chen *et al.*, "A novel "energy fiber" by coaxially integrating dye-sensitized solar cell and electrochemical capacitor," *Journal of Materials Chemistry A*, vol. 2, no. 6, pp. 1897-1902, 2014.
- [113] J. Liang *et al.*, "MoS₂-based all-purpose fibrous electrode and self-powering energy fiber for efficient energy harvesting and storage," *Advanced Energy Materials*, vol. 7, no. 3, p. 1601208, 2017.
- [114] Z. Chai *et al.*, "Tailorable and wearable textile devices for solar energy harvesting and simultaneous storage," *ACS nano*, vol. 10, no. 10, pp. 9201-9207, 2016.
- [115] F. Zhang *et al.*, "Transparent conducting oxide-and Pt-free flexible photo-rechargeable electric energy storage systems," *RSC advances*, vol. 7, no. 83, pp. 52988-52994, 2017.
- [116] K. Gangotri and J. Meena, "Role of surfactants in photogalvanic cells for solar energy conversion and storage," *Energy sources*, vol. 28, no. 8, pp. 771-777, 2006.
- [117] C. Lal, "Use of mixed dyes in a photogalvanic cell for solar energy conversion and storage: EDTA–thionine–azur-B system," *Journal of power sources*, vol. 164, no. 2, pp. 926-930, 2007.
- [118] J. R. Bolton, "The photochemical conversion and storage of solar energy: An historical perspective," *Solar energy materials and solar cells*, vol. 38, no. 1-4, pp. 543-554, 1995.

- [119] P. Koli, "Solar energy conversion and storage: Fast Green FCF-Fructose photogalvanic cell," *Applied energy*, vol. 118, pp. 231-237, 2014.
- [120] A. Malviya and P. P. Solanki, "Photogalvanics: A sustainable and promising device for solar energy conversion and storage," *Renewable and Sustainable Energy Reviews*, vol. 59, pp. 662-691, 2016.
- [121] K. Kalyanasundaram and M. Graetzel, "Artificial photosynthesis: biomimetic approaches to solar energy conversion and storage," *Current opinion in Biotechnology*, vol. 21, no. 3, pp. 298-310, 2010.
- [122] J. Connolly, *Photochemical conversion and storage of solar energy*. Elsevier, 2012.
- [123] C. Lal, "PHOTOGALVANIC CELL: AN EFFICIENT DEVICE FOR PHOTOCHEMICAL CONVERSION AND STORAGE OF SOLAR ENERGY," *Environmental Science and Technology*, vol. 2, p. 428, 2016.
- [124] W. J. Albery, "Development of photogalvanic cells for solar energy conservation," *Accounts of Chemical Research*, vol. 15, no. 5, pp. 142-148, 1982. [Online]. Available: <http://dx.doi.org/10.1021/ar00077a003>.
- [125] W. J. Albery and M. D. Archer, "Photogalvanic cells—I. The potential of zero current," *Electrochimica Acta*, vol. 21, no. 12, pp. 1155-1163, 1976, doi: 10.1016/0013-4686(76)85173-0.
- [126] W. J. Albery and M. D. Archer, "Optimum efficiency of photogalvanic cells for solar energy conversion," *Nature*, 10.1038/270399a0 vol. 270, no. 5636, pp. 399-402, 1977. [Online]. Available: <http://dx.doi.org/10.1038/270399a0>.
- [127] W. J. Albery and M. D. Archer, "Photogalvanic Cells," *Journal of The Electrochemical Society*, vol. 124, no. 5, pp. 688-697, 1977. [Online]. Available: <http://dx.doi.org/10.1149/1.2133384>.
- [128] P. G. Ang and A. F. Sammells, "Photoelectrochemical systems with energy storage," *Faraday Discussions of the Chemical Society*, vol. 70, pp. 207-222, 1980.
- [129] K. Xiao, L. Chen, L. Jiang, and M. Antonietti, "Carbon nitride nanotube for ion transport based photo-rechargeable electric energy storage," *Nano Energy*, vol. 67, p. 104230, 2020.
- [130] J. E. Halls and J. D. Wadhawan, "Photogalvanic Cells, Principles and Perspectives," in *Encyclopedia of Applied Electrochemistry*, G. Kreysa, K.-i. Ota, and R. F. Savinell Eds. New York, NY: Springer New York, 2014, pp. 1556-1578.
- [131] K. Genwa and M. Genwa, "Photogalvanic cell: A new approach for green and sustainable chemistry," *Solar energy materials and solar cells*, vol. 92, no. 5, pp. 522-529, 2008.
- [132] K. Knehr and E. Kumbur, "Open circuit voltage of vanadium redox flow batteries: Discrepancy between models and experiments," *Electrochemistry Communications*, vol. 13, no. 4, pp. 342-345, 2011.
- [133] B. Aljafari, S. K. Indrakar, M. K. Ram, P. K. Biswas, E. Stefanakos, and A. Takshi, "A Polyaniline-Based Redox-Active Composite Gel Electrolyte with Photo-Electric and Electrochromic Properties," *ChemElectroChem*, vol. 6, no. 23, pp. 5888-5895, 2019.
- [134] B. Aljafari, F. Khorramshahi, M. K. Ram, and A. Takshi, "Photo-Electric Properties of Polypyrrole Based Gel Electrolyte for Hybrid Photoactive Supercapacitors," *ECS Transactions*, vol. 92, no. 9, p. 7, 2019.

- [135] A. Takshi, J. D. Madden, A. Mahmoudzadeh, R. Saer, and J. T. Beatty, "A photovoltaic device using an electrolyte containing photosynthetic reaction centers," *Energies*, vol. 3, no. 11, pp. 1721-1727, 2010.
- [136] L. De La Garza *et al.*, "Enzyme-based photoelectrochemical biofuel cell," *The Journal of Physical Chemistry B*, vol. 107, no. 37, pp. 10252-10260, 2003.
- [137] H. Usui, S. Nonaka, S. Suzuki, Y. Domi, and H. Sakaguchi, "Photosynthesis-Inspired Electrolyte Additives Enhancing Photoelectrochemical Charge–Discharge Property of TiO₂/MnO₂ Composite Electrode," *ACS Applied Electronic Materials*, vol. 1, no. 6, pp. 823-827, 2019.
- [138] M. A. Mahmoudzadeh, A. R. Usgaocar, J. Giorgio, D. L. Officer, G. G. Wallace, and J. D. Madden, "A high energy density solar rechargeable redox battery," *Journal of Materials Chemistry A*, vol. 4, no. 9, pp. 3446-3452, 2016.
- [139] P. Liu, Y. I. Cao, G. R. Li, X. P. Gao, X. P. Ai, and H. X. Yang, "A solar rechargeable flow battery based on photoregeneration of two soluble redox couples," *ChemSusChem*, vol. 6, no. 5, pp. 802-806, 2013.
- [140] L. Cao, M. Skyllas-Kazacos, and D. W. Wang, "Solar redox flow batteries: Mechanism, design, and measurement," *Advanced Sustainable Systems*, vol. 2, no. 8-9, p. 1800031, 2018.
- [141] P. Leung, X. Li, C. P. De León, L. Berlouis, C. J. Low, and F. C. Walsh, "Progress in redox flow batteries, remaining challenges and their applications in energy storage," *Rsc Advances*, vol. 2, no. 27, pp. 10125-10156, 2012.
- [142] X. Zhou, T. Zhao, L. An, Y. Zeng, and L. Wei, "Critical transport issues for improving the performance of aqueous redox flow batteries," *Journal of Power Sources*, vol. 339, pp. 1-12, 2017.
- [143] P. Leung *et al.*, "Recent developments in organic redox flow batteries: a critical review," *Journal of Power Sources*, vol. 360, pp. 243-283, 2017.
- [144] L. F. Arenas, C. P. de León, and F. C. Walsh, "Redox flow batteries for energy storage: their promise, achievements and challenges," *Current Opinion in Electrochemistry*, vol. 16, pp. 117-126, 2019.
- [145] A. Takshi, H. Yaghoubi, T. Tevi, and S. Bakhshi, "Photoactive supercapacitors for solar energy harvesting and storage," *Journal of Power Sources*, vol. 275, pp. 621-626, 2015.
- [146] B. Aljafari, M. K. Ram, and A. Takshi, "Integrated electrochemical energy storage and photovoltaic device with a gel electrolyte," in *Physics, Simulation, and Photonic Engineering of Photovoltaic Devices VIII*, 2019, vol. 10913: International Society for Optics and Photonics, p. 1091318.
- [147] X. Huang, X. Zhang, and H. Jiang, "Photovoltaically self-charging cells with WO₃·H₂O/CNTs/PVDF composite," *RSC advances*, vol. 6, no. 99, pp. 96490-96494, 2016.
- [148] J. Cai, C. Lv, and A. Watanabe, "High-performance all-solid-state flexible carbon/TiO₂ micro-supercapacitors with photo-rechargeable capability," *RSC advances*, vol. 7, no. 1, pp. 415-422, 2017.
- [149] A. Roy *et al.*, "A photoelectrochemical supercapacitor based on a single BiVO₄-RGO bilayer photocapacitive electrode," *Electrochimica Acta*, vol. 329, p. 135170, 2020.
- [150] S. Roy *et al.*, "Self-charging photo-power cell based on a novel polymer nanocomposite film with high energy density and durability," *Polymer Journal*, vol. 51, no. 11, pp. 1197-1209, 2019.

- [151] Z. Ouyang *et al.*, "Monolithic integration of anodic molybdenum oxide pseudocapacitive electrodes on screen-printed silicon solar cells for hybrid energy harvesting-storage systems," *Advanced Energy Materials*, vol. 7, no. 9, p. 1602325, 2017.
- [152] J. Liang *et al.*, "Integrated perovskite solar capacitors with high energy conversion efficiency and fast photo-charging rate," *Journal of Materials Chemistry A*, vol. 6, no. 5, pp. 2047-2052, 2018.
- [153] S. Lau *et al.*, "A three-electrode integrated photo-supercapacitor utilizing graphene-based intermediate bifunctional electrode," *Electrochimica Acta*, vol. 238, pp. 178-184, 2017.
- [154] Y.-H. Lee *et al.*, "Wearable textile battery rechargeable by solar energy," *Nano letters*, vol. 13, no. 11, pp. 5753-5761, 2013.
- [155] L. D. Partain and L. M. Fraas, *Solar cells and their applications*. Wiley, 2010.
- [156] S. Kalasina, P. Pattanasattayavong, M. Suksomboon, N. Phattharasupakun, J. Wutthiprom, and M. Sawangphruk, "A new concept of charging supercapacitors based on the photovoltaic effect," *Chemical Communications*, vol. 53, no. 4, pp. 709-712, 2017.
- [157] Y. Wang, X. Yang, A. G. Pandolfo, J. Ding, and D. Li, "High-Rate and High-Volumetric Capacitance of Compact Graphene–Polyaniline Hydrogel Electrodes," *Advanced Energy Materials*, vol. 6, no. 11, p. 1600185, 2016.
- [158] K. Wang *et al.*, "Chemically crosslinked hydrogel film leads to integrated flexible supercapacitors with superior performance," *Advanced materials*, vol. 27, no. 45, pp. 7451-7457, 2015.
- [159] W. Li, F. Gao, X. Wang, N. Zhang, and M. Ma, "Strong and robust polyaniline-based supramolecular hydrogels for flexible supercapacitors," *Angewandte Chemie*, vol. 128, no. 32, pp. 9342-9347, 2016.
- [160] H. Huang *et al.*, "Reinforced polyaniline/polyvinyl alcohol conducting hydrogel from a freezing–thawing method as self-supported electrode for supercapacitors," *Journal of materials science*, vol. 51, no. 18, pp. 8728-8736, 2016.
- [161] X. Cheng, J. Pan, Y. Zhao, M. Liao, and H. Peng, "Gel polymer electrolytes for electrochemical energy storage," *Advanced Energy Materials*, vol. 8, no. 7, p. 1702184, 2018.
- [162] Z. Tang *et al.*, "Preparation of PAA-g-CTAB/PANI polymer based gel-electrolyte and the application in quasi-solid-state dye-sensitized solar cells," *Electrochimica acta*, vol. 58, pp. 52-57, 2011.
- [163] B. C. Nath, B. Gogoi, M. Boruah, M. Khannam, G. A. Ahmed, and S. K. Dolui, "High performance polyvinyl alcohol/multi walled carbon nanotube/polyaniline hydrogel (PVA/MWCNT/PAni) based dye sensitized solar cells," *Electrochimica Acta*, vol. 146, pp. 106-111, 2014.
- [164] X. Jin, L. You, Z. Chen, and Q. Li, "High-efficiency platinum-free quasi-solid-state dye-sensitized solar cells from polyaniline (polypyrrole)-carbon nanotube complex tailored conducting gel electrolytes and counter electrodes," *Electrochimica Acta*, vol. 260, pp. 905-911, 2018.
- [165] S. B. Aziz, T. J. Woo, M. Kadir, and H. M. Ahmed, "A conceptual review on polymer electrolytes and ion transport models," *Journal of Science: Advanced Materials and Devices*, vol. 3, no. 1, pp. 1-17, 2018.
- [166] K. S. Ngai, S. Ramesh, K. Ramesh, and J. C. Juan, "A review of polymer electrolytes: fundamental, approaches and applications," *Ionics*, vol. 22, no. 8, pp. 1259-1279, 2016.

- [167] L. Hu *et al.*, "Highly conductive paper for energy-storage devices," *Proceedings of the National Academy of Sciences*, vol. 106, no. 51, pp. 21490-21494, 2009.
- [168] R. Gangopadhyay, A. De, and G. Ghosh, "Polyaniline–poly (vinyl alcohol) conducting composite: material with easy processability and novel application potential," *Synthetic Metals*, vol. 123, no. 1, pp. 21-31, 2001.
- [169] J. Han *et al.*, "ZnO nanotube-based dye-sensitized solar cell and its application in self-powered devices," *Nanotechnology*, vol. 21, no. 40, p. 405203, 2010.
- [170] W. Jing, C. H. Lai, W. S. Wong, and M. D. Wong, "A comprehensive study of battery-supercapacitor hybrid energy storage system for standalone PV power system in rural electrification," *Applied Energy*, vol. 224, pp. 340-356, 2018.
- [171] A. Das, S. Deshagani, R. Kumar, and M. Deepa, "Bifunctional photo-supercapacitor with a new architecture converts and stores solar energy as charge," *ACS applied materials & interfaces*, vol. 10, no. 42, pp. 35932-35945, 2018.
- [172] A. Takshi, B. Aljafari, T. Kareri, and E. Stefanakos, "A Critical Review on the Voltage Requirement in Hybrid Cells with Solar Energy Harvesting and Energy Storage Capability," *Batteries & Supercaps*, vol. 4, no. 2, pp. 252-267, 2021.
- [173] T. Kareri, B. Aljafari, and A. Takshi, "Impedance spectroscopy study of hybrid photovoltaic supercapacitors," in *New Concepts in Solar and Thermal Radiation Conversion III*, 2020, vol. 11496: International Society for Optics and Photonics, p. 114960D.
- [174] M. Vangari, T. Pryor, and L. Jiang, "Supercapacitors: review of materials and fabrication methods," *Journal of Energy Engineering*, vol. 139, no. 2, pp. 72-79, 2013.
- [175] Z. Yang, J. Tian, Z. Yin, C. Cui, W. Qian, and F. Wei, "Carbon nanotube-and graphene-based nanomaterials and applications in high-voltage supercapacitor: a review," *Carbon*, vol. 141, pp. 467-480, 2019.
- [176] G. A. Snook, P. Kao, and A. S. Best, "Conducting-polymer-based supercapacitor devices and electrodes," *Journal of power sources*, vol. 196, no. 1, pp. 1-12, 2011.
- [177] T. Tevi, S. W. Saint Birch, S. W. Thomas, and A. Takshi, "Effect of Triton X-100 on the double layer capacitance and conductivity of poly (3, 4-ethylenedioxythiophene): poly (styrenesulfonate)(PEDOT: PSS) films," *Synthetic Metals*, vol. 191, pp. 59-65, 2014.
- [178] W. Lu and L. Dai, *Carbon nanotube supercapacitors*. IntechOpen, 2010.
- [179] Y. Wang, Y. Song, and Y. Xia, "Electrochemical capacitors: mechanism, materials, systems, characterization and applications," *Chemical Society Reviews*, vol. 45, no. 21, pp. 5925-5950, 2016.
- [180] W. Raza *et al.*, "Recent advancements in supercapacitor technology," *Nano Energy*, 2018.
- [181] M. Cakici, R. R. Kakarla, and F. Alonso-Marroquin, "Advanced electrochemical energy storage supercapacitors based on the flexible carbon fiber fabric-coated with uniform coral-like MnO₂ structured electrodes," *Chemical Engineering Journal*, vol. 309, pp. 151-158, 2017.
- [182] Y. Wang, J. Guo, T. Wang, J. Shao, D. Wang, and Y.-W. Yang, "Mesoporous transition metal oxides for supercapacitors," *Nanomaterials*, vol. 5, no. 4, pp. 1667-1689, 2015.
- [183] A. Afzal, F. A. Abuilaiwi, A. Habib, M. Awais, S. B. Waje, and M. A. Atieh, "Polypyrrole/carbon nanotube supercapacitors: Technological advances and challenges," *Journal of Power Sources*, vol. 352, pp. 174-186, 2017.

- [184] S. Park, M. Vosguerichian, and Z. Bao, "A review of fabrication and applications of carbon nanotube film-based flexible electronics," *Nanoscale*, vol. 5, no. 5, pp. 1727-1752, 2013.
- [185] T. Chen and L. Dai, "Flexible supercapacitors based on carbon nanomaterials," *Journal of Materials Chemistry A*, vol. 2, no. 28, pp. 10756-10775, 2014.
- [186] Y. Shao *et al.*, "Graphene-based materials for flexible supercapacitors," *Chemical Society Reviews*, vol. 44, no. 11, pp. 3639-3665, 2015.
- [187] T. Qin *et al.*, "Flexible and wearable all-solid-state supercapacitors with ultrahigh energy density based on a carbon fiber fabric electrode," *Advanced Energy Materials*, vol. 7, no. 20, p. 1700409, 2017.
- [188] X. Cheng *et al.*, "Design of a hierarchical ternary hybrid for a fiber-shaped asymmetric supercapacitor with high volumetric energy density," *The Journal of Physical Chemistry C*, vol. 120, no. 18, pp. 9685-9691, 2016.
- [189] K. Wang, Q. Meng, Y. Zhang, Z. Wei, and M. Miao, "High-performance two-ply yarn supercapacitors based on carbon nanotubes and polyaniline nanowire arrays," *Advanced materials*, vol. 25, no. 10, pp. 1494-1498, 2013.
- [190] Z. Cai, L. Li, J. Ren, L. Qiu, H. Lin, and H. Peng, "Flexible, weavable and efficient microsupercapacitor wires based on polyaniline composite fibers incorporated with aligned carbon nanotubes," *Journal of Materials Chemistry A*, vol. 1, no. 2, pp. 258-261, 2013.
- [191] X. Chen *et al.*, "Novel electric double-layer capacitor with a coaxial fiber structure," *Advanced Materials*, vol. 25, no. 44, pp. 6436-6441, 2013.
- [192] L. Liu, Y. Yu, C. Yan, K. Li, and Z. Zheng, "Wearable energy-dense and power-dense supercapacitor yarns enabled by scalable graphene-metallic textile composite electrodes," *Nature communications*, vol. 6, no. 1, pp. 1-9, 2015.
- [193] D. S. Patil *et al.*, "Electrochemical supercapacitor electrode material based on polyacrylic acid/polypyrrole/silver composite," *Electrochimica Acta*, vol. 105, pp. 569-577, 2013.
- [194] P. K. Kalambate, R. A. Dar, S. P. Karna, and A. K. Srivastava, "High performance supercapacitor based on graphene-silver nanoparticles-polypyrrole nanocomposite coated on glassy carbon electrode," *Journal of Power Sources*, vol. 276, pp. 262-270, 2015.
- [195] B. Aljafari, T. Alamro, M. K. Ram, and A. Takshi, "Polyvinyl alcohol-acid redox active gel electrolytes for electrical double-layer capacitor devices," *Journal of Solid State Electrochemistry*, vol. 23, no. 1, pp. 125-133, 2019.
- [196] A. Fakhruddin *et al.*, "Fiber-Shaped Electronic Devices," *Advanced Energy Materials*, vol. 11, no. 34, p. 2101443, 2021.
- [197] P. Li *et al.*, "A General Electrode Design Strategy for Flexible Fiber Micro-Pseudocapacitors Combining Ultrahigh Energy and Power Delivery," *Advanced Science*, vol. 4, no. 8, p. 1700003, 2017.
- [198] W. Liu *et al.*, "A wire-shaped flexible asymmetric supercapacitor based on carbon fiber coated with a metal oxide and a polymer," *Journal of Materials Chemistry A*, vol. 3, no. 25, pp. 13461-13467, 2015.
- [199] C. Shen, Y. Xie, M. Sanghadasa, Y. Tang, L. Lu, and L. Lin, "Ultrathin coaxial fiber supercapacitors achieving high energy and power densities," *ACS applied materials & interfaces*, vol. 9, no. 45, pp. 39391-39398, 2017.

- [200] G. Qu *et al.*, "A fiber supercapacitor with high energy density based on hollow graphene/conducting polymer fiber electrode," *Advanced materials*, vol. 28, no. 19, pp. 3646-3652, 2016.
- [201] X. Fu *et al.*, "A fiber-shaped solar cell showing a record power conversion efficiency of 10%," *Journal of Materials Chemistry A*, vol. 6, no. 1, pp. 45-51, 2018.
- [202] G. Liu, M. Peng, W. Song, H. Wang, and D. Zou, "An 8.07% efficient fiber dye-sensitized solar cell based on a TiO₂ micron-core array and multilayer structure photoanode," *Nano Energy*, vol. 11, pp. 341-347, 2015.
- [203] G. Liu *et al.*, "A novel photoanode with high flexibility for fiber-shaped dye sensitized solar cells," *Journal of Materials Chemistry A*, vol. 4, no. 16, pp. 5925-5931, 2016.
- [204] R. Li, X. Xiang, X. Tong, J. Zou, and Q. Li, "Wearable double-twisted fibrous perovskite solar cell," *Advanced Materials*, vol. 27, no. 25, pp. 3831-3835, 2015.
- [205] B. Dong *et al.*, "High-Efficiency Fiber-Shaped Perovskite Solar Cell by Vapor-Assisted Deposition with a Record Efficiency of 10.79%," *Advanced Materials Technologies*, vol. 4, no. 7, p. 1900131, 2019.
- [206] D. Liu *et al.*, "Solid-state, polymer-based fiber solar cells with carbon nanotube electrodes," *Acs Nano*, vol. 6, no. 12, pp. 11027-11034, 2012.
- [207] S. Pan *et al.*, "Novel wearable energy devices based on aligned carbon nanotube fiber textiles," *Advanced Energy Materials*, vol. 5, no. 4, p. 1401438, 2015.
- [208] K. Liu *et al.*, "A self-supported graphene/carbon nanotube hollow fiber for integrated energy conversion and storage," *Nano-micro letters*, vol. 12, no. 1, pp. 1-11, 2020.
- [209] T. Kareri, B. Aljafari, and A. Takshi, "Hybrid photovoltaic-supercapacitors: effect of the counter electrode on the device performance," in *New Concepts in Solar and Thermal Radiation Conversion IV*, 2021, vol. 11824: International Society for Optics and Photonics, p. 1182407.
- [210] F. Rahimi and A. Takshi, "Energy storage capability of the dye sensitized solar cells via utilization of highly porous carbon electrodes," in *Next Generation Technologies for Solar Energy Conversion VII*, 2016, vol. 9937: International Society for Optics and Photonics, p. 99370T.
- [211] C. Zhao, X. Li, Q. Wu, and X. Liu, "A thread-based wearable sweat nanobiosensor," *Biosensors and Bioelectronics*, p. 113270, 2021.
- [212] X. Li, C. Zhao, and X. Liu, "A paper-based microfluidic biosensor integrating zinc oxide nanowires for electrochemical glucose detection," *Microsystems & Nanoengineering*, vol. 1, no. 1, pp. 1-7, 2015.
- [213] T. Kareri, R. L. Yadav, and A. Takshi, "Image processing analysis of supercapacitors with twisted fiber structures and a gel electrolyte," *Journal of Applied Electrochemistry*, vol. 52, no. 1, pp. 139-148, 2022.
- [214] A. Guerra *et al.*, "ZnO/carbon nanowalls shell/core nanostructures as electrodes for supercapacitors," *Applied Surface Science*, vol. 481, pp. 926-932, 2019.
- [215] N. R. Chodankar *et al.*, "True meaning of pseudocapacitors and their performance metrics: asymmetric versus hybrid supercapacitors," *Small*, vol. 16, no. 37, p. 2002806, 2020.
- [216] M. K. Ram, D. Y. Goswami, A. Takshi, and E. Stefanakos, "A new chromic (TouchChromic) thin film," *Acta Materialia*, vol. 121, pp. 325-330, 2016.

- [217] L. Qiu, J. Deng, X. Lu, Z. Yang, and H. Peng, "Integrating perovskite solar cells into a flexible fiber," *Angewandte Chemie International Edition*, vol. 53, no. 39, pp. 10425-10428, 2014.
- [218] M.-S. White, D. Olson, S. Shaheen, N. Kopidakis, and D. S. Ginley, "Inverted bulk-heterojunction organic photovoltaic device using a solution-derived ZnO underlayer," *Applied Physics Letters*, vol. 89, no. 14, p. 143517, 2006.
- [219] G. Georgousis, E. Kontou, A. Kyritsis, P. Pissis, M. Mičušík, and M. Omastová, "Piezoresistivity of conductive polymer nanocomposites: Experiment and modeling," *Journal of Reinforced Plastics and Composites*, vol. 37, no. 17, pp. 1085-1098, 2018.
- [220] M. Shiraishi and M. Ata, "Work function of carbon nanotubes," *Carbon*, vol. 39, no. 12, pp. 1913-1917, 2001.
- [221] R. Gao, Z. Pan, and Z. L. Wang, "Work function at the tips of multiwalled carbon nanotubes," *Applied Physics Letters*, vol. 78, no. 12, pp. 1757-1759, 2001.
- [222] H. Emrah Unalan, "Flexible organic photovoltaics from zinc oxide nanowires grown on transparent and conducting single walled carbon nanotube thin films," *Journal of Materials Chemistry*, vol. 18, no. 48, pp. 5909-5912, 2008.
- [223] Y. Dong, Y. Zou, J. Song, Z. Zhu, J. Li, and H. Zeng, "Self-powered fiber-shaped wearable omnidirectional photodetectors," *Nano Energy*, vol. 30, pp. 173-179, 2016.
- [224] X.-B. Xiang, Y. Yu, W. Wen, and J.-M. Wu, "Construction of hierarchical Ag@TiO₂@ZnO nanowires with high photocatalytic activity," *New Journal of Chemistry*, vol. 42, no. 1, pp. 265-271, 2018.
- [225] A. Wibowo *et al.*, "ZnO nanostructured materials for emerging solar cell applications," *Rsc Advances*, vol. 10, no. 70, pp. 42838-42859, 2020.

Appendix A: Copyright Permissions

The permission below is for the use of materials in Chapter 2 (A Critical Review on the Voltage Requirement in Hybrid Cells with Solar Energy Harvesting and Energy Storage Capability).

RE: Reprint and Reuse Permission

Wiley Global Permissions <permissions@wiley.com>

Thu 3/3/2022 10:40 AM

To: Tareq Kareri <tkareri@usf.edu>

Dear Tareq

As one of the authors of the paper, you do not need Permission to re-use.

Kind regards

Mary O'Connell

Sales Co-Ordinator, GSP

Chichester, United Kingdom


WILEY

From: Tareq Kareri <tkareri@usf.edu>

Sent: 02 March 2022 17:16

To: Wiley Global Permissions <permissions@wiley.com>

Subject: Reprint and Reuse Permission

 This is an external email.

Hello,

I would like to request permission for my paper (A Critical Review on the Voltage Requirement in Hybrid Cells with Solar Energy Harvesting and Energy Storage Capability), A. Takshi, B. Aljafari, T. Kareri, E. Stefanakos, Batteries & Supercaps 2021, 4, 252, to reuse the full article in my dissertation (Fiber-based Electrical Energy Storage and Harvesting Devices for Wearable Electronics).

Thanks,
Tareq Kareri

The permission below is for the use of materials in Chapter 3 (Impedance Spectroscopy Study of Hybrid Photovoltaic Supercapacitors).

3/3/22, 10:35 PM

Mail - Tareq Kareri - Outlook

RE: Reprint and Reuse Permission SPIE 2020

Karleena Burdick <karleenab@spie.org>

Wed 3/2/2022 3:53 PM

To: Tareq Kareri <tkareri@usf.edu>

Cc: reprint_permission <reprint_permission@spie.org>

Dear Tareq Kareri,

Thank you for seeking permission from SPIE to reprint material from our publications. SPIE shares the copyright with you, so as author you retain the right to reproduce your paper in part or in whole.

Publisher's permission is hereby granted under the following conditions:

- (1) the material to be used has appeared in our publication without credit or acknowledgment to another source; and
- (2) you credit the original SPIE publication. Include the authors' names, title of paper, volume title, SPIE volume number, and year of publication in your credit statement.

Please let me know if I may be of any further assistance.

Best,
Karleena Burdick
Editorial Assistant, Publications
SPIE – the international society for optics and photonics
karleenab@spie.org
1 360 685 5515

SPIE.

From: Tareq Kareri <tkareri@usf.edu>

Sent: Wednesday, March 2, 2022 9:37 AM

To: reprint_permission <reprint_permission@spie.org>

Subject: Reprint and Reuse Permission SPIE 2020

Hello,

I would like to request permission for my paper.

Title and author:

(Impedance spectroscopy study of hybrid photovoltaic supercapacitors), Tareq Kareri, Belqasem Aljafari, Arash Takshi,

Volume, issue, and page numbers:

(2020, August), (Vol. 11496, pp. 8-14)

What you would like to reproduce:

To reuse the full article in my dissertation (Fiber-based Electrical Energy Storage and Harvesting Devices for Wearable Electronics).

Where you will republish the requested material:

University of South Florida

Regards,
Tareq

<https://outlook.office.com/mail/inbox/id/AAQkADlhMTBmYzgwLWUzZWUtNGYyMy05NTQ2LTYSZDg5NzI5MDhmOQAQAEfELVEm4QxOokJL%2BnVfi%2...> 1/2

The permission below is for the use of materials in Chapter 4 (Hybrid Photovoltaic-Supercapacitors: Effect of the Counter Electrode on the Device Performance).

3/3/22, 10:36 PM

Mail - Tareq Kareri - Outlook

RE: Reprint and Reuse Permission

Karleena Burdick <karleenab@spie.org>

Wed 3/2/2022 3:55 PM

To: Tareq Kareri <tkareri@usf.edu>

Cc: reprint_permission <reprint_permission@spie.org>

Dear Tareq Kareri,

Thank you for seeking permission from SPIE to reprint material from our publications. SPIE shares the copyright with you, so as author you retain the right to reproduce your paper in part or in whole.

Publisher's permission is hereby granted under the following conditions:

- (1) the material to be used has appeared in our publication without credit or acknowledgment to another source; and
- (2) you credit the original SPIE publication. Include the authors' names, title of paper, volume title, SPIE volume number, and year of publication in your credit statement.

Please let me know if I may be of any further assistance.

Best,
Karleena Burdick
Editorial Assistant, Publications
SPIE – the international society for optics and photonics
karleenab@spie.org
1 360 685 5515

SPIE.

From: Tareq Kareri <tkareri@usf.edu>
Sent: Wednesday, March 2, 2022 9:32 AM
To: reprint_permission <reprint_permission@spie.org>
Subject: Reprint and Reuse Permission

Hello,

I would like to request permission for my paper:

Title and author:

Hybrid photovoltaic-supercapacitors: effect of the counter electrode on the device performance),
Tareq Kareri, Belqasem Aljafari, Arash Takshi.

Volume, issue, and page numbers:

(2021, August), (Vol. 11824, p. 1182407).

What you would like to reproduce:

To reuse the full article in my dissertation (Fiber-based Electrical Energy Storage and Harvesting Devices for Wearable Electronics).

Where you will republish the requested material:

University of South Florida

Regards,
Tareq

<https://outlook.office.com/mail/inbox/id/AAQkADlhMTBmYzgwLWUzZWUtNGYyMy05NTQ2LTYSZDg5NzI5MDhmOQAQAPIJdZleOb9HrTuhzeNAJGc%3D?...> 1/2

The permission below is for the use of materials in Chapter 5 (Image Processing Analysis of Supercapacitors with Twisted-Fiber Structures and a Gel Electrolyte).



My Orders > Orders > All Orders

License Details

This Agreement between University of South Florida -- Tareq Kareri ("You") and Springer Nature ("Springer Nature") consists of your license details and the terms and conditions provided by Springer Nature and Copyright Clearance Center.

[Print](#) [Copy](#)

License Number	5260340748256
License date	Mar 01, 2022
Licensed Content Publisher	Springer Nature
Licensed Content Publication	Journal of Applied Electrochemistry
Licensed Content Title	Image processing analysis of supercapacitors with twisted fiber structures and a gel electrolyte
Licensed Content Author	Tareq Kareri et al
Licensed Content Date	Sep 4, 2021
Type of Use	Thesis/Dissertation
Requestor type	academic/university or research institute
Format	print and electronic
Portion	full article/chapter
Will you be translating?	no
Circulation/distribution	50000 or greater
Author of this Springer Nature content	yes
Title	Fiber-based Electrical Energy Storage and Harvesting Devices for Wearable Electronics
Institution name	University of South Florida
Expected presentation date	Mar 2022
Order reference number	2
Requestor Location	University of South Florida 4202 E Fowler Ave, Tampa TAMPA, FL 33620 United States Attn: University of South Florida

The submission confirmation letter below is for Chapter 6 (A Flexible Fiber-Shaped Hybrid Cell with a Photoactive Gel Electrolyte for Concurrent Solar Energy Harvesting and Charge Storage).

Submission Confirmation for A Flexible Fiber-Shaped Hybrid Cell with a Photoactive Gel Electrolyte for Concurrent Solar Energy Harvesting and Charge Storage (adfm.202202189)



em.afm-journal.0.798e33.4ab49582@editorialmanager.com on behalf of Advanced Functional Materials <em@editorialmanager.com>

Wed 2/23/2022 12:29 PM

To: Tareq Kareri

You are being blind carbon copied ("bcc:d") on an e-mail "To" "Arash Takshi" atakshi@usf.edu

Dear Dr. Takshi,

Your submission entitled "A Flexible Fiber-Shaped Hybrid Cell with a Photoactive Gel Electrolyte for Concurrent Solar Energy Harvesting and Charge Storage" has been received by journal Advanced Functional Materials. The manuscript number for your submission is adfm.202202189.

To view your submission, please login to <https://www.editorialmanager.com/afm-journal/> by entering your username (*****) and password and selecting the "Author Login" option. Please note that the current status of your submission will remain "Under consideration" until an editorial decision is made, at which time you will be notified by e-mail.

If the manuscript is accepted for publication, this author's affiliation will be used to determine eligibility for some open access funding (click [here](#) for details).

This journal offers a number of license options; information about this is available [here](#). The submitting author has confirmed that all co-authors have the necessary rights to grant in the submission, including in light of each co-author's funder's policies. If any author's funder has a policy that restricts which kinds of license they can sign, for example if the funder is a member of Coalition S, please make sure the submitting author is aware.

This message has been sent to all named co-authors listed in the submission process to serve as notification of submission.

Thank you for submitting your work to the journal.

Kind regards,

Editorial Office

Advanced Functional Materials
E-mail: afm@wiley-vch.de

Appendix B: Supporting Information for Chapter 5

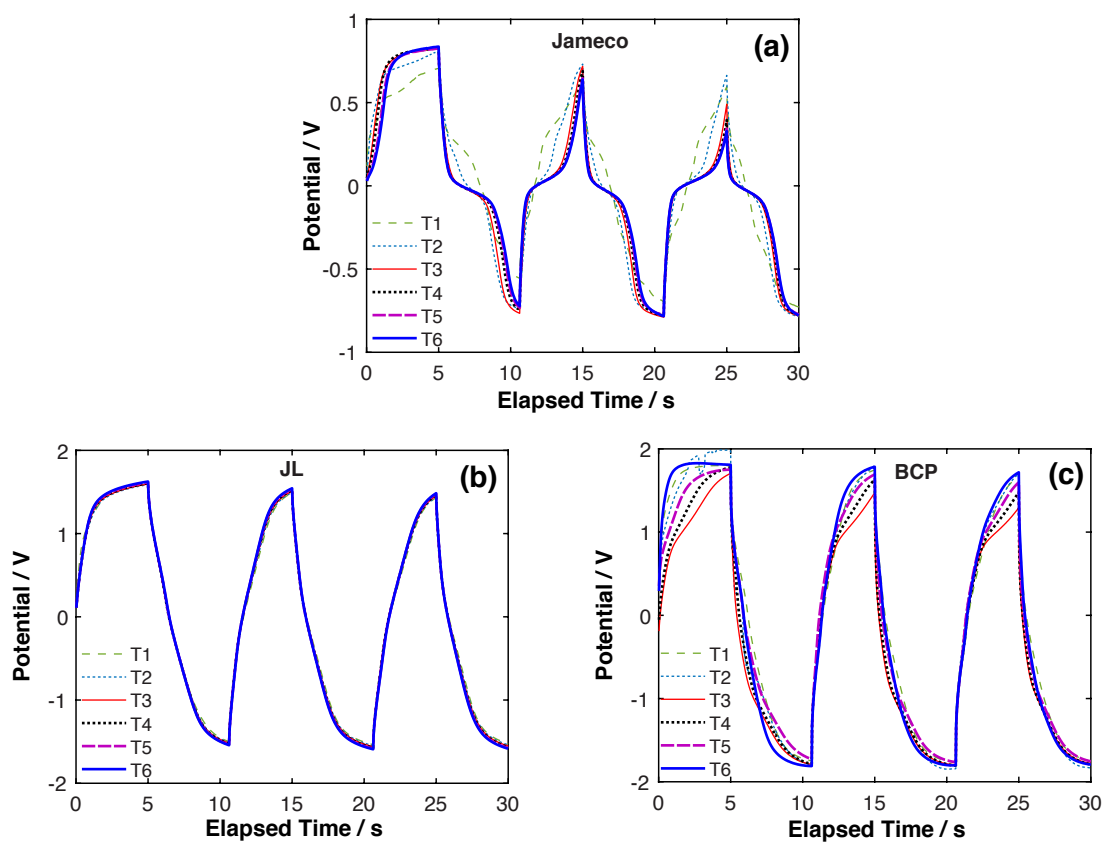


Figure S1: Galvanostatic charge-discharge results of the supercapacitor with (a) Jameco, (b) JL, and (c) BCP fibers and different twisting turns.

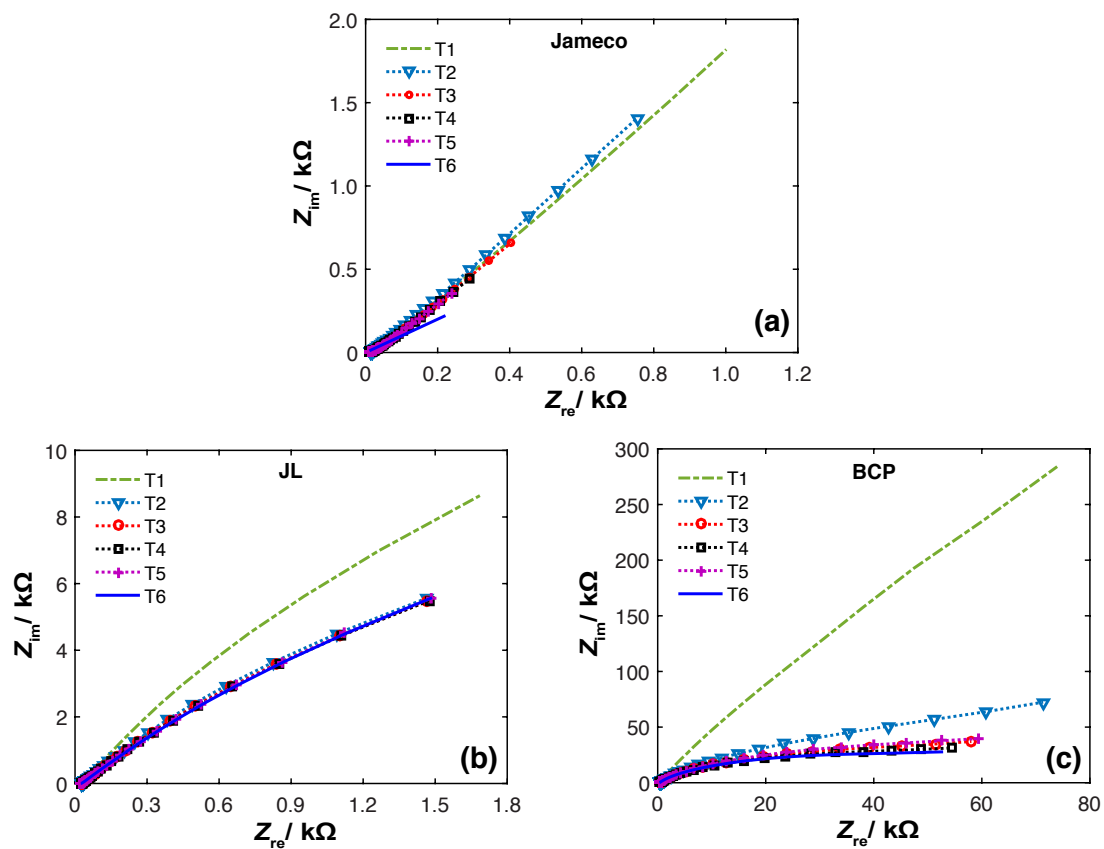


Figure S2: Nyquist plots of the device with (a) Jameco, (b) JL, and (c) BCP fibers.



Figure S3: Jameco thread coated with a layer of gel electrolyte before making the twisted-fiber capacitor.

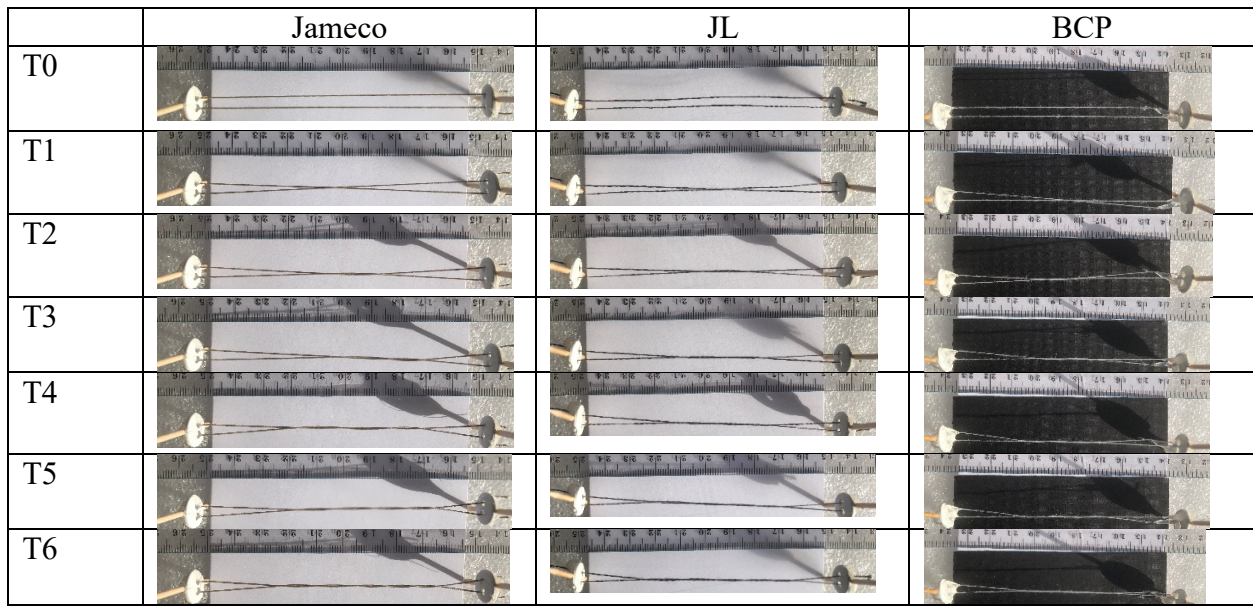


Figure S4: Cropped images of the Jameco, JL, and BCP devices at different number of turns.

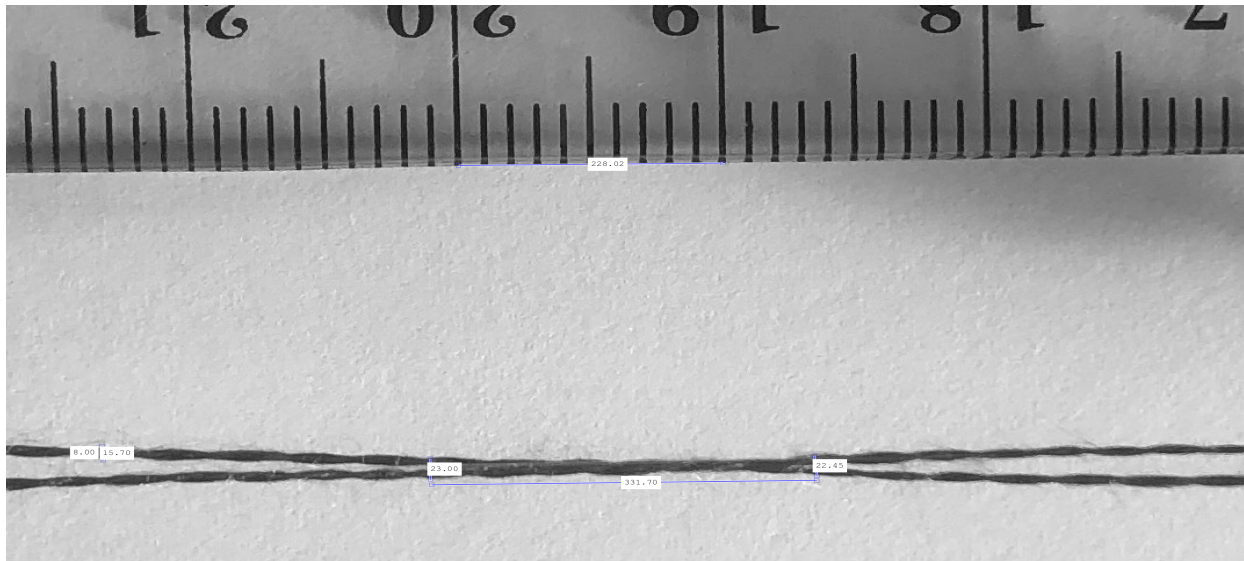


Figure S5: Zoomed in picture of T2 in the JL sample, showing the double layer structure of each JL thread and its effect on the structure of twisted two threads.

Appendix C: Supporting Information for Chapter 6

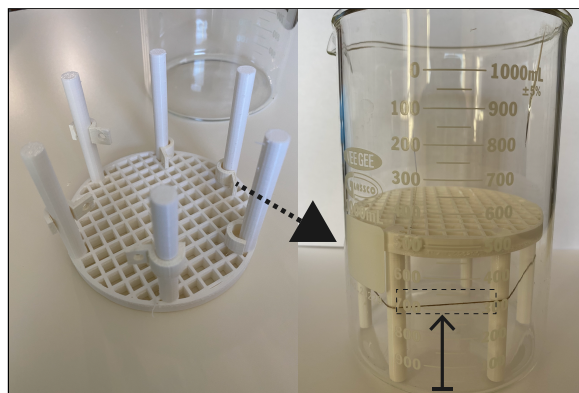


Figure S6: A picture of the 3D printed threads holder for the hydrothermal process.

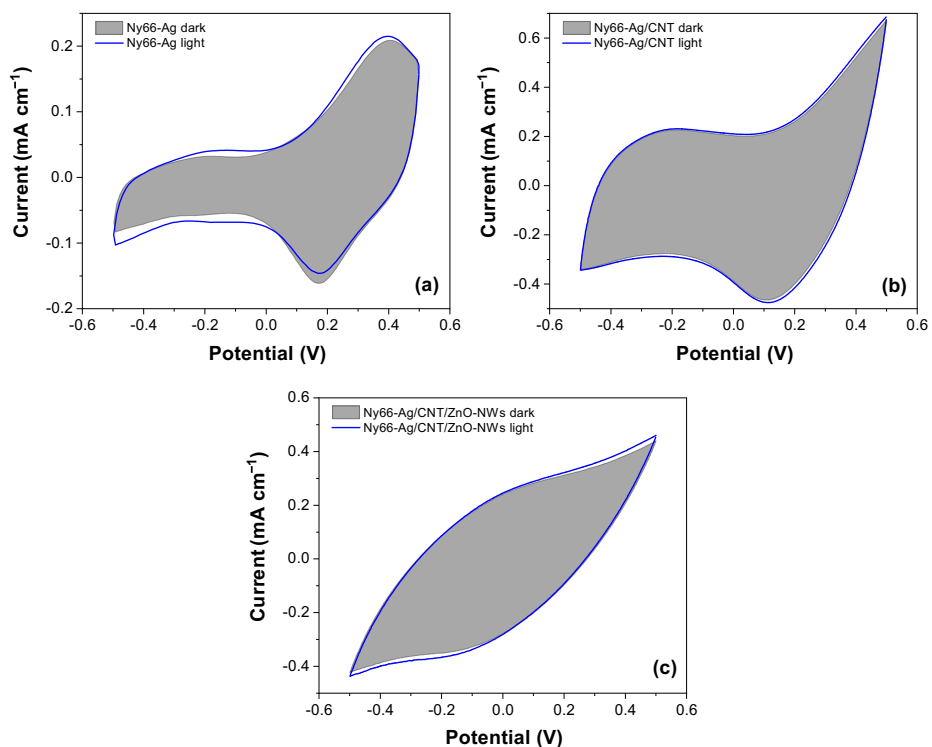


Figure S7: Cyclic voltammetry results of the fiber-shaped hybrid devices with (a) Ny66-Ag, (b) Ny66-Ag/CNT, and (c) Ny66-Ag/CNT/ZnO-NWs electrode in dark and under illumination.

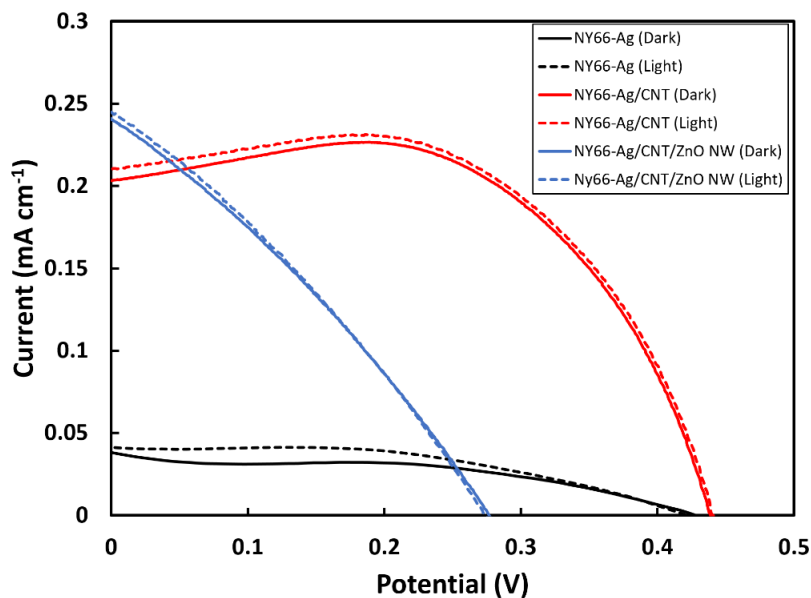


Figure S8: I-V response of the fiber-shaped hybrid devices with (a) Ny66-Ag, (b) Ny66-Ag/CNT, and (c) Ny66-Ag/CNT/ZnO-NWs electrode in dark and under illumination.

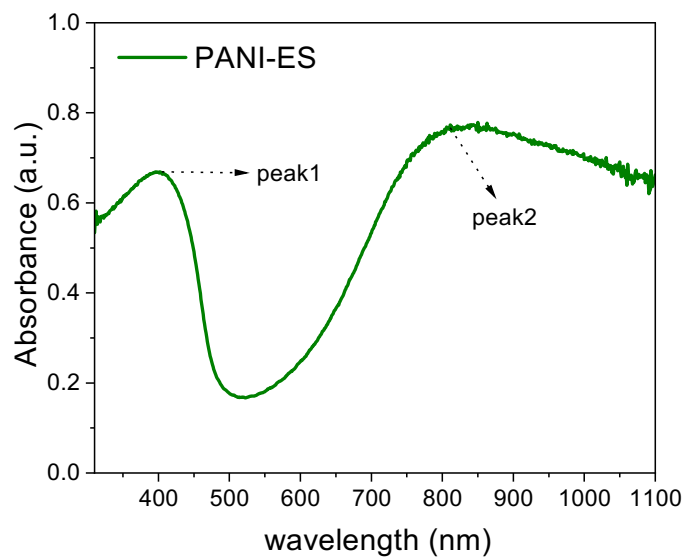


Figure S9: UV-visible absorption spectrum of the photoactive PANI gel in emeraldine salt form.

Table S1: Impedance parameters of the fiber-shaped hybrid devices in dark and under illumination.

Anode Electrodes	R_s [Ω]	R_p [Ω]	C_{dl} [μF]	C_{gel} [μF]	R_{gel} [Ω]	R_e [Ω]	$0 < n < 1$	Q [$S s^n$]
Ny66-Ag Dark	102.46	2284.4	14.64	746.8	33134	29.5	0.691	84.1×10^{-5}
Ny66-Ag Light	98.96	1505.1	21.29	577.6	18853	34.8	0.692	100.9×10^{-5}
Ny66-Ag/CNT Dark	111.68	11562	2.83	3755.7	7231.5	21.1	0.337	99.9×10^{-4}
Ny66-Ag/CNT Light	111.18	11504	2.91	3785.5	7936.2	21.4	0.352	101.6×10^{-4}
Ny66- Ag/CNT/ZnO-NWs Dark	1733.3	1156.7	2.26	2136	16232	42.4	0.463	34.1×10^{-4}
Ny66- Ag/CNT/ZnO-NWs Light	1713.4	951.59	2.27	2215.3	13504	16.3	0.418	50.4×10^{-4}